# ICE DEFORMATION ASSOCIATED WITH A GLACIER-DAMMED LAKE IN ALASKA AND THE IMPLICATIONS FOR OUTBURST FLOOD HYDRAULICS

by

MICHELLE L. CUNICO

A thesis submitted in partial fulfillment of the
requirements for the degree of

MASTER OF SCIENCE
in
GEOLOGY

Portland State University
2003

THESIS APPROVAL

The abstract and thesis of Michelle L. Cunico for the Master of Science in Geology were presented April 4, 2003, and accepted by the thesis committee and the department.

COMMITTEE APPROVALS:

_____
Andrew G. Fountain, Chair

_____
Joseph S. Walder

_____
Christina Hulbe

_____
Dan Johnson
Representative of the Office of Graduate Studies

DEPARTMENT APPROVAL:

_____
Michael L. Cummings, Chair
Department of Geology

**Abstract**

An abstract of the thesis of Michelle L. Cunico for the Master of Science in Geology presented April 4, 2003.

Title: Ice deformation associated with a glacier-dammed lake in Alaska and the implications for outburst flood hydraulics

Glacial outburst floods, or jökulhlaups, occur when water is released from a body of water impounded by, within, or beneath a glacier. This study focuses on outburst floods from Hidden Creek Lake, a lake that forms in a tributary valley that is blocked by Kennicott Glacier, Alaska. Two field seasons (1999 and 2000) were spent monitoring the lake and ice dam before and during the outburst flood in order to better understand the hydrological and mechanical interactions associated with outburst floods. A water balance study was used to ascertain whether the glacier stores lake water prior to the flood. Displacements of the ice dam were measured using survey methods while simultaneously measuring lake stage to determine how the glacier responds to changing lake levels.

For both years vertical displacements of the ice dam were largest nearest the ice front but decreased dramatically with distance from the lake. Correspondingly, the ice thickness also decreased with distance from the lake. Horizontal velocities

increased significantly after the onset of the flood by a factor of 21 nearest the lake to a factor of < 2 at the targets farthest from the lake.

The results from both the water balance study and the vertical displacements of the ice suggest that a significant volume of water is stored beneath the ice dam prior to the flood. Using a water balance approach, the stored water volume was estimated as 2 million $m^3 \pm 1$ million $m^3$. The stored water volume determined from vertical ice displacement was between 2 and 4 million $m^3$. The stored water is probably hydraulically connected to the lake but is separated from the glacier's main drainage system by an internal drainage divide.

ACKNOWLEDGEMENTS

I would first like to thank my two advisors Andrew G. Fountain (PSU) and Joseph S. Walder (USGS – CVO) who provided me with the opportunity to work on this fascinating project in beautiful Alaska. As one of my earlier professors, Andrew G. Fountain was key in sparking my interest in glaciology. I would also like to thank my other committee members Christina Hulbe and Dan Johnson from the Geology and Geography departments respectively at PSU.

This thesis was a small part of a larger collaborative project and would not have been possible without Suzanne P. Anderson and Robert S. Anderson (Univ. of CA, Santa Cruz). In addition I would like to express my gratitude to every member of the Kennicott team all of whom contributed to this thesis in some manner; Robert Schlichting, Steven Malone (Univ. of WA), Christy Swindling (UCSC), and Sharon Longacre (UCSC). I would like to offer a special thanks to Andrew Malm (St. Olaf College) who performed all of the ice-radar measurements, Robert Jacobal (St. Olaf College) for providing the ice radar instrumentation, Erin Kraal (UCSC) for her friendship and for having a (much-needed) shower ready for us when we got out of the field, and Donald Lindsey (PSU) for always keeping us entertained. I would especially like to thank Dennis Trabant (USGS – Fairbanks) for being a great mentor and delightful field companion as we shared the most beautiful campsite in the world.

Our entire team benefited greatly from the generosity and support provided by the Wrangell Mountain Institute. The National Park Service, U.S. Geological Survey field office in Anchorage, and Nancy Eriksson (PSU) all provided logistical support

while we were in the field. Financial support was provided by a grant from the National Science Foundation Office of Polar Programs/Arctic Science section.

I would like to thank everyone in the PSU glacier group for the invaluable conversations at our weekly meetings. I am grateful for Robin Johnston's friendship and support through undergraduate and graduate school.

Finally, I will be forever grateful to my family and husband for their patience, love, understanding, and emotional support.

TABLE OF CONTENTS

## LIST OF TABLES

LIST OF FIGURES

# CHAPTER 1

# INTRODUCTION AND PROJECT DESCRIPTION

## 1.1 Introduction

Outburst floods, also known by the Icelandic word jökulhlaup, are caused by the sudden drainage of a body of water impounded by, within, or beneath a glacier. Commonly, water drainage occurs subglacially although some ice-dammed lakes can drain through a breach between the glacier and valley wall. The study of outburst floods is important to the hydrology and geomorphology of glaciated areas. A glacier flood can initiate migration of the river channel, channel erosion, flood plain inundation, and increase sediment load. In populated areas they may also threaten human life, property, bridges, and roads. Evidence of the destructive nature of outburst floods is exposed in the "Channeled Scablands", a landscape that stretches across Montana, Idaho, Oregon and Washington (Baker and Fairbridge, 1981). The Channeled Scablands were formed by episodic outburst floods from Pleistocene-age glacial Lake Missoula, Montana, impounded by the Cordilleran ice sheet (Bretz, 1969). Outbursts of Lake Missoula may have released as much as 2,184 $km^3$ of water (Clarke et al., 1984) scouring out the loess and basalt deposits of the Columbia Plateau (Baker and Fairbridge, 1981) leaving behind deeply dissected gorges, flood channels and such large-scale depositional features as giant gravel bars and current dunes.

Glacial outburst floods are common in glaciated regions all over the world. Some of the largest and most spectacular Holocene floods from ice-dammed lakes have been documented in Iceland and are associated with geothermal activity (Björnsson, 1974; Björnsson, 1992; Fowler, 1999; Nye, 1976; Thorarinsson, 1939). For example, outburst floods from the subglacial lake Grímsvötn beneath the Vatnajökull Ice Cap occur every 4 to 6 years with peak discharges up to 10,000 $m^3/s$ and volumes as great as 3.0 $km^3$ (Björnsson, 1992). Other outburst floods have been reported in Norway, Switzerland, China, South America, Greenland, Canada, and North America (Tweed and Russell, 1999; Walder and Costa, 1996). Outburst floods also occur on glaciated volcanoes of Mount Rainier and Mount Hood in the Cascade Range of Washington and Oregon, and are associated with the release of subglacially or englacially stored water (Driedger and Fountain, 1989; Walder and Driedger, 1995). These events occur during the melt season and are probably triggered by large influxes of meltwater and/or rainfall (Walder and Driedger, 1994). Outburst floods released by Tahoma Glacier on Mount Rainier have resulted in destructive debris flows in the Tahoma Creek River Valley, Washington, covering roads and recreational areas with mud and debris (Driedger and Fountain, 1989; Walder and Driedger, 1994).

Although outburst floods are relatively common events, they remain poorly studied owing to their unpredictable and transient nature. Specifically, little is known about the mechanical and hydrological interactions between an ice-dammed lake and the impounding glacier prior to and during an outburst flood. The primary purpose of this thesis is to examine how an ice dam mechanically deforms in response to

changing lake levels to better understand the fundamental mechanisms governing the storage and release of impounded water. This study will focus on a sub-aerial lake that is situated at the margin of a glacier and drains subglacially. The work presented here is a portion of a larger collaborative project studying various aspects of outburst floods from inception to the flood outflow at the terminus. Other institutions involved in this project in addition to Portland State University include the University of California, Santa Cruz and the United States Geological Survey.

## 1.2 Hypothesis

Nye (1976) conducted extensive research on outburst floods from the Vatnajökull ice cap in Iceland. Nye suggested that prior to an outburst flood there is a drainage divide that separates water hydraulically connected to the lake from water hydraulically connected to the glacier's main drainage system. As the water pressure in the lake increases, the thinnest portions of the ice will begin to rise creating a cantilever effect on the still-grounded ice. The cantilever effect is caused by the finite time necessary for the buoyantly supported ice to attain isostatic equilibrium. Drainage of the lake occurs once the water pressure in the lake exceeds the overburden pressure of the thickest ice, adjusted for the cantilever effect (Nye, 1976). This scenario may be applied to an outburst flood that occurs on a subaerial ice dammed lake with the geometry of Hidden Creek Lake and Kennicott Ice Dam.

My hypothesis follows from Nye's (1976) analysis. Prior to the flood, a large volume of water enters into storage beneath the ice dam. The water is hydraulically

isolated from the main subglacial drainage system by a drainage divide. Catastrophic drainage of the lake occurs when the subglacially stored water pressure becomes great enough to breach the drainage divide, eventually connecting with the main drainage system of the glacier. To test aspects of this hypothesis I will examine the mechanical response of the ice dam to changing lake levels, determine if any portion of the ice dam is floating prior to the flood, determine the volume of stored water beneath the ice dam prior to drainage, and estimate the location of the subglacial drainage divide if it exists. I will do this using survey data and ice radar data collected on the surface of the ice dam, water level data from Hidden Creek Lake, and water level data collected from boreholes drilled in the ice dam.

### 1.3 Study Area

Hidden Creek Lake (HCL) was chosen for this study because there is a relatively complete historical record of outburst floods dating back to 1909 (Rickman and Rosenkrans, 1997), the outflow stream can be readily gaged, and the glacier is accessible by road. HCL is situated at 61$^{o}$ 34'N, 143$^{o}$ 05'W in Wrangell-St. Elias National Park and Preserve in southeastern Alaska (Figure 1.1). The lake forms in a tributary valley dammed by Kennicott Glacier and fed by Hidden Creek. At its maximum extent, HCL has a surface area of approximately 1.0 km$^2$, being 0.8 km wide at the ice dam and 1.3 km long. Annual drainage of HCL occurs sometime in mid summer or early fall and typically lasts for 2-3 days, leaving the lake basin choked with ice debris (Figure 1.2). The lake drains subglacially or englacially and

discharges at the terminus of the glacier, 15 km downstream from the lake, where it adds to the normal flow of the Kennicott River.

The term “ice dam” is used in this thesis to refer to the portion of the glacier that enters into the tributary valley (Figure1.3 a). HCL is the largest of six glacier-dammed lakes in the Kennicott River Basin (Figure 1.2). Erie Lake tends to drain around the same time as HCL while Donoho Lake and Jumbo Lake typically drain earlier in the summer or spring and Gates Lakes and Bonanza Lakes drain later in the summer or fall (Rickman and Rosenkrans, 1997). During drainage of HCL, Donoho Lake and Jumbo Lake have been observed to refill with sediment-laden water, then to empty again as the HCL flood wanes, indicating at least a temporary hydraulic connection through the glacier between the lakes in the Kennicott basin (Rickman and Rosenkrans, 1997).

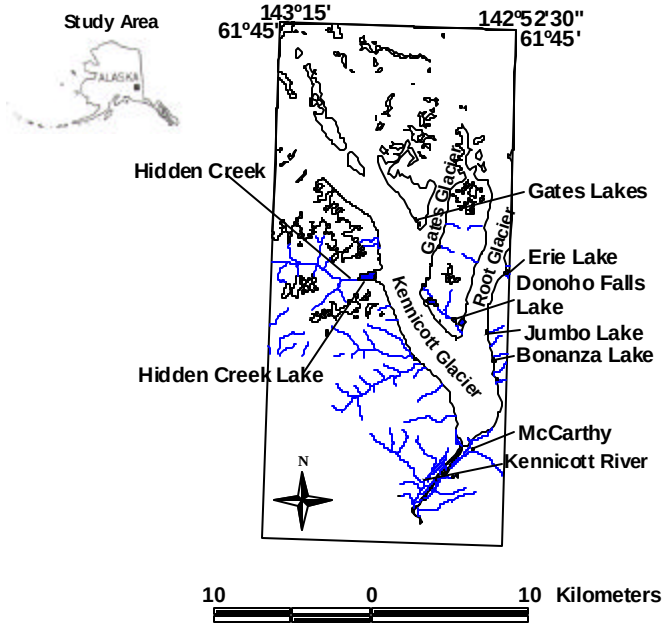


Figure 1.1 Location of the study area.

a.

b.

Figure 1.2 Photographs of HCL before (a) and after (b) the 1999 outburst flood. View is from the survey station looking southwest. The ice dam can be seen on the left side of each photo. Notice the ice debris (b) that accumulates in the basin from the collapse of the ice dam during and after the flood. These photos were taken over a four-day period.

The lake and the ice dam are situated below the equilibrium line of Kennicott Glacier. The equilibrium line separates the accumulation zone (glacier area of net yearly mass gain) from the ablation zone (glacier area of net yearly mass loss). Below the equilibrium line, broad medial moraines cover most of the surface of the glacier. The ice dam is mantled with rock debris and heavily crevassed including a series of north trending arcuate shaped crevasses that extend to approximately 300 m from the ice dam/lake interface and point away from the lake (Figure 1.3 b). Closer to the lake, the crevasses maintain a N-S orientation but are much straighter.

### *McCarthy, Alaska*

The town of McCarthy, Alaska is located adjacent to the Kennicott River, about 1.5 km from the glacier terminus (Figure 1.1). The McCarthy area attracts several thousand visitors annually due to its recreational opportunities and the historic Kennecott Copper Mine. In the past, outburst floods from HCL increased the normal summer discharge of the Kennicott River by as much as a factor of 10, creating hazardous flooding conditions for residents and tourists. Access to McCarthy requires crossing the Kennicott River. Until the establishment of a footbridge in 1997, temporary bridges were repeatedly washed out by outburst floods from HCL (Rickman and Rosenkrans, 1997).

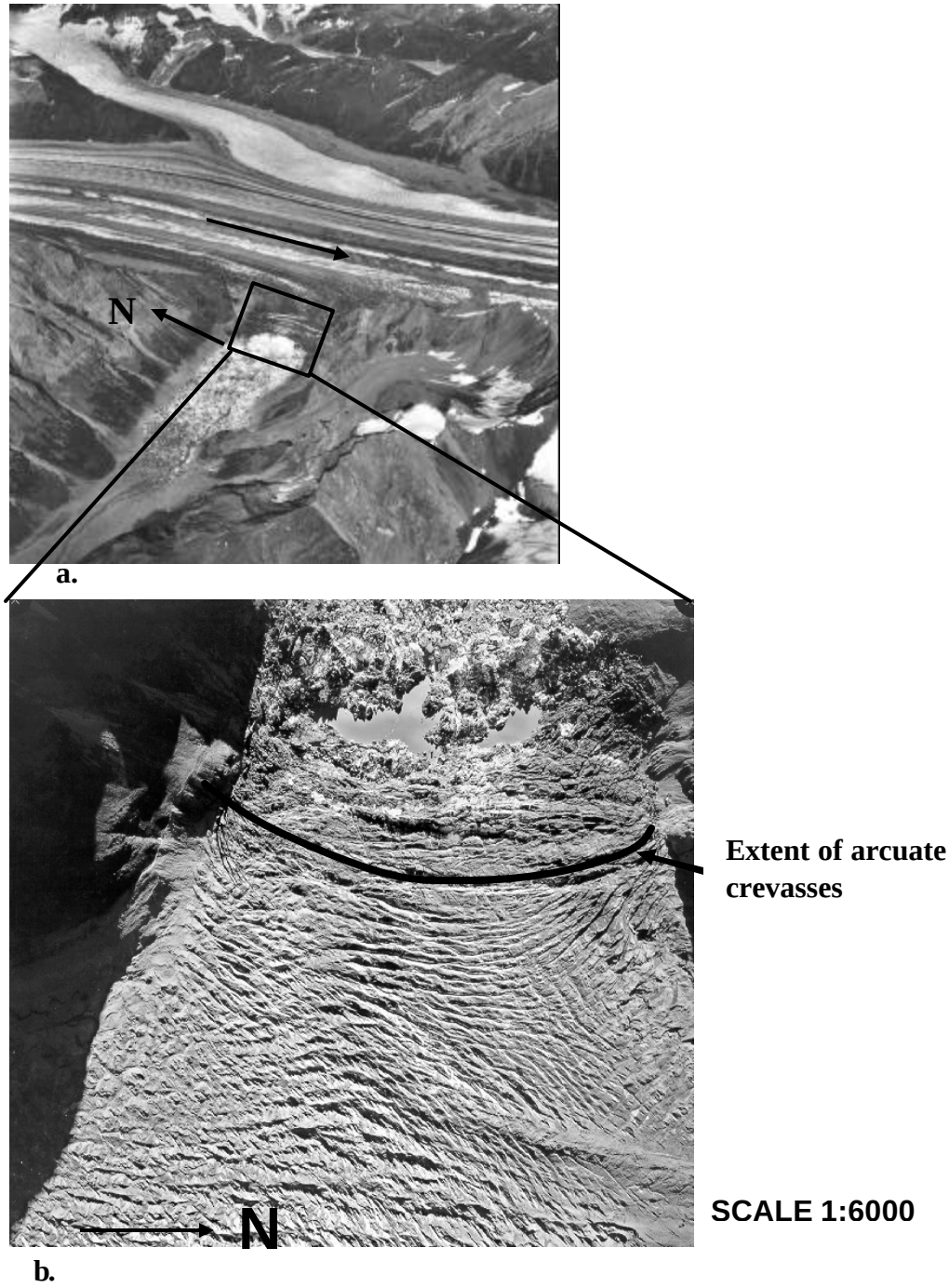


Figure 1.3 Aerial photographs of the Kennicott ice-dam showing (a) the approximate extent of the effective "ice dam" and (b) the extent of arcuate crevassing. The lake had begun to refill (top of bottom photo) at the time the photo was taken in mid August 1999.

### *Topography*

The Kennicott Glacier basin contains several large peaks: Mount Blackburn (4,996 m), Atna Peaks (4,225 m & 4,145 m) and Regal Mountain (4,220 m). Kennicott Glacier is approximately 45 km long and originates from both the southeast side of Mount Blackburn and the south side of Atna Peaks. The Gates and Root glaciers both flow from Regal Mountain and merge with the Kennicott Glacier at elevations of 1,067 m and 762 m, respectively. The terminus of the Kennicott Glacier has retreated by approximately 610 m over the years 1909 – 1995 (Rickman and Rosenkrans, 1997).

### *Climate*

The climate in the Kennicott Basin is influenced by the wet, temperate climate of the coast and the drier, colder interior of Alaska (Rickman and Rosenkrans, 1997). Climate data are recorded by the National Weather Service from the nearest weather station, located in McCarthy (station 3 SW) 61º 25’ N 143º 00’ W at an elevation of 381 m, and are averaged over the years 1999-2000. The station is located near McCarthy, approximately 15 km down-glacier from the lake. Temperatures during the summer (June – Aug.) average 20.7º C for the high and 12.3º C for the low. Temperatures during the winter (Dec. – Feb.) average –10.5º C for the high and –21.6º C for the low. Average total annual precipitation is 0.5 m, with an average total snowfall of 2.1 m.

*Geology*

The geology in the Kennicott Basin is diverse and reflects a complicated geologic history. Mount Blackburn is one of the oldest (3.0 – 4.5 million years old) remnant volcanoes in the Wrangell Volcanic Field, which began as a volcanic arc that drifted northward and eventually began accreting onto the North American plate approximately 100 million years ago (Richter et al., 1995). The Wrangell Mountains comprise a series of large volcanoes that erupted over the past 26 million years that covered an area of 10,400 $km^2$ with lava (Richter et al., 1995). The ancient terrane making up the basement rocks of the Wrangell Mountains consists of basalt and marine limestone derived from the shallow seas that once inundated the region (Richter et al., 1995). The Kennicott Basin consists of Tertiary age andesite and pyroclastic rocks at higher elevations near Mount Blackburn (MacKevett, 1972). The Triassic-age Nikolai Greenstone and the Chitistone and Nizina Limestones are exposed at the surface from the intersection of the Gates Glacier with the Kennicott Glacier down to its terminus, as well as in Hidden Creek Valley (MacKevett, 1972).

Structurally, the Kennicott Basin is dominated by northeast trending high angle normal faults (MacKevett, 1972). One of these high angle faults is inferred to cut across the HCL basin where it intersects Kennicott Glacier to the north (MacKevett, 1972).

## 1.4 Thesis Structure

The thesis is organized into five chapters. A discussion of pertinent research related to outburst floods is presented in Chapter Two. Hydrological data from HCL as well as Hidden Creek is included in Chapter Three. These data include lake drawdown, bathymetry and discharge, along with discharge records from Hidden Creek. Chapter Four discusses the geometry of the ice dam interpreted from ice radar, ice displacement results and an analysis of triggering mechanisms. This chapter also includes a discussion on water storage beneath the ice dam. Finally, Chapter Five concludes with a synthesis of the research findings and suggestions for future research.

# CHAPTER 2

# BACKGROUND RESEARCH

## 2.1 Mechanisms of drainage initiation

The most systematic research on outburst floods has centered on the subglacial lake Grímsvötn on the Vatnajökull ice cap in Iceland. The lake forms at the base of the ice cap due to intense geothermal melting and periodically drains subglacially (Björnsson, 1992). From Thorarinsson's (1939) early research on Grímsvötn, he theorized that the triggering mechanism for outburst floods is simply flotation of the ice dam once the hydrostatic pressure from the lake exceeds the pressure of the ice at its thinnest location. Subsequent Icelandic lake studies showed that outburst floods commonly occurred at water levels 20-50 m less than that required for the flotation condition (Björnsson, 1974, 1992).

Glen (1954) proposed a somewhat similar mechanism for flood initiation. He theorized that outburst floods occur when the hydrostatic pressure from the water body exceeds the vertical ice overburden pressure allowing the water to escape beneath the ice dam in sheet flow. Eventually the escaping water would form a tunnel that links up with a pre-existing subglacial conduit system. Nye (1976) attempted to explain the drainage via a hydrostatic cantilever effect. He suggested that as the lake water rises, the buoyant force causes the thinnest ice to flex upward as the ice adjusts towards a new isostatic equilibrium. The effect of the cantilever is to reduce the pressure at the

bottom of the thicker grounded ice. The reduction in pressure at the base of the ice would allow drainage to occur at lower water stages than would flotation for a given ice thickness.

Nye's (1976) theory assumes that prior to the flood, there is a tight hydraulic seal at the location of the grounded ice. However, Kasper's (1989) water balance study on an ice-dammed marginal lake on the Kaskawulsh Glacier, Yukon Territory revealed that substantial leakage of the lake may have occurred ($1.95 \times 10^7$ $m^3$) before the lake drained. In addition, Fisher (1973) injected dye into glacier-dammed Summit Lake, British Columbia, and detected it in the Salmon River downstream from the glacier terminus. Water must have leaked from the lake into the glacier's main drainage system.

Although previous research has greatly advanced our knowledge of outburst floods, the theories have not been well tested with field data. The reported flood volumes in Iceland, for example, are based on the outflow hydrograph with little or no independent knowledge of the volume of stored water or the rate of release. By implementing a comprehensive and collaborative field study, we have obtained detailed data that better constrain models of outburst floods.

Other studies of outburst floods have focused on the prediction of peak discharge. Clague and Mathews (1973), updated by Walder and Costa (1996), used observations of maximum lake level and peak discharge to develop a relationship between the two. Nye (1976) developed a theoretical model for predicting discharge using the governing equations for unsteady water flow in subglacial tunnels, which he

applied to the outburst floods of Grímsvötn Lake, Iceland. Clarke (1982) expanded Nye's (1976) model by introducing other factors such as lake temperature, reservoir geometry, and creep closure. Clarke (1982) tested his own model by comparing measured discharge from an outburst flood at Hazard Lake, Yukon Territory to the simulated discharge.

Ice dam deformation in response to filling and draining of an ice-dammed lake has only been reported once. Kasper (1989), measured the vertical displacement of an ice dam on the Kaskawulsh Glacier, Yukon Territory, as it's lake filled and drained. She determined that maximum displacement occurred nearest the ice front and decreased drastically within a few hundred meters from the lake, indicating that the ice dam nearest the lake may be floating.

## 2.2 Review of subglacial hydrology

The subglacial drainage system can be divided into "fast" and "slow" subsystems (Raymond et al., 1995). "Fast" drainage systems include channelized conduit systems and "slow" drainage systems include distributed or widely spread drainage systems that transport water over a larger portion of the bed. I omit from this review the sheet flow and subglacial till components of the distributed system because the volume of water that is transported and stored in these systems is relatively small and is not deemed significant to this study.

*“Fast” drainage systems*

In the fast drainage system, water is transported efficiently. For instance, in fast drainage systems, dye injected instantaneously into the glacier emerges from the proglacial stream relatively quickly, within hours, as a single concentrated pulse indicating that little dispersion or storage is occurring during transport (Seaberg et al., 1988; Willis et al., 1990). Fast drainage is thought to be accomplished via two types of channels; “Röthlisberger” or R – channels that are incised into the ice and “Nye” or N – channels that are incised into the substratum (Nye, 1973).

R-channels and N-channels form under different conditions and produce different glacier drainage characteristics. R-channels tend to close by creep when the water pressure is less than the ice overburden pressure but can remain open if the water pressure equals the ice overburden pressure, aided by frictional melting of the channel walls (Röthlisberger, 1972). Under steady flow conditions, there is an inverse relationship between discharge and channel water pressure (Röthlisberger, 1972). As water discharge increases, it generates more frictional heat that enlarges the conduit walls allowing more water to flow thereby lowering the water pressure. This relationship leads to the tendency of large R-channels to capture smaller ones, resulting in an arborescent conduit network of smaller channels funneling into a single large channel. N-channels can occur as single conduits or in networks as observed in deglaciated bedrock (Walder and Hallet, 1979). The development of N-channels often occurs where water flow and erosion are concentrated along the same route such as occurs in steep bedrock topography (Benn and Evans, 1998).

*“Slow” drainage systems*

Slow drainage systems are less efficient at transporting water than fast drainage systems. In contrast to the fast drainage system, dye emerges slowly (days to weeks) as multiple pulses over a longer period of time, indicating dispersion and the temporary storage of water. The type of slow drainage system pertinent to this thesis is the linked cavity system.

Cavities form between the base of the ice and the substratum where the glacier flows over rough bedrock topography (Figure 2.1). Smaller links or orifices form between cavities where the topography is less advantageous to cavity development. Under steady flow conditions, there is a direct relationship between water discharge and water pressure within the cavities (Kamb, 1987). With large transients in water pressure, the cavities and orifices can grow unstably and may convert to a system of R-channels thus allowing for a more efficient evacuation of water (Kamb, 1987). Likewise, when the pressure drops the R-channels can collapse and revert back to a system of linked cavities (Walder, 1986).

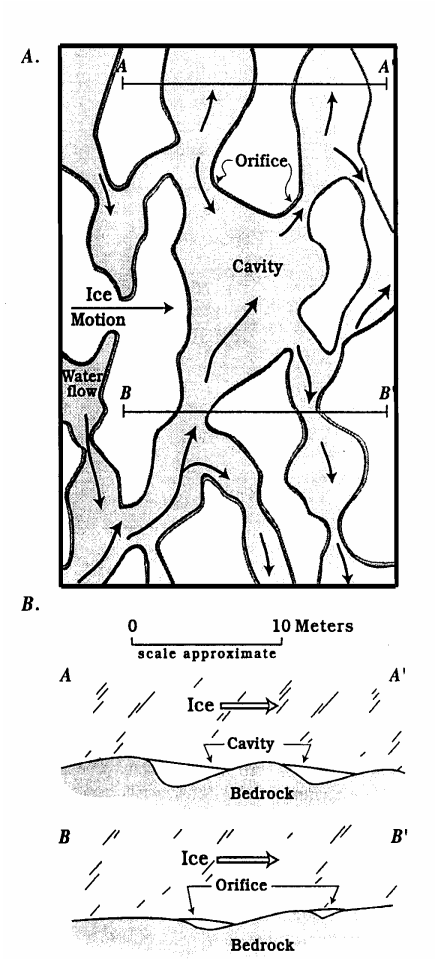


Figure 2.1 (a) Schematic drawing of a basal linked cavity drainage system in plan view; (b) Cross section diagram showing the formation of cavities (Kamb, 1987).

## 2.3 Prior research in study area

The most comprehensive description of HCL is by Rickman and Rosenkrans (1997), who compiled a history of outburst floods, conducted a survey of the lake basin after drainage, and estimated the lake volume. In addition, stage and stream flow measurements were taken on the Kennicott River near the terminus of the glacier. The

survey data proved to be valuable to this study because we were unable to survey the lake basin, except for a few locations, due to the danger posed by ice debris.

Other, more directed studies have also been conducted. Friend (1988), used data collected from an outburst of HCL to test the proposed models of Clague and Mathews (1973) and Clarke (1982). Previous fieldwork directly related to ice-dam motion was conducted by J. Walder and C. Driedger (1994 pers. comm.), who placed a time lapse camera aimed at HCL and the ice dam, documenting the movement of the ice dam before, during and after the flood.

# CHAPTER 3

# HYDROLOGICAL MEASUREMENTS

## 3.1 Introduction

Hydrological measurements of HCL were fundamental for establishing the upstream boundary conditions for the flood, namely the water pressure at the ice dam and water flux during the flood. These measurements are necessary for understanding the process of storage and release as well as the timing and hydraulic response of the subglacial drainage system during the flood (Kraal, 2001). Lake stage was recorded during the filling and draining period to determine the water pressure at the ice dam. With knowledge of the hypsometry and change in stage, we can determine flux into the lake prior to outburst and the flux from the lake during the flood.

## 3.2 Field Methods

The majority of the HCL measurements were conducted using an inflatable Zodiac boat. On July 14, 1999 we arrived in the field intending to have two to three weeks for setting up instruments and to begin collecting data before the flood initiation. Unfortunately, one day after our arrival (July 15, 1999), the lake stage began to drop slowly indicating the onset of the outburst flood. We managed to collect data on lake level change during the flood event but lacked any pre-flood data. Based on

the experience of 1999, we initiated the fieldwork earlier the next season (July 5) and managed to collect data for almost three weeks before the flood onset (July 25).

During both field seasons, lake stage was measured by lowering non-vented and sealed pressure transducers to the bottom of the lake. The transducers were weighted and placed in the lake as deep as possible. The pressure transducers were all calibrated in the lab prior to deployment in the field (Appendix A1). Two Campbell Scientific CR10 data loggers were used that were powered by rechargeable batteries and solar panels. The data loggers were programmed to collect data at 20-minute intervals. The water stage record was referenced to an elevation datum by periodically surveying to a reflector manually held at the current water line on the shore.

*1999 field season*

During the 1999 field season we placed one 100 psi (70 m ± 0.08 m) and two 300 psi (210 m ± 0.24 m) pressure transducers in the lake. The transducers were at a maximum depth of about 55.5 m and were attached to 305 m of electrical cable. Based on what is now known about the bathymetry of the lake, we estimate that the maximum depth of the lake may have been close to 100 m.

*2000 field season*

Four pressure transducers were initially placed in the lake at the beginning of the 2000 field season: two 70m (100 psi) transducers (on 305 m and 610 m of cable) and two 210 m (300 psi) transducers (on 305 m and 610 m of cable). Rickman and

Rosenkrans (1997) showed that the deepest part of the lake was at the glacier-lake interface. We used a sonar depth finder to determine water depth and were able to place the transducers at a depth of about 90 m. We were unable to place the transducers at a greater depth due to the dangers of calving ice. A barometer was placed next to the data loggers to measure the atmospheric changes that may induce pressure variations in the non-vented transducers.

On Julian Day 199 (July 17, 2000) at 16:37, a large portion of the ice dam (~0.15 $km^2$ in area) calved, floated out approximately 20 m, then became grounded in the vicinity of the deep water transducers. The fact that the ice mass did not shift in response to the prevailing wind direction but remained relatively stationary is evidence for grounding. Our initial deployment of transducers produced data of poor quality due to the random noise in the records. We suspect water leaked into the transducers or cables. After the calving event, the data made no sense and we concluded that the transducers were destroyed. We then placed two vented and sealed 50 psi (35 m ± 0.02 m) pressure transducers attached to 100 m of underwater cable in the water near the shoreline. Because of the short cable we were only able to measure about 3.0 m of head change. As a backup, survey measurements (under the direction of Dennis Trabant – USGS) were made to the lake surface relative to a pointed rock spire located across the lake from the survey site. These survey angles were recorded at four-hour intervals before and two-hour intervals after Julian Day 192 (July 10, 2000). Also, a survey reflector was attached to the top of a plastic bucket that was placed into the lake and tethered to the shoreline by rocks. Distance measurements were made to the

reflector at the same intervals as the survey angle measurements. All of the HCL field measurements were conducted in collaboration with Joseph S. Walder (USGS – Cascades Volcano Observatory).

*Bathymetry*

To supplement the survey data compiled by Rickman and Rosenkrans (1997), we used a sonar depth finder with a paper chart recorder to map the bathymetry of the lake during the 2000 field season. Straight line transects were run across the lake as close to the ice front as was deemed safe. A small electric motor propelled the boat and allowed us to maintain a fixed speed. The starting and ending transect positions were recorded using a handheld Garmin GPS unit. Unfortunately, the paper chart recordings were lost and only one position and depth sounding was salvaged. This point will be referred to later in the bathymetric analysis section.

*Hidden Creek*

Hidden Creek flows directly into HCL from the west and is the primary source of input into the lake. Glacial meltwater and precipitation are secondary sources. The stage and discharge of Hidden Creek were measured in 2000 for use in the water balance study. Robert Anderson and Erin Kraal (University of California) set up the instruments and performed the discharge calculations. The water stage was recorded by suspending an acoustic water stage sensor over the stream following the methods of Anderson et al. (1999) and Dick et al. (1997). The data were recorded using a

Campbell Scientific CR10 data logger programmed to measure stage at 2-second intervals and store an average value every 15 minutes. Several salt discharge readings were conducted before and after the flood following the method of Kite (1993). Discharge was additionally measured using a hand held Price AA current meter and wading rod following standard USGS stream gaging methods (Wahl et al., 1995). Plotting the stream discharge with the corresponding stream stage resulted in a rating curve (Appendix A2). The rating curve was then used to convert the stage data to discharge for the entire field season.

## 3.3 Results

*HCL stage – 1999 Field Season*

The 100 psi pressure transducer recorded data for the longest time period from Julian Day 196.61 (July 15, 1999 15:04 until Julian Day 198.65 (July 17, 1999 16:00). The record ends when either the transducer stopped functioning or the water level fell below the transducer. The maximum head was 56.1 m (Figure 3.1). The two 300 psi transducer records can be found in Appendix A3.

*HCL stage – 2000 Field Season*

Because the 100 and 300 psi pressure transducers were destroyed during the calving event and the data collected prior to their destruction is questionable, the data were discarded. A combination of the 50-psi transducers and the two independent survey records were used instead. To avoid confusion, the survey made to the target

floating in the lake will be referred to as “floating target” and the survey angle measurements made from the lake surface up to the spire will be referred to as “spire target”. The largest probable measurement errors for both the survey records are 5 cm, with the floating target measurements being slightly more accurate. The floating target measurements utilized a reflector, allowing us to focus on the cross hair for each measurement. With the survey angle measurements, there was nothing that precise to focus on. Larger errors are more likely to occur in the morning or evening, when atmospheric refraction can be a problem and on sunny days when the instrument is less stable (D. Trabant, pers. comm. 2000). From the four uncombined records (Figure 3.2), it is evident that although the two 50 psi transducers are similar, noise exists in the data (of magnitude about 10 cm) above instrument error.

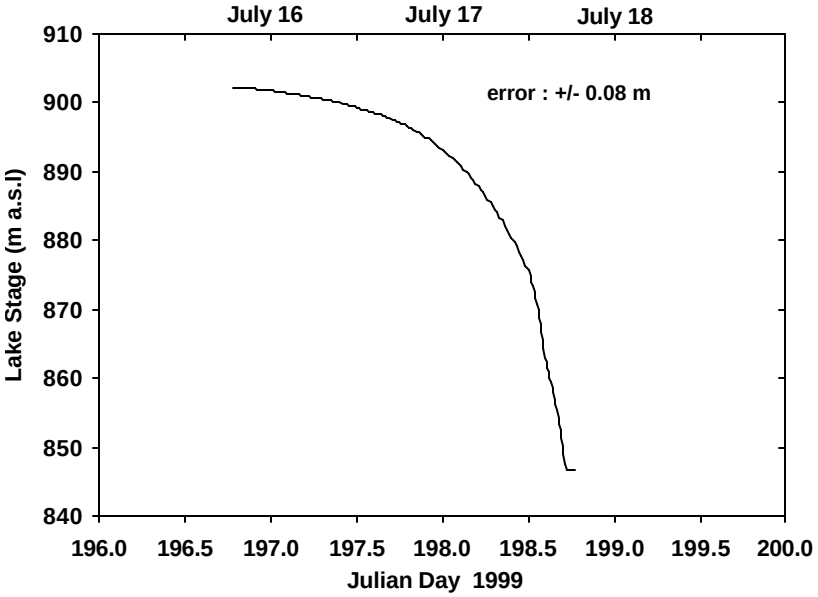


Figure 3.1 1999 lake stage recorded by the 100 psi pressure transducer.

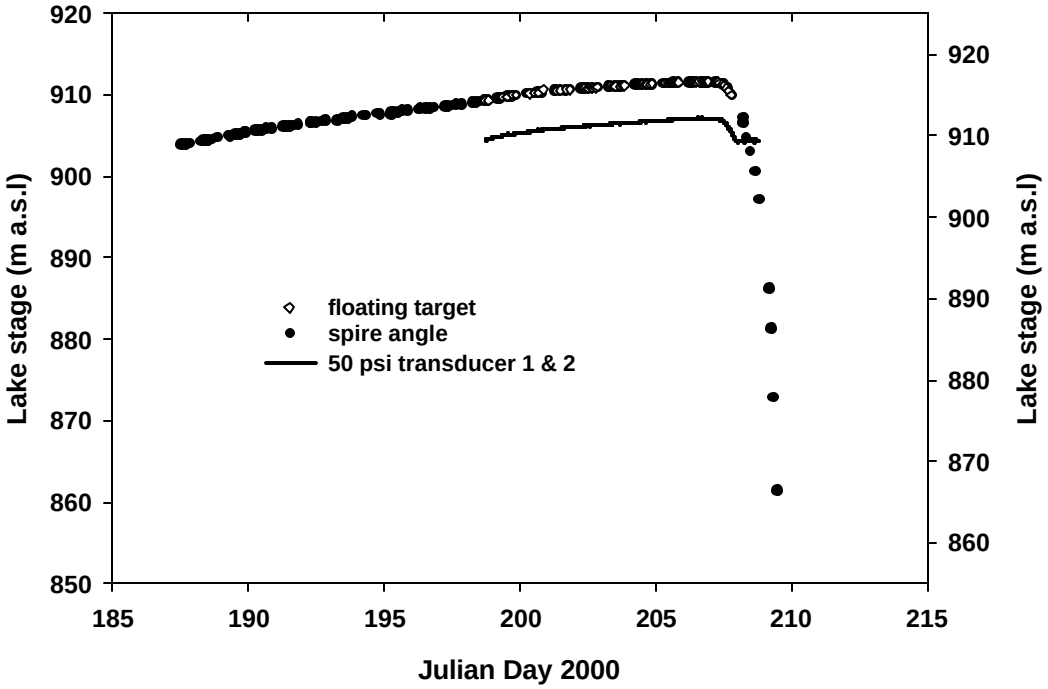


Figure 3.2 Lake stage time series recorded by the two 50-psi pressure transducers and the two survey measurements. Notice that the secondary y-axis corresponds to the 50 psi transducer data and has been slightly offset to see the comparison.

With the exception of the two 50 psi transducers, the four data sets were not collected simultaneously nor at the same time intervals. To construct a unified record, the transducer records were merged with the survey measurements. For a summary of the methods used to combine the records see Appendix A4. The final record from the four water stage measurements shows a total drawdown of 47.7 m (Figure 3.3). The largest error from the four different records is about 0.05 m and is used as error for the combined drawdown record.

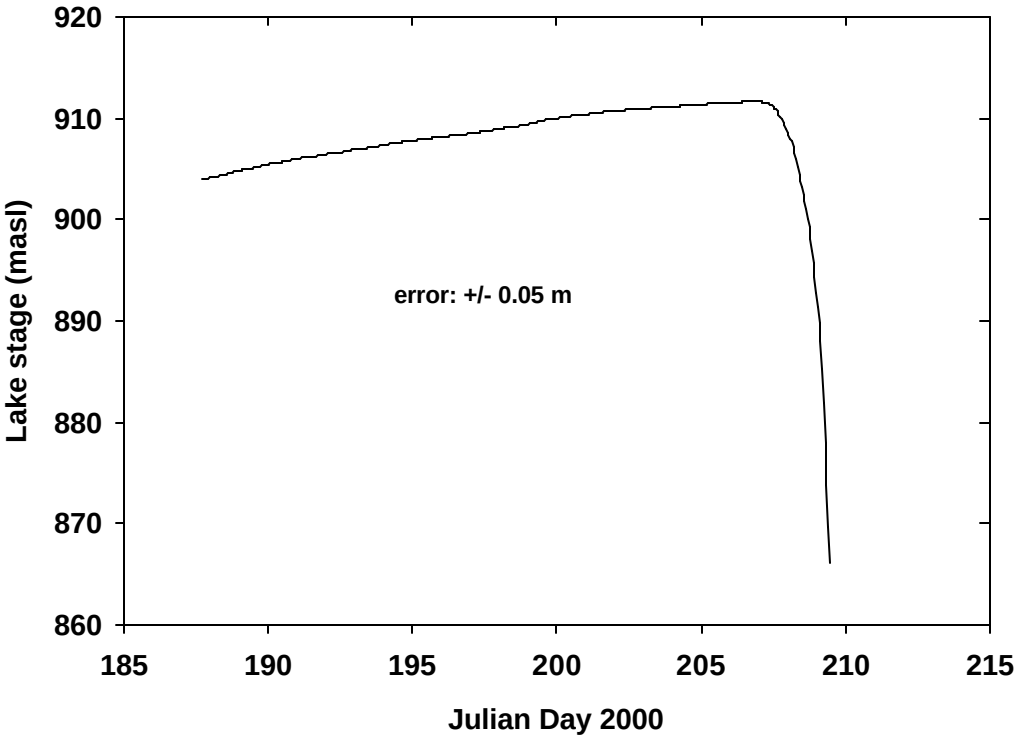


Figure 3.3 HCL drawdown record for the 2000 season incorporating all of the four stage records.

## 3.4 Hydrological Analysis

*Water Stage Records*

We cannot precisely compare the two lake stage records during the period of rise because of our late arrival in 1999; however, the levels are similar. The highest lake stage recorded in 1999 was 902.49 m. This measurement, taken at the onset of the 1999 flood, is probably close to the maximum stage because the initial drainage rate was slow. The maximum lake stage recorded in 2000 was 911.68 m. The records show that the rate of peak drainage was greater in 1999 (175 m/day) than it was in 2000 (70 m/day). The flood initiation occurred during July for both years. In 1999, the lake

stage began to drop during the night prior to Julian Day 196 (July 15, 1999) before we were able to place our instruments into the lake. During the 2000 field season the lake stage began to drop on Julian Day 206.75 (July 24, 2000).

*HCL bathymetry*

A bathymetric map was constructed by combining the 1994 and 1995 lake basin survey data from Rickman and Rosenkrans (1997), supplemented with survey data that was collected by our field team during the 1999 and 2000 field season. The automated contouring did not produce realistic results in the deeper depths of the lake because of the sparse distribution of measured data in that area. To improve the automated contours, five manually interpolated points were added to the deep basin. The location of data points used in the interpolation can be found in Appendix A5.

The point values of elevation were spatially interpolated by kriging and then contoured to construct a bathymetric map (Figure 3.4). The bathymetric map reveals steep bed topography nearest the ice front with a deep trough then a decreasing slope with distance from the ice dam. Although heavily covered with ice debris, the lake basin topography is visible after drainage. In order to characterize the topographic surface of the lake bottom and obtain area and volume statistics, a Triangulated Irregular Network (TIN) was applied to the kriged data using ArcView Geographic Information System (GIS) with the Spatial Analyst ArcView extension. The area and volume statistics were calculated at 2 m intervals up to the highest measured lake stage. The volume vs. stage relationship is shown in Figure 3.5.

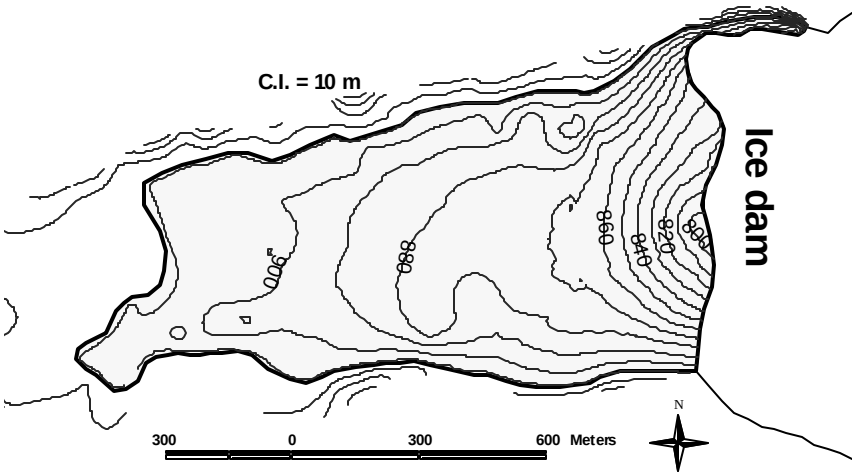


Figure 3.4 Bathymetric map of HCL. The outline of the lake is shaded.

*Error analysis*

The sparseness of data within the lake basin, in addition to the survey error, produces inherent errors in the bathymetry of the lake basin. The change in slope of the lake basin is large near the ice dam, hence in this vicinity there is a large volume change associated with small variations in water level. Unfortunately, this area is lacking data and points were manually interpolated to improve contours. The automated grid interpolation was very sensitive to the placement and value of the manually added data points. I ascribed an error of ± 5m to the manually interpolated elevations and the volume and area vs. stage relationship were re-calculated (Figure 3.5).

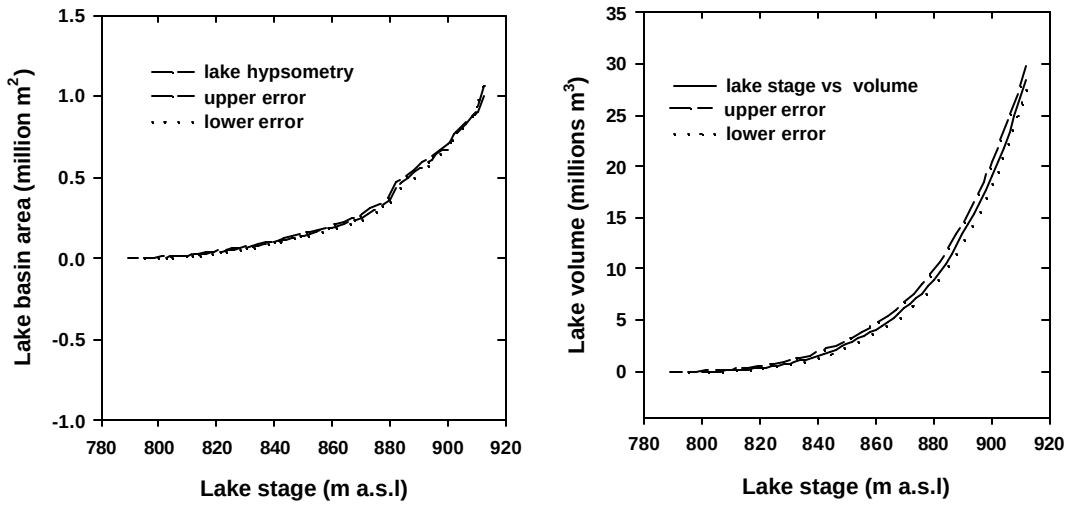


Figure 3.5 Graphs showing the hypsometry and lake volume with stage relationship for HCL. The dashed and dotted lines indicate an upper and lower bound based on an error bar of ± 5 m for the interpolated data points.

*HCL discharge*

The hypsometry of the lake basin was used to convert change in lake stage to change in volume by the following relations:

$$\frac{dV_{lake}}{dt} = Q_{in} - Q_{out} \quad (3.1)$$

$$\frac{dV_{lake}}{dt} = A(h)\frac{dh}{dt} \quad (3.2)$$

where $Q_{in}$ is the discharge going into the lake, $Q_{out}$ is the discharge leaving the lake, $V$ is lake volume, $t$ is time, $h$ is lake stage, and $A(h)$ is the surface area of the visible lake as a function of stage. Substituting equation 3.2 into 3.1 yields,

$$Q_{out} = Q_{in} - A(h)\frac{dh}{dt} \quad (3.3)$$

When determining the discharge, three estimates of *dV/dh* were made. The 1999 and 2000 lake drawdown rate (*dh/dt)* were calculated using the finite difference method. The final calculated discharge including a lower and upper bound for both 1999 and 2000 are shown in Figure 3.6. The upper and lower discharge values are used here to illustrate the error in the discharge values and will not be used. The maximum lake volumes from the 1999 and 2000 field season were approximately 21 x $10^6$ $m^3$ ± 2 x $10^5$ $m^3$ and 28 x $10^6$ $m^3$ ± 3 x $10^5$ $m^3$, respectively. These volumes do not account for displacement due to the grounding of icebergs, which would reduce the water volume. Because the grounding of icebergs changes with time, it is unclear how to account for this factor.

A direct comparison of the two hydrographs in Figure 3.7 shows that the lake discharge initially increased rapidly in 2000, reaching a peak discharge of 323 $m^3$/s approximately 1 day after the drainage began. In 1999, the discharge increased slowly and although peak lake discharge is unknown, it was still rising 2 days after onset of drainage. Note that the 2000 drawdown curve is smoother than the 1999 drawdown curve due to combining the four different stage records and interpolating.

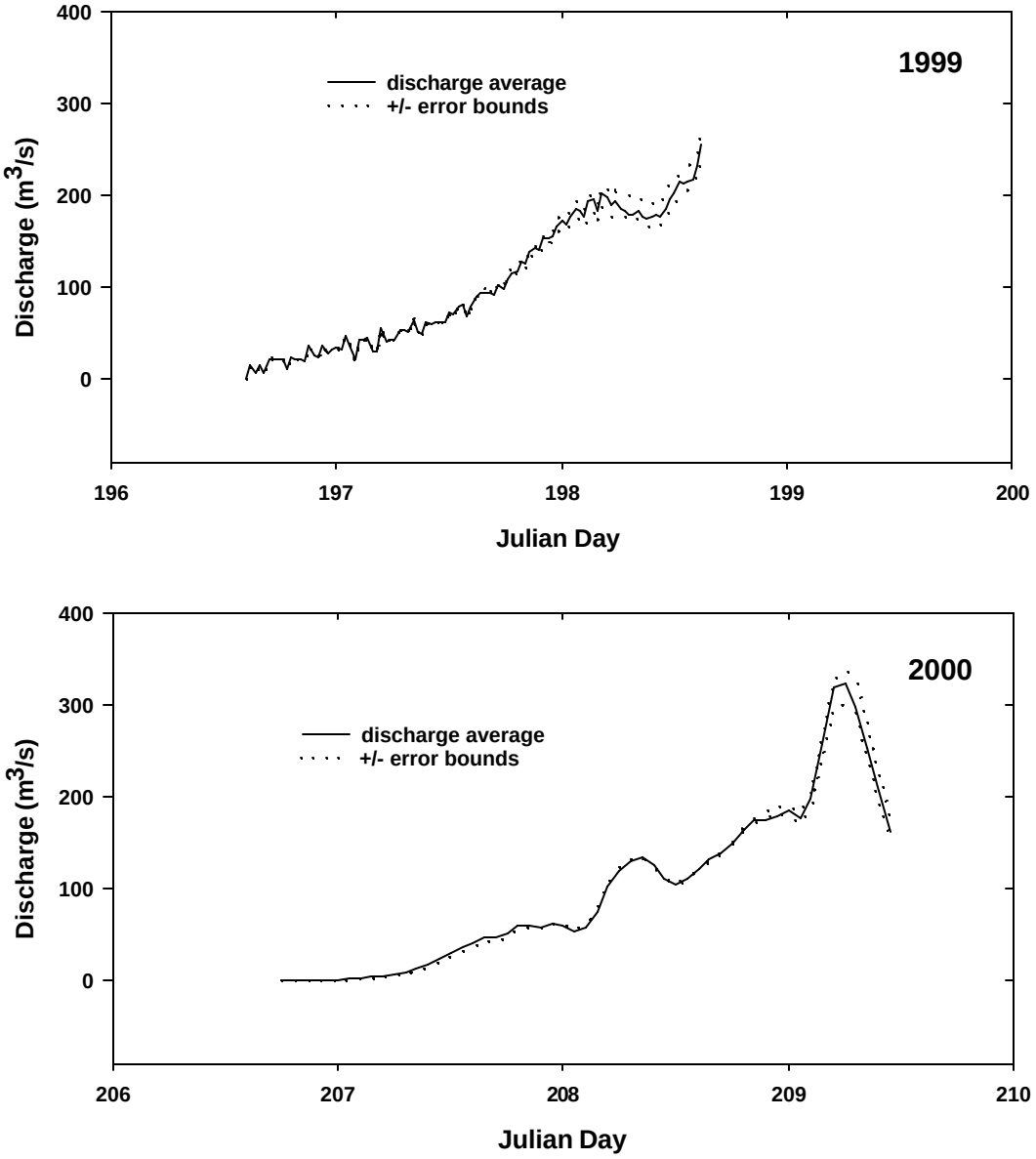


Figure 3.6 HCL flood hydrographs for 1999 (upper) and 2000 (lower). Each hydrograph includes an upper and lower bound corresponding to the error bars on the lake hypsometry.

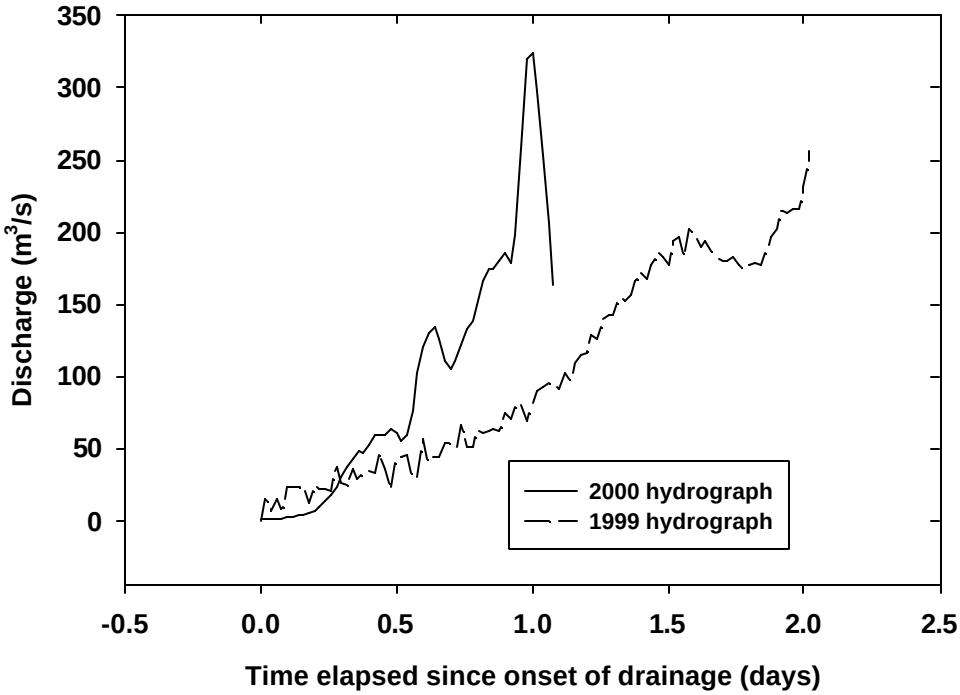


Figure 3.7 Comparison between the 1999 and 2000 hydrographs.

Because we were unable to submerge the pressure transducers in the lowest part of the lake, neither the 1999 nor the 2000 hydrographs are complete. Based on the volume vs lake stage relationship, there may have been as much as 2 million $m^3$ of water left in the basin when the pressure transducers went dry in 1999 and 5 million $m^3$ left in 2000. To extrapolate the hydrographs to complete drainage of the lake, we assumed that the drawdown rate is constant after the last record (Figure 3.8). For comparison, a third order polynomial curve was fit to the 1999 drawdown rate and was extrapolated to complete drainage. A third order polynomial curve was fit to both the

1999 and 2000 drawdown data yielding essentially the same results as the linear curve fit in 1999. The polynomial curve fit did not approximate the 2000 data well.

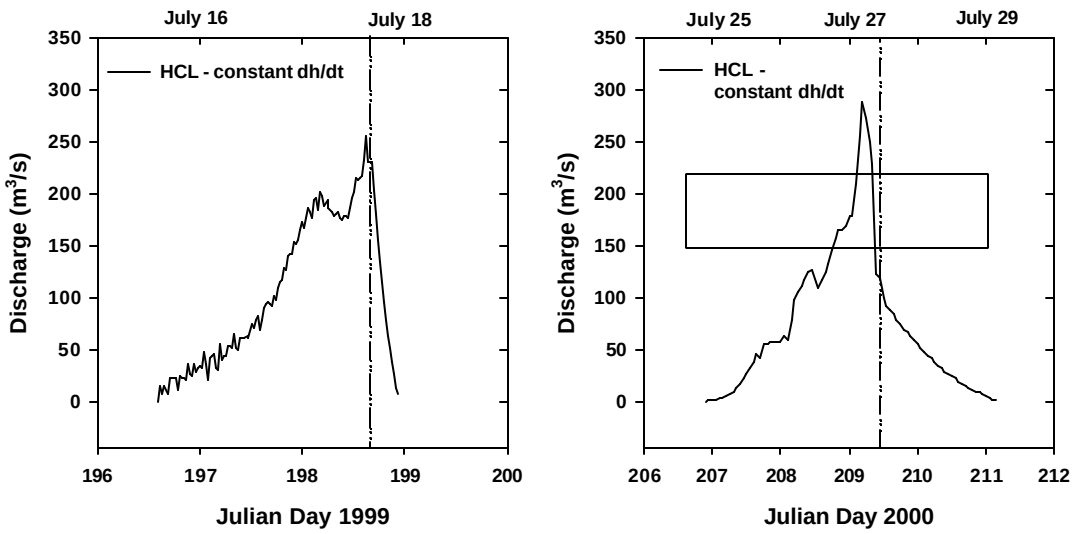


a. b.

Figure 3.8 Extrapolation of the HCL hydrograph for (a) 1999 based on a constant dh/dt after the transducer record ends and (b) 2000 based on a constant dh/dt after the transducer record ends. The curves to the right of the vertical line represent the extrapolated portion of the data.

*Hidden Creek*

Hidden Creek discharge was relatively high (5.0 – 7.0 $m^3/s$) during the early part of July (Figure 3.9), corresponding with early summer melting of the snow pack. The discharge declines during mid – July and continues to decline into late July with the exception of a large peak in discharge (7.0 $m^3/s$) during a warm period of weather, Julian Day 198 – 201 (July 16 – 19). The errors on the measurements are estimated as 20%. The discharge of Hidden Creek over the time period of measurement, Julian Day

187 to 207 (July 5 – July 25, 2000), yielded a total water input into the lake of 6 x $10^6$ $m^3$ ± 1.2 x $10^6$ $m^3$.

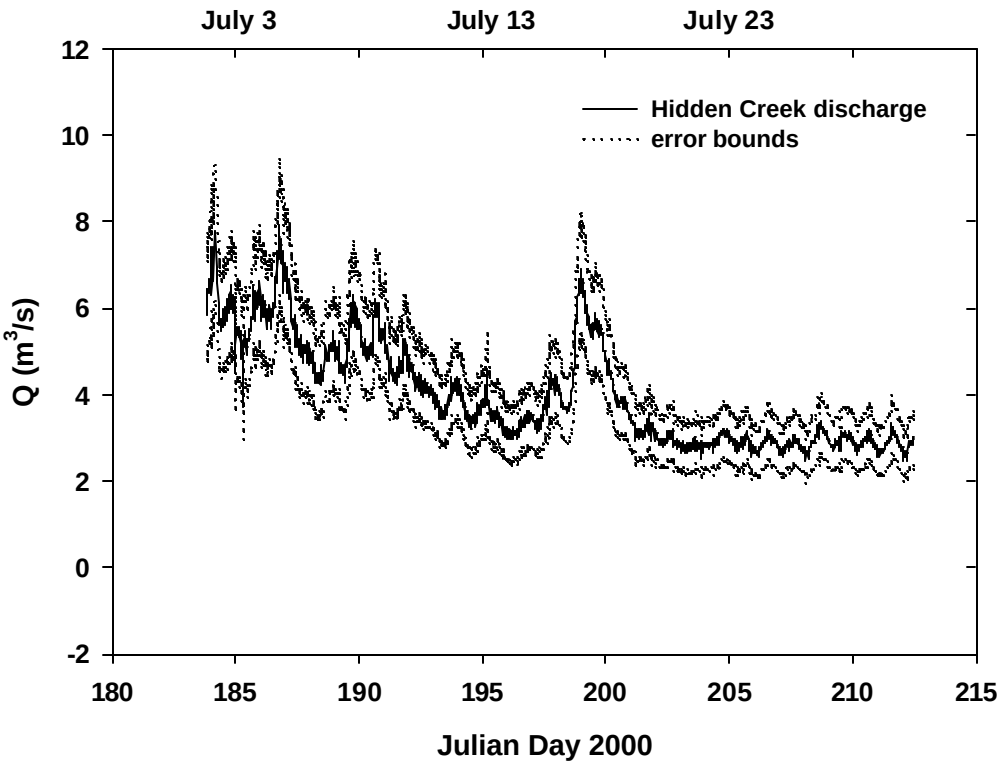


Figure 3.9 Hidden Creek hydrograph for the 2000 field season. The dotted lines indicate the approximate error bounds on the measurements.

To make a rough estimate of the water budget in the lake basin, the discharge values for Hidden Creek and HCL were converted to cumulative volume inputs beginning at the same time our lake measurements began (Figure 3.10). The graph shows that the stream volume change is nearly identical to the lake volume change.

However, the following paragraph will take a more comprehensive approach to the water balance that includes other factors such as ablation and precipitation.

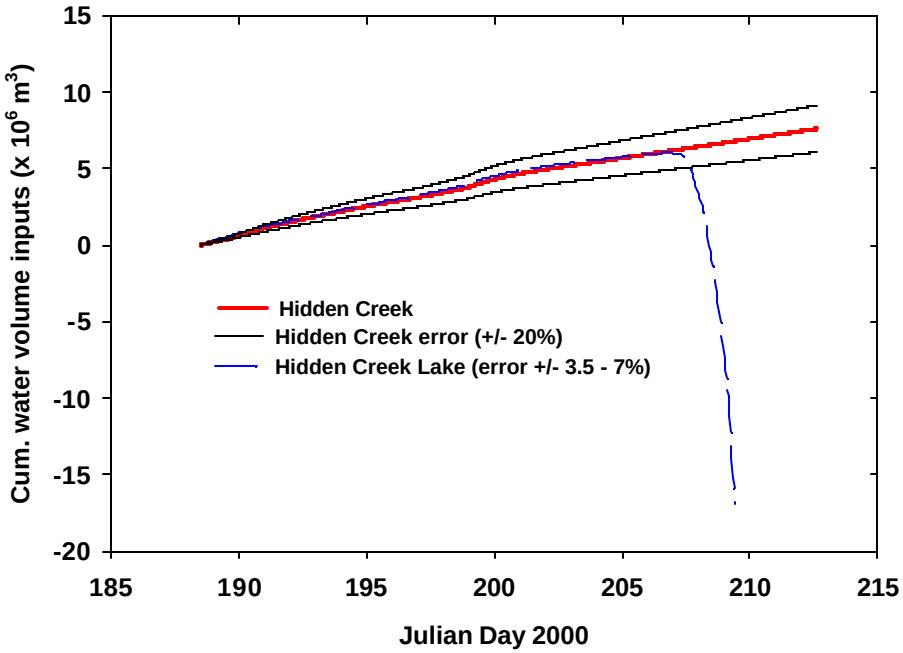


Figure 3.10 Cumulative water volume inputs from Hidden Creek and cumulative water volume of HCL.

*Water budget*

An analysis of the water budget in the HCL basin is used to determine if there is storage of water prior to the flood. The basic governing equation for the conservation of mass is outputs minus inputs equals a change in water storage. The total water balance incorporating all of the appropriate terms results in:

$$V_{HC} + P + A \pm E = ?\ storage \quad (3.4)$$

Where $V_{HC}$ is the water volume for Hidden Creek during the lake filling period, $P$ is the volume from rain and $A$ is the volume of meltwater derived from ablation. $(E)$ is evaporation and is assumed to be negligible. As an example, a graph was used to predict a range of typical evaporation values for lakes (Roberts and Stall, 1967). Using an average summer temperature and solar radiation value obtained from the McCarthy weather station (3SW) averaged over the years 1999-2000, the graph shows an average of 0.01 to 0.02 inches/day (0.02 to 0.05 cm/day) of evaporation depending on dew point temperature and wind speed. If we apply these evaporation values to the maximum surface area of Hidden Creek Lake (1.0 $km^2$), the volume of evaporated water over a 30-day period would be 6,000 to 15,000 $m^3$. Therefore, compared to the magnitude of the other water balance terms, evaporation is considered to be an insignificant component.

*Glacier Runoff*

Three factors control the routing of water on the surface of the glacier: surface slope, englacial pathways, and the presence of a subglacial or englacial drainage divide. The surface slope of the ice dam would be the primary control if the water stayed on the surface. However, the ice-dam is highly crevassed and the water enters the body of the glacier after relatively short path lengths. More probable is the presence of a subglacial drainage divide located near the ice dam, analogous to Nye's (1976) analysis. The divide separates drainage pathways hydraulically connected to

the lake and pathways associated with the glacier's main drainage network. The routing of water through englacial conduits must also be considered. The approximate area over which surface water from the glacier drains to the lake is determined by the position of the subglacial drainage divide and the routing of water from the surface via englacial conduits. We determined the position of the drainage divide by calculating the hydraulic bed potential, using water level from boreholes drilled in the ice, and by estimating the flow by englacial pathways.

*Hydraulic bed potential*

Subglacial water will tend to flow perpendicular to equipotential contours at the bed. The potential ($F$) in units of pressure can be calculated:

$$F = r_w gB + r_i g(H - B) \quad (3.5)$$

(Shreve, 1972), where $r_w$ and $r_i$ represent the density of water and ice (1000 kg/m$^3$ and 910 kg/m$^3$ respectively), $B$ is the elevation of the bed, $g$ is the gravitational acceleration (9.81 m/s$^2$) and $H$ is the elevation of the ice surface. The following equation can be used to calculate the hydraulic potential in terms of head ($Q$):

$$Q = B + 0.91(H - B) \quad (3.6)$$

In equations 3.5 and 3.6, the value for ice density is assumed to be for pure ice. The effect of crevasses, which may influence the effective density, is not considered. Although the effect of crevasses may be an important factor, it is difficult to quantify. To assess the thickness of the glacier, we used ice radar surveys conducted by Andrew Malm (St. Olaf College), the methods for which are explained in the next chapter. A

triangulated irregular network (TIN) was applied to the potential data and contoured to produce the equipotentials (Figure 3.11)

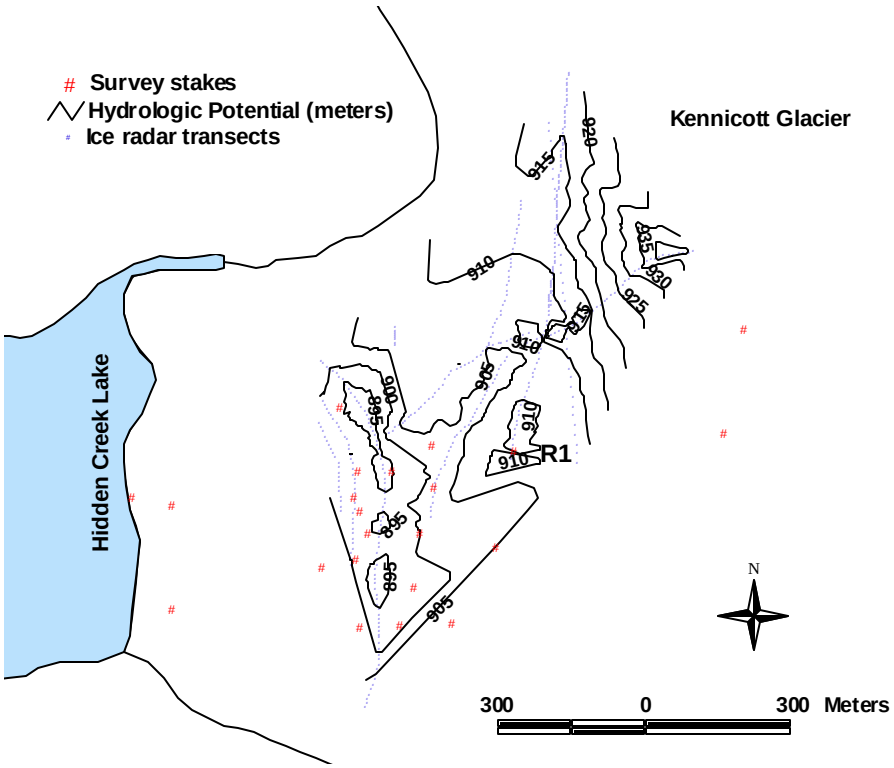


Figure 3.11. Equipotential contour lines at the bed of the glacier in meters.

Although our ice radar surveys do not cover the entire ice dam area, the data available are useful. In particular, where the bed potential reaches a local maximum, it is assumed that an internal drainage divide must exist that separates water flowing into the lake from water entering the glacier's main drainage system.

The two far target (BL1 and MLN) exhibited very little vertical displacements upward in response to lake rise, thereby indicating that they are not hydraulically

connected to the lake and lie eastward of the drainage divide. Based on this circumstantial information the drainage divide was interpreted to be located west of targets BL1 and MLN despite the lack of equipotential contours to the west of these two data points. The borehole water levels will be used later in this chapter to substantiate this interpretation.

One source of error in using the radar data for this interpretation is that if any water is stored beneath the glacier, the radar will be reflected at the bottom of the glacier at the ice-water interface rather than at the valley bottom. We attributed an error of ± 5 to 15 m to normal ice radar operation. Depending on the location and the timing of the ice radar transects the bed potential contours may have an error of as much as 17 m closest to the lake and 0.5 m farthest from the lake attributed to the ice displacement survey data.

*Borehole transducers*

To supplement the interpretations from the bed potential map, the borehole water levels will be used to aid in locating the drainage divide. Water levels were monitored in boreholes in the ice dam during the 2000 observation period (Lindsey, 2003). Transducers were lowered into the holes and the water head recorded at 20 minute intervals. The debris concentration in the ice was large enough that the hot-water drill could not reach the bed of the glacier. However, the boreholes appeared to intersect englacial pathways. The location of the boreholes relative to the equipotential contours and survey stakes in 2000 are shown in Figure 3.12.

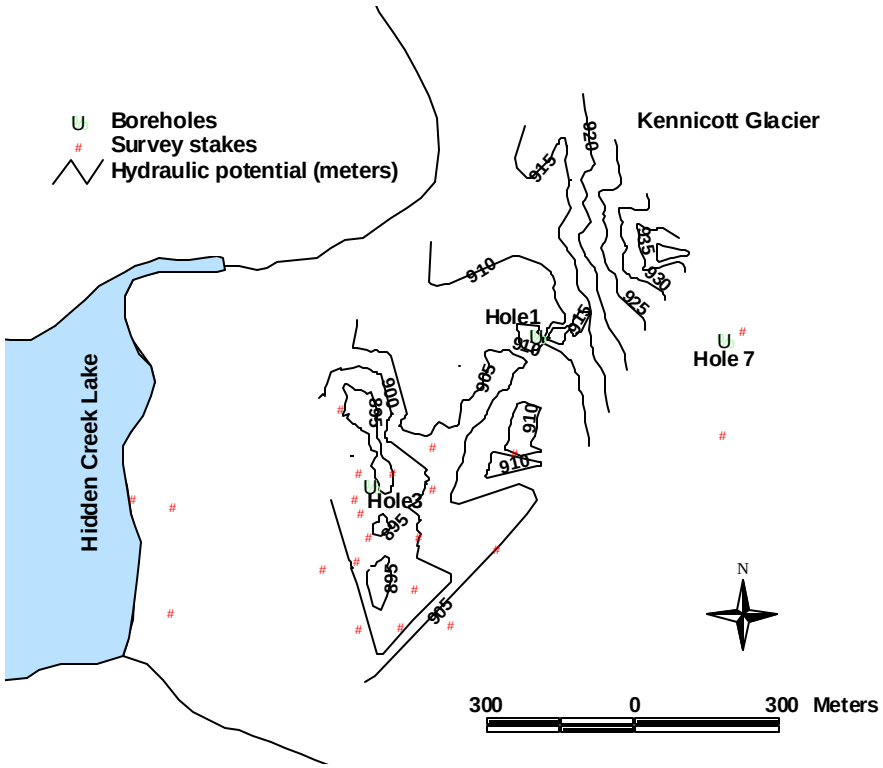


Figure 3.12 Location of boreholes relative to equipotential contours, ice radar transects, and survey stakes.

Borehole water levels, corrected for changes in ice-surface elevation, are plotted against the lake levels in Figure 3.13. Prior to JD 200, the water level in borehole 1 rose slightly during the lake filling period but remained relatively constant, while the water level in borehole 3 closely matched the lake stage. After JD 200, the water level in both boreholes 1 and 3 tracked the lake stage closely and fell in unison with the lake level during the flood. This indicates a direct hydraulic connection between the lake and englacial drainage system. In contrast, the water level in

borehole 7 fluctuated diurnally prior to and after the flood and did not appear to be hydraulically connected to the lake. After Julian Day 208, the water level began to fall in borehole 7, probably in response to lake drainage, but continued to have clear diurnal fluctuations. The data from these three boreholes suggests that the drainage divide separating the lake water from the glacier's main drainage system lies east of borehole 1 but west of borehole 7. After the drainage divide is breached and the flood begins, borehole 7 is then hydraulically responding to the lake drainage. This supports the conclusion obtained from the equipotential map that a drainage divide may exist west of target R1. The lack of data south of target R1 prevents us from determining the orientation of the drainage divide.

*Englacial drainage*

The englacial drainage system may capture and direct surface meltwater, in effect altering the effective size of the surface catchment area. Shreve (1972) argued that the englacial drainage system is a network of tree-like pattern of passages from the glacier surface to the bed. The pressure in the ice governs the direction of water flow and depends on the slope of the ice surface and the local bed topography (Shreve, 1972).

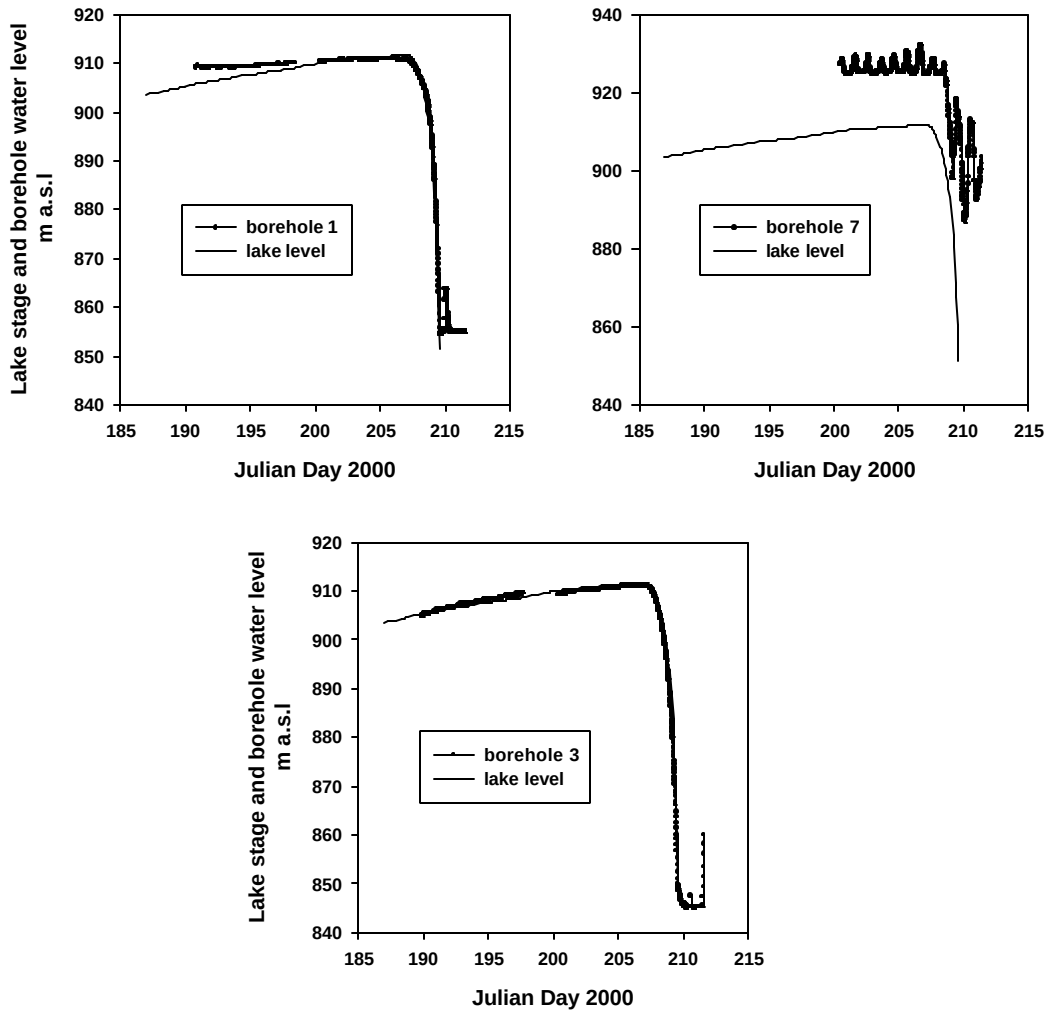


Figure 3.13 Water level above sea level in boreholes drilled into the ice compared to lake stage.

Drainage from the surface will flow perpendicular to the contours of equal potential, which slope at an average angle of:

$$a = arctan\left[\frac{r_i \left|grad\ H\right|}{(r_w - r_i)}\right] \quad (3.7)$$

where $H$ is the surface gradient, $r_w$ and $r_i$ represent the density of water and ice respectively. If we use the ice surface slope in the central part of the ice dam in 2000 and assume it is a plane, then H = 0.062 (3.5º) and α = 29º. Consequently, the englacial drainage should trend downslope at an angle of 61º from the horizontal. If we assume the drainage divide is located east of borehole 3 along the 910 m equipotential contour, we can use the local ice thickness, determined from the ice radar, to calculate the surface area east of the drainage divide (routing into the main glacier drainage system) using equation 3.7. This portion of the surface area is assumed to contribute water to the lake via englacial flow (Figure 3.14). The surface slope is small and may be assumed to be horizontal. The distance westward above the drainage divide is calculated (Shreve, 1972):

$$x = \frac{T_i}{tan(\frac{p}{2} - a)} \quad (3.8)$$

where $x$ is the distance from a point on the surface of the glacier that lies directly above the drainage divide. $T_i$ is the ice thickness and $a$ is the angle of the drainage paths with respect to horizontal. In the area of the estimated drainage divide, the ice thickness ranges from 300 to 350 m. Therefore, the distance on the surface eastward of the drainage divide providing water to the lake is about 200 m. The glacier surface area that provides recharge to the lake is about 0.9 $km^2$.

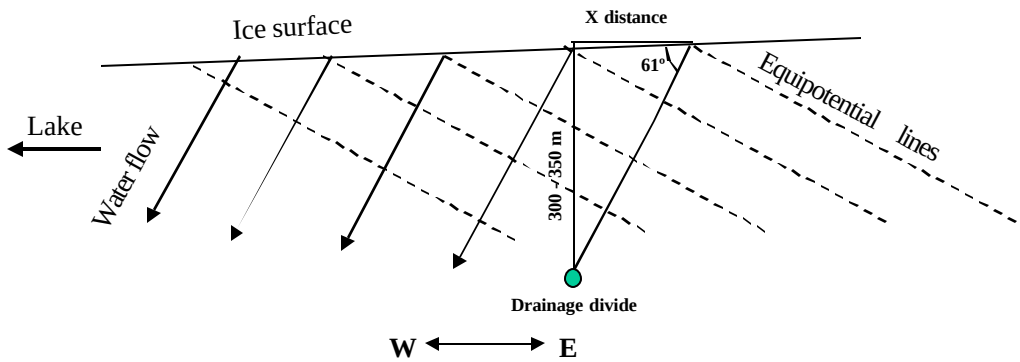


Figure 3.14 Diagram illustrating how surface water originating (x) distance away from the drainage divide will intersect the drainage divide at the bed.

*Precipitation and Ablation*

We had not initially planned to conduct a full water balance study during the summer of 2000 so we did not place a rain gauge near the lake or on the glacier. Instead we used the nearest weather station (McCarthy 3 SW) from the National Weather Service to estimate the amount of precipitation that fell during the field season in July 2000. The weather station is located approximately 15 km down glacier from the lake. The total precipitation over our observation period (July 5 – 24, 2000) was 28 mm. The drainage area was constrained by the topographic divides surrounding the lake basin and the ice dam area determined as previously described. The total area contributing rainfall to the lake including the glacier surface is about 7.1 $km^2 \pm 1.8\ km^2$, resulting in a volume of $0.20 \times 10^6\ m^3 \pm 0.05 \times 10^6\ m^3$ of precipitation input to the lake for the entire month of July.

Ablation was measured at each survey stake. A wood plug was inserted into each stake to prevent the survey poles from melting into the ice. The pole length exposed above the ice surface was noted at the time the poles were drilled and during the last survey of each day. Any increase in the length of exposed pole was revealed by an increase in the measured angle and attributed to ablation. Table 3.1 shows the total ablation during the pre-flood period, total ablation during the period of measure and daily average rate of ablation for each target. We were unable to obtain ablation measurements at stakes F6, F7, F4 and BL1. The total ablation is measured in meters water equivalent and an average total ablation for all the targets was used. The average ablation (1.31 m) during the pre-flood period of measurement is converted to water equivalent by multiplying by the ratio of ice density (900 kg/m$^3$) to water density (1000 kg/m$^3$) resulting in an ablation of 1.18 meters water equivalent (weq). The average ablation is then applied over the total glacier area that drains into the lake (0.9 km$^2$), resulting in an approximate total water volume input to the lake from ablation of $1.1 \times 10^6$ m$^3 \pm 0.3 \times 10^6$.

Table 3.1 Total ablation during the pre-flood period, total ablation for the entire period, and the daily average average rate of ablation for each target.

| Target | ablation mweq (preflood) | ablation rate preflood (mweq/day) | ablation mweq (total period) | ablation rate total period (mweq/day) |
|---|---|---|---|---|
| LL1 | 0.96 | 0.05 | 1.22 | 0.05 |
| Rx | 1.07 | 0.05 | 1.29 | 0.06 |
| C2 | 1.13 | 0.06 | 1.53 | 0.07 |
| D1 | 1.16 | 0.06 | 1.40 | 0.06 |
| M1 | 1.28 | 0.07 | 1.52 | 0.07 |
| C1 | 1.25 | 0.06 | 1.56 | 0.07 |
| M2 | 1.20 | 0.06 | 1.39 | 0.06 |
| M3 | 1.19 | 0.06 | 1.41 | 0.06 |
| M6 | 1.06 | 0.05 | 1.24 | 0.05 |
| M4 | 1.24 | 0.06 | 1.46 | 0.06 |
| M5 | 1.34 | 0.07 | 1.59 | 0.07 |
| R3 | 1.38 | 0.07 | 1.57 | 0.07 |
| R2 | 1.53 | 0.08 | 1.82 | 0.08 |
| R1 | 0.88 | 0.04 | 1.06 | 0.05 |
| MLN | 0.98 | 0.05 | 1.13 | 0.05 |
| avg: | 1.18 | 0.06 | 1.41 | 0.06 |

*Water balance summary*

The change in storage is calculated using Equation 2.6 and results in an estimated storage volume of $7.3 \times 10^6$ $m^3 \pm 1.2 \times 10^6$ $m^3$. The values used for each factor used in the equation are shown in Table 3.2. Based on the lake hypsometry, the accumulated volume of lake water during the pre-flood period is $6 \times 10^6$ $m^3 \pm 6 \times 10^4$ $m^3$. Thus, a volume of water 1.3 million $m^3 \pm$ 1.2 million $m^3$ accounts for a change in storage of water from the lake.

Table 3.2 The values of each factor used in the water balance calculation.

| Factor | Water Volume ($x\ 10^6\ m^3$) | Possible Error ($x\ 10^6\ m^3$) |
|---|---|---|
| Precipitation | 0.2 | 0.05 |
| Ablation | 1.1 | 0.3 |
| $V_{HC}$ | 6 | 1.2 |

## 3.5 Discussion

*Water balance*

The water balance in the HCL basin reveals that approximately $2 \times 10^6\ m^3 \pm 1 \times 10^6\ m^3$ of water was lost from the lake. Displacement of water by icebergs that become grounded was ignored and may be a significant cause of change in lake level, and thus a significant source of error in the present calculation. Kasper's (1989) water balance study of an ice-dammed lake adjacent to the Kaskawulsh Glacier also revealed a loss of water from the lake prior to the flood. Kasper (1989) also states that her water balance may include $1 \times 10^6\ m^3$ of water stored beneath the dam. It is difficult to make a direct comparison between the Kaskawulsh and HCL water balance studies because the errors in the Kaskawulsh water balance components were not quantified and are likely as large as those determined from the HCL water balance components.

## 3.6 Summary and Conclusions

Two upstream boundary conditions on the flood were quantified, the changing pressure head at the lake and the water flux. These boundary conditions are critical in

determining the response of the ice dam to changing lake levels, which help to better understand the triggering mechanisms behind outburst floods (Chapter 4). When combined with the water balance results, the outflow hydrograph from the glacier (Kennicott River) is useful to study the evolution of the glacier's drainage system during the flood (Kraal, 2001).

The quantification of lake stage data is presented here but its primary use will be in Chapter 4, where it is compared to the ice dam deformation. The lake reached a higher stage (911.68 m) in 2000 and had a greater volume ($28 \times 10^6$ $m^3 \pm 3 \times 10^5$ $m^3$) than it did in 1999 with a stage of 902.49 m and a volume of $21 \times 10^6$ $m^3 \pm 2 \times 10^5$ $m^3$. However, the maximum rate of lake level drop was greater (175 m/s) in 1999 than in 2000 (70 m/s). The peak flood discharge from HCL was 323 $m^3$/s in 2000 but is unknown in 1999. For comparison, the flood volume measured at the Kennicott River in 2000 was approximately $38 \times 10^6$ $m^3$ with a peak discharge of 470 $m^3$/s (S. Anderson, pers. comm., 2000).

An estimate of the full water balance revealed that $2 \times 10^6$ $m^3 \pm 1 \times 10^6 m^3$ of water was lost from the lake. However, the water balance equations is subject to large errors. Chapter 4 addresses the issue of water storage using another type of measurement, displacement of ice adjacent to the lake.

# CHAPTER 4

# ICE DAM DISPLACEMENTS

## 4.1 Introduction

Understanding how an ice dam deforms in response to changes in lake level can provide insight into the fundamental mechanisms governing the storage and release of impounded water. To evaluate the ice dam mechanics, surface displacements of the ice were measured by theodolite survey. In addition, a qualitative record of ice motion was recorded using a time lapse camera placed on the lakeshore.

## 4.2 Methods

*Survey methods*

The surveying was planned and implemented with Dennis Trabant from the United States Geological Survey in Fairbanks, Alaska. For the 1999 and 2000 field seasons, a Wild Heerbrug theodolite and electronic distance meter (EDM) was used. The North American Datum of 1983 (NAD83) was used as the horizontal datum and the National Geodetic Vertical Datum of 1929 (NGVD29) for the vertical datum. The survey data was georeferenced into Universal Transverse Mercator (UTM) coordinates by placing a GPS (global positioning system) unit beneath the survey station and referencing it to a GPS base station positioned on a USGS benchmark located near the town of McCarthy, Alaska.

Each survey stake consisted of a corner reflector attached to the top end of electrical conduit 3.0 m in length. The poles were drilled into the ice to a depth of about 2 m using a hand auger. A wood plug was hammered into the ice end of the pole to reduce the melt rate of the poles into the ice. Details of the surveying techniques and accuracy of the measurements are discussed in Appendix B1.

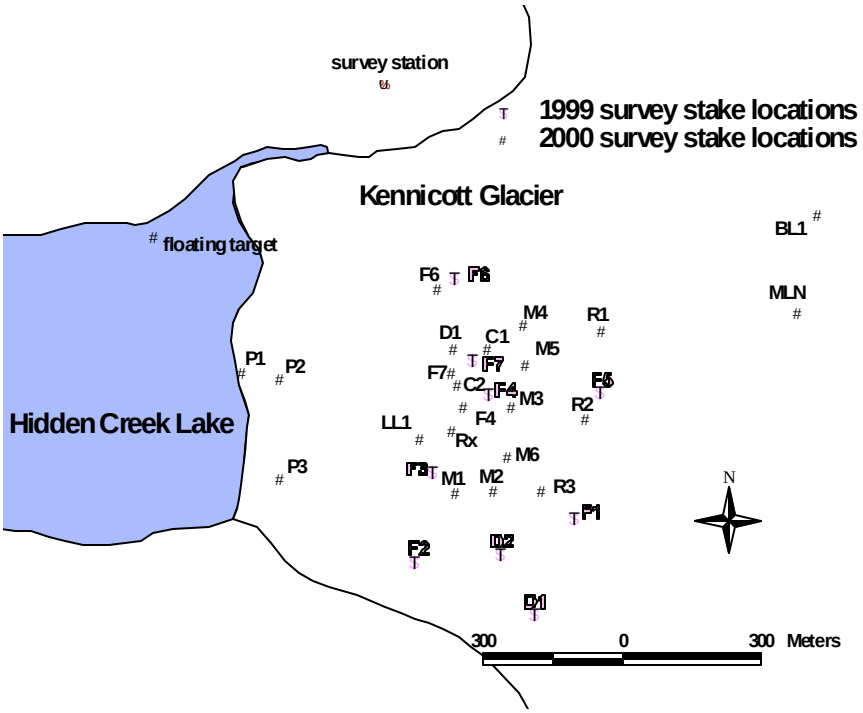


Figure 4.1 Map of the ice-dam and HCL showing the locations of the survey markers and survey station for the 1999 and 2000 field seasons.

In 1999 we managed to place 9 survey stakes on the ice dam but only measured surface displacements as the lake drained. Surveys were conducted at two-

hour intervals from Julian Day 196 (July 15, 1999) to Julian Day 201 (July 20, 1999). The distribution of survey markers extended from about 400 m to 700 m from the lake (Figure 4.1).

During the 2000 field season we placed a total of 22 survey reflectors on the ice dam and captured both the rise and drop of the ice prior to and during the flood. With helicopter support we were able to place reflectors near the edge of the ice dam. Due to the likelihood of losing those targets nearest the lake (P1, P2, and P3) we used three 0.7 m squares of retro-reflective road sign material instead of traditional and more expensive reflectors. Surveys were conducted at 4-hour intervals from 8:00 am to 8:00 pm until Julian Day 192 (July 10, 2000) when the interval was decreased to 2 hours. The distribution of survey markers extended from the ice front to about 1.0 km from the lake (Figure4.1).

*Time Lapse Camera*

During the 1999 and 2000 field seasons a 35 mm time-lapse camera with a wide-angle lens was placed in a watertight metal barrel with a glass cover on one end. The barrel was positioned on the north hillslope overlooking the lake and ice dam (Figure4.2). Photographs were taken at 4-hour intervals but the interval was decreased to 2-hour intervals closer to the time of the outburst. The photographs were made into two separate videos to illustrate the movement of the ice dam and lake with time. The videos for both years can be viewed by visiting the following website:

http://www.geol.pdx.edu/Glaciers/kennicott. Comparison of photos prior to the flood and after the flood (Figure 4.3) reveals the magnitude of ice dam displacement.

Figure 4.2 Photograph showing the barrel that holds the time lapse camera pointed directly at the ice dam. Note the copious amount of ice debris that collects in the basin after the flood.

Figure 4.3 Photographs of the ice-dam A) before and B) after lake drainage. The ice dam is approximately 900 m wide.

*Ice radar*

Ice penetrating radar was used to determine ice thickness and subglacial bed topography. The radar fieldwork and processing was performed by Andrew Malm under the guidance of Dr. Robert Jacobel, St. Olaf College. Ice radar transmits pulses of microwaves into the ice through an antenna laid on the ice surface. The transmitted energy reflects from the bed (or features in the ice) and is received by another antenna. The travel time between transmitted and received waveform divided by the wave's velocity in ice determines the distance traveled using two-way travel time. Waveforms were recorded at discrete points every 10 m along straight line transects. Although point measurements make it difficult to distinguish between the high energy scatter returns caused by englacial voids and the weaker subglacial bed returns (Fountain and Jacobel, 1997), continuous radar profiling was not feasible due to rough ice and debris on the surface. Andrew Malm (St. Olaf College) processed the ice radar profiles using a procedure called migration to transform the data recorded at the surface into the correct positions in the subsurface (Telford et al., 1990). In this case the raw data were processed by migrating the data two dimensionally then filtered with a bandpass filter ranging from 4 – 10 MHz. Two processed radar profiles are shown in Figure 4.4.

The radar returned stacked 256 measurements at each point to improve the signal to noise ratio. Depending on the need, either a 5 MHz or 10 MHz resistively damped antenna with a pulsed transmitter was used. Higher frequencies yield increased scatter (noise) when englacial water-filled voids are present (Watts and England, 1976). Although a 5 – 10 MHz centered wave has a lower resolution than

higher frequency antennae, the lower frequencies are necessary for penetrating large depths. The transmitting and receiving antennae were separated at their centers by a distance of 60 m. A 222A Tektronix 100 MHz digital oscilloscope was used as the waveform recorder. The waveforms were transferred to a laptop computer for storage. The positions of the radar transects on the glacier surface were constrained by surveying to a handheld reflector approximately every 50 meters. A piece-wise linear interpolation of the surveyed radar transect positions was applied between each 50 meter reading.

We were able to complete more radar measurements during the 2000 field season than during the 1999 field season. All of the (1999 & 2000) ice penetrating radar transect positions on the ice dam are shown in Figure 4.5. The radar transect locations were limited by crevasses which increase in number and size as one moves closer to the lake, making travel difficult. The average estimated error associated with the ice radar returns varies across the glacier. Near the middle of the glacier, where bed returns are not influenced by edge effects of the valley walls, the error is estimated to be ± 5 m. Towards the sides of the glacier the error is estimated to be ± 10 m. In places where the bed return was weak and difficult to discern, but was not discounted, a maximum error of ± 15 m is suggested by A. Malm (2000, pers. comm.)

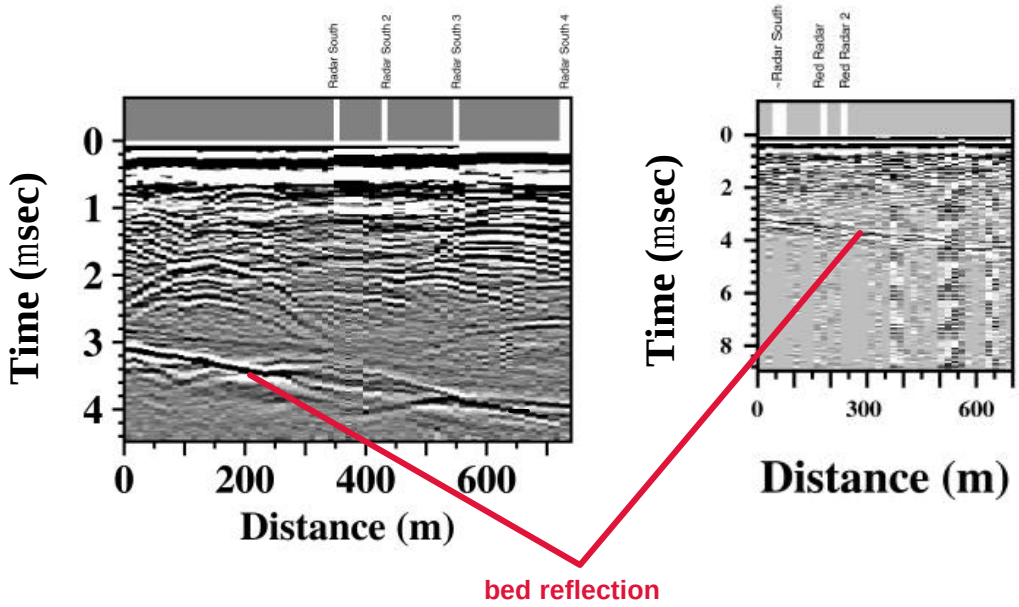


Figure 4.4 Example of two ice radar profiles after migration. Time is two-way travel time.

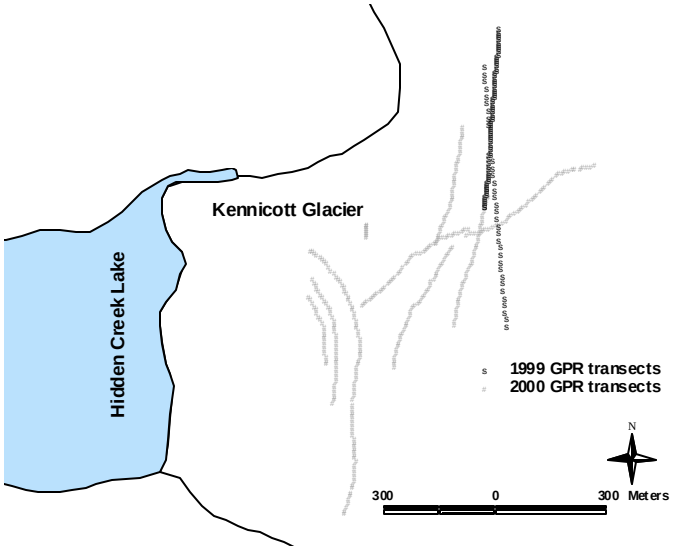


Figure 4.5 Location of ice penetrating radar transects conducted during the 1999 and 2000 field season.

*Crevasse mapping*

Crevasse orientations and lengths were mapped prior to the flood to infer the stress distribution in the ice dam. Transects across the glacier were conducted using a Brunton compass to mark the orientation of crevasses. The center location of the crevasses was determined by using a handheld GPS unit while the lengths of the crevasses were estimated. Much of the ice dam is not accessible by foot due to large crevasses so photographs taken from a helicopter and from the survey site were used in conjunction with field mapping.

## 4.3 Ice Dam Results

*Vertical Displacements*

Vertical displacement of the ice surface has two components, that due to normal glacier flow and that related to the lake and it's drainage. Thus, to accurately analyze the ice dam deformation it is necessary to remove the vertical displacement resulting from normal glacier flow from the measured vertical displacements. Mathematically, this is expressed:

$$Dh_z = Dh_s + Dh_v \qquad (4.1)$$

where $Dh_z$ represents the total measured vertical displacement from the survey data, $Dh_s$ is the component of vertical displacement attributed to bed-parallel ice flow, and $Dh_v$ is the component of vertical displacement attributed to changes in lake level. In this analysis, we are assuming a steady state shape and the absence of ablation. It is likely that the latter assumption is trivial over the time span of our measurements.

However, the assumption of a steady state shape could be inaccurate over the same time span. The component $Dh_s$ can be defined by:

$$D\,h_s = \frac{\partial h}{\partial N} dN + \frac{\partial h}{\partial E} dE \quad (4.2)$$

where $Dh_s$ is the change in the vertical component associated with gross glacier flow, the terms ¶ *h/¶N and ¶h/¶E* represent the average surface slope of the ice dam while *dE* and *dN* represent the incremental changes in the easting and northing direction. This equation follows from the basic principle that particles of ice stay at the surface, moving up or down the surface slope as they advect downstream. Therefore, with a constant reference surface, we can estimate the vertical displacement at a point on the glacier that is attributed to glacier flow. Any deviation away from this reference frame is then likely associated with filling and drainage of the lake. An average surface slope was defined from the survey targets using the first time period of measurements for both years, Equation 4.2 is modified to define the reference plane:

$$Dh_s = h_0 + \frac{\partial h_0}{\partial N} dN + \frac{\partial h_0}{\partial E} dE \quad (4.3)$$

where, $h_0$ is the initial elevation for each target at the beginning of the survey measurements for each year, ¶ $h_0$/¶*N and* ¶$h_0$/¶*E* represent the average surface slope of the ice dam at $t_0$ , which is the time at $h_0$ or the start of each year's field measurements. *dE* and *dN* represent the incremental changes in the easting and northing direction for each target. The assumption is made that the glacier slope is constant in time and that

the observed displacement is a combination of movement down the slope and changes in elevation of the ice surface itself.

The average surface slope was estimated using the elevation of the survey targets at the beginning of our measurements. Defining an average surface slope was difficult because the data are irregularly spaced. The 1999 reference plane was defined by fitting a smooth surface via a triangulated irregular network (TIN) to the 8 survey targets shown in Figure 4.1. The resulting surface was nearly a plane with a slope of 0.070 in the northwest direction and a strike of S10ºW. The apparent dip is 0.069 to the west and 0.012 to the south. Figure 4.5 shows the adjusted cumulative vertical displacements for the 1999 survey targets during the flood period. Target F2 was excluded from further analysis because the data contained large errors derived from a problem with the reflector.

The slope of the ice dam in 2000 is more complex than in 1999, mainly because we had more survey targets and have more information on the nature of the deformation. The large number of survey targets in 2000, were divided into four groups based on similarities in total vertical displacement characteristics (Figure 4.7). The cluster of survey targets in groups 2 and 3 were used to define the reference plane. Group 1 was not used because it only contained three targets. Group 4 is located farthest from the lake, in a region that was not considered part of the ice dam as described later. The slope of the fitted surface slopes 0.062 in a northwest direction and strikes S10ºW. This results in a slope that is 0.061 to the west and 0.011 to the south, which is similar to the 1999 slope results.

The group 4 targets are used to define the reference plane after JD 196. Prior to JD 196, the negative (downward) vertical displacements of the two targets from group 4 are small and are consistent with normal glacier flow downslope. After JD 196 the group 4 targets began to experience small positive (upward) vertical displacements. The mean rate of motion for the group 4 targets prior to JD 196, 0.015 m/day, can be used to define the reference plane after JD 196 by assuming that the cluster of targets would have continued moving along a surface of constant slope, were it not for other glaciological events:

$$H(r) = h_0 - (0.015\ m/day)(?t) \qquad (4.4)$$

Where $H(r)$ defines the reference elevation at time $t$, $h_0$ is the initial reference elevation, and $?t$ is the time interval. Figure 4.8 shows the adjusted cumulative vertical displacements for the 2000 targets prior to and during the flood. The sign convention is (+) for uplift and (-) for downdrop of the ice.

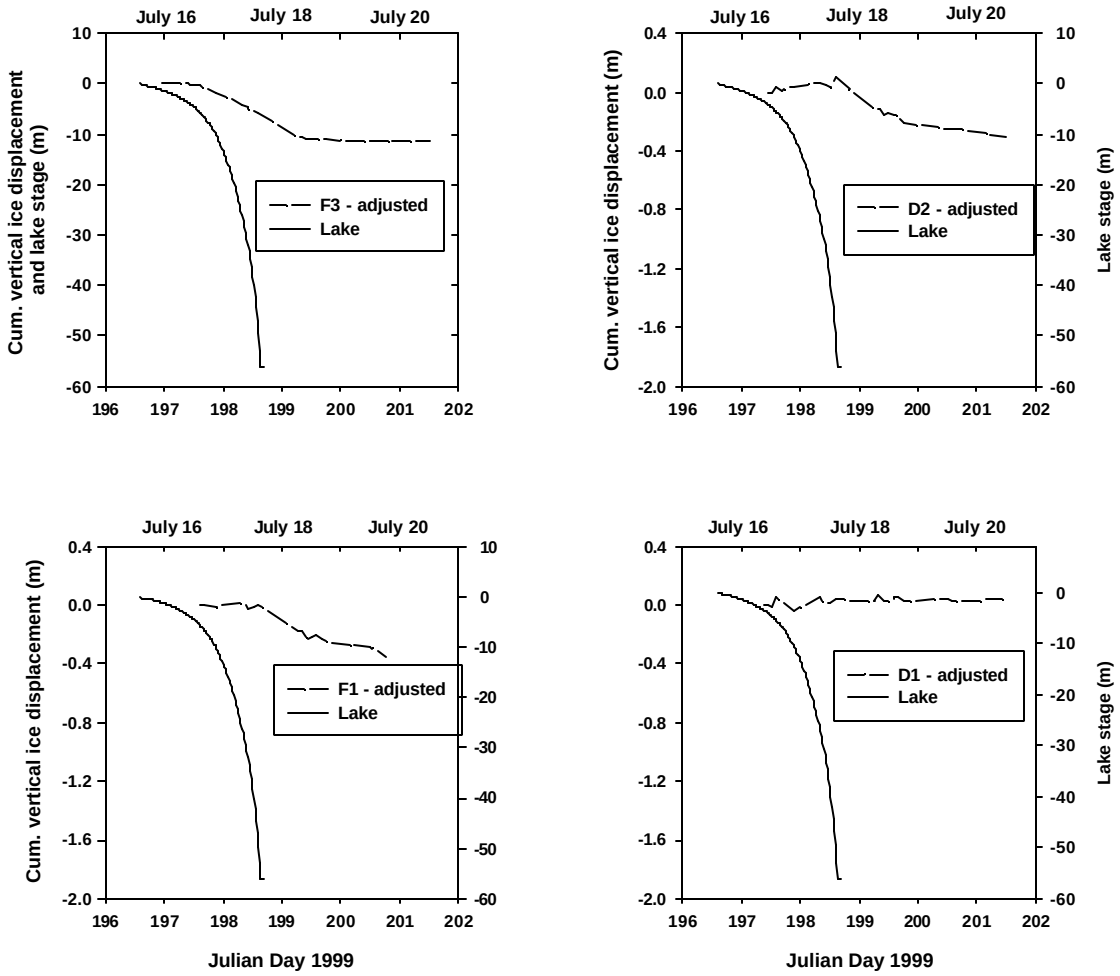


Figure 4.6 Cumulative vertical displacements of the 1999 survey targets after they have been adjusted to remove the amount of displacement due to gross glacier flow. Notice the different scale for the graph of target F3.

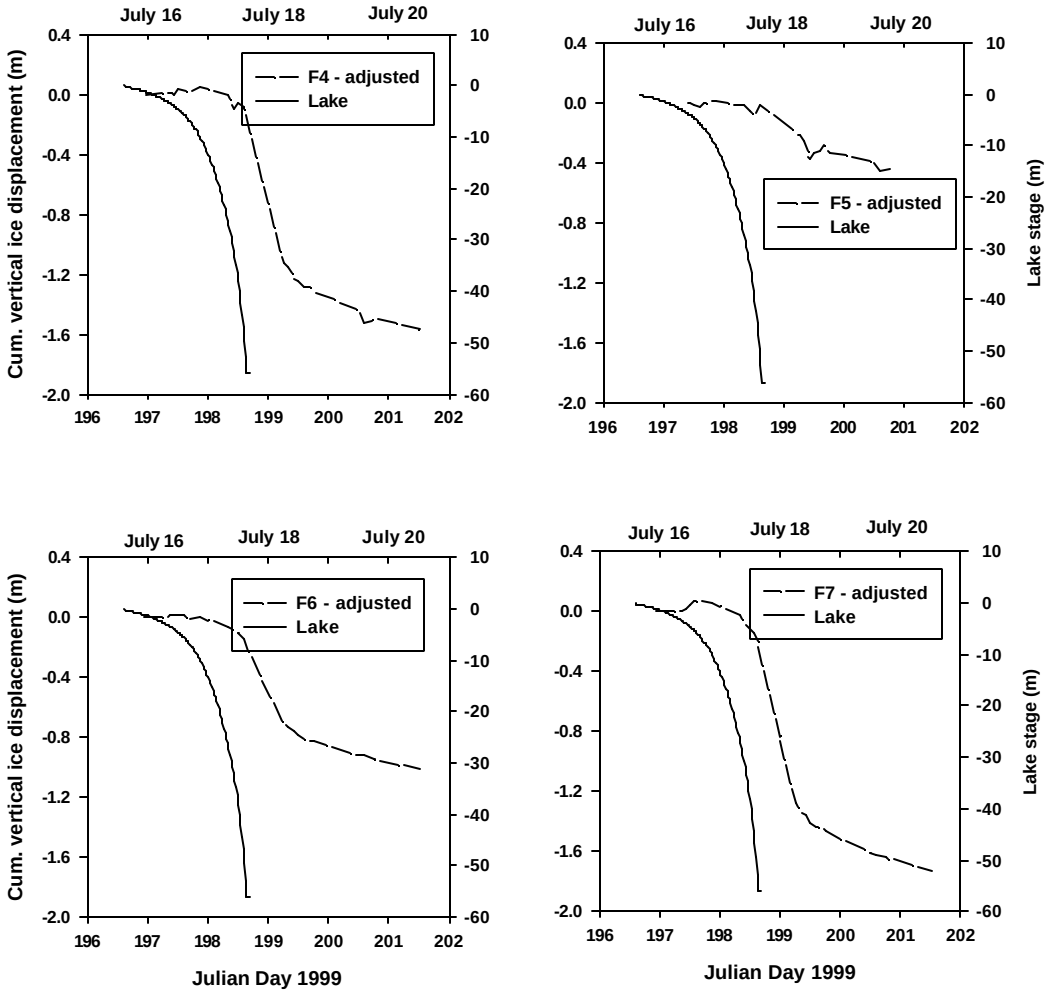


Figure 4.6 cont. Cumulative vertical displacements of the 1999 survey targets after they have been adjusted to remove the amount of displacement due to gross glacier flow.

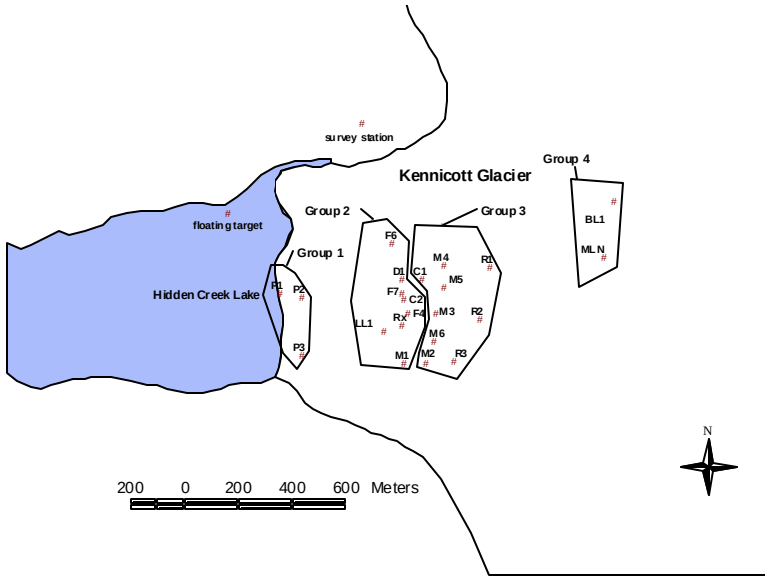


Figure 4.7 Location map of survey stakes for the 2000 field season. The boxes indicate the four different groupings of targets based on vertical displacement behavior.

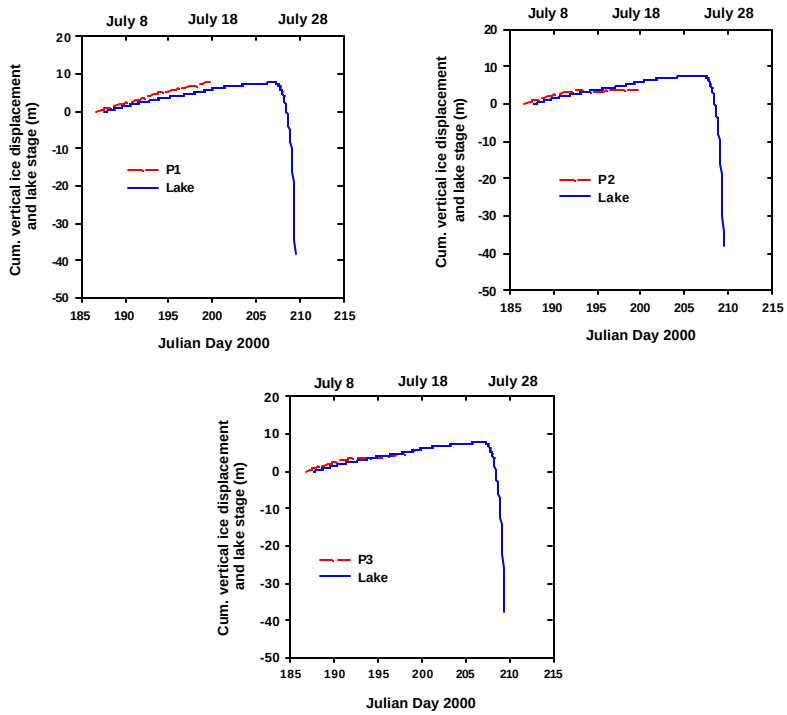


Figure 4.8 (a) Cumulative vertical displacements of targets in group 1 from the raw survey data.

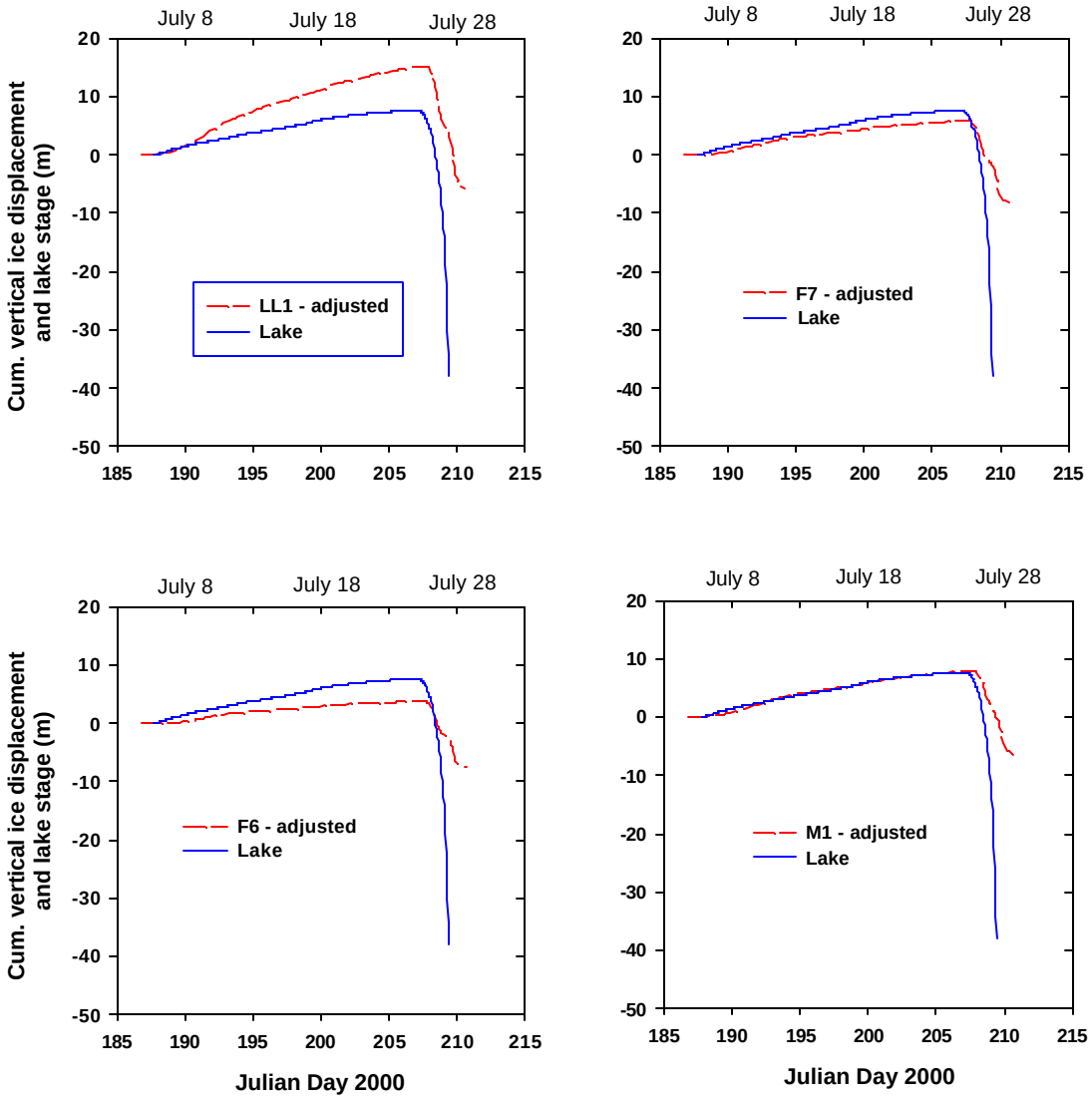


Figure 4.8 (b) Cumulative vertical displacements of targets in group 2 after they have been adjusted to remove the displacement due to gross glacier flow.

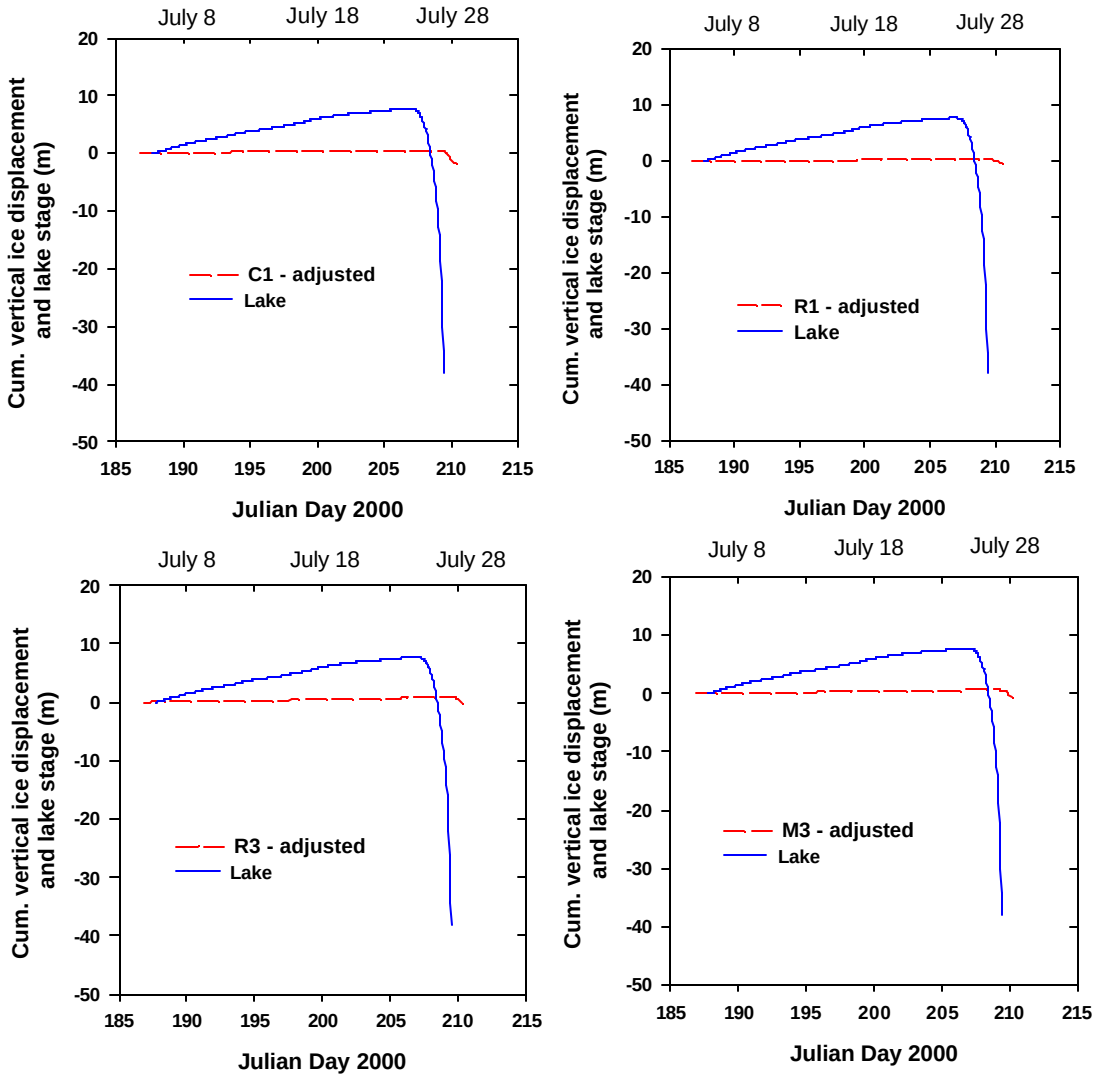


Figure 4.8 (c) Cumulative vertical displacements of targets in group 3 after they have been adjusted to remove the displacement due to gross glacier flow.

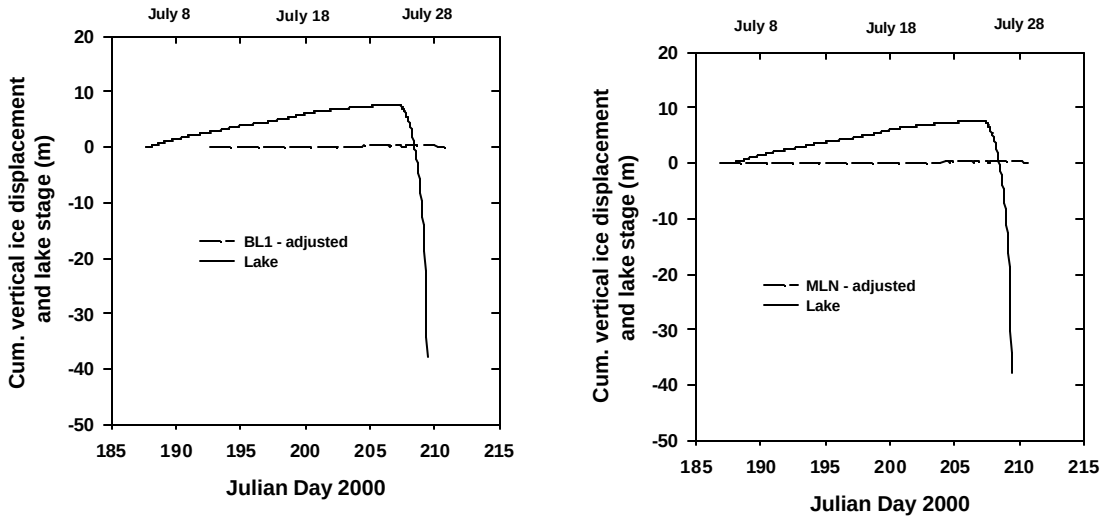


Figure 4.8 (d) Cumulative vertical displacements of targets in group 4 after they have been adjusted to remove the displacement due to gross glacier flow.

The vertical displacements measured at each target with the two components associated with changes in lake stage and gross glacier flow are reported in Table 4.1. For both years, the displacements associated with changes in lake level are much larger than those associated with gross glacier flow, particularly for those targets located nearest the lake. Figure 4.9 provides a comparison of the magnitude of vertical displacements from target C2 over the complete 2000 observation interval. For reference, C2 is located about 500 m from the lake and about mid-way between the valley walls.

Table 4.1 Table showing the total measured vertical displacements and the components due to changes in lake level and to gross glacier flow.

| 1999 | | | | 2000 | | | |
|---|---|---|---|---|---|---|---|
| target | measured vert. | vertical D lake stage | vertical gross | target | measured vert. displ. | vertical D lake | vertical gross |
| D1 | 0.06 | 0.05 | 0.01 | LL1 | -25.47 | -21.45 | -4.02 |
| D2 | -0.39 | -0.31 | -0.08 | F6 | -13.48 | -11.53 | -1.95 |
| F1 | -0.39 | -0.35 | -0.04 | Rx | -18.38 | -15.61 | -2.77 |
| F3 | -12.32 | -11.48 | -0.84 | F7 | -16.93 | -14.43 | -2.50 |
| F4 | -1.89 | -1.57 | -0.32 | C2 | -15.97 | -13.56 | -2.41 |
| F5 | -0.5 | -0.44 | -0.06 | F4 | -15.46 | -13.21 | -2.25 |
| F6 | -1.05 | -1.01 | -0.04 | D1 | -14.71 | -12.56 | -2.15 |
| F7 | -2.02 | -1.73 | -0.29 | M1 | -17.12 | -14.7 | -2.42 |
| | | | | C1 | -1.45 | -2.69 | -1.24 |
| | | | | M2 | -3.76 | -3.68 | -0.08 |
| | | | | M3 | -1.93 | -1.88 | -0.05 |
| | | | | M6 | -2.14 | -2.45 | -0.31 |
| | | | | M4 | -1.08 | -1.07 | -0.01 |
| | | | | M5 | -1.27 | -1.34 | -0.07 |
| | | | | R3 | -1.13 | -1.41 | -0.28 |
| | | | | R2 | -1.23 | -1.23 | -0.00 |
| | | | | R1 | -0.71 | -0.73 | -0.02 |
| | | | | MLN | -0.36 | -0.26 | -0.10 |
| | | | | BL1 | -0.30 | -0.18 | -0.12 |

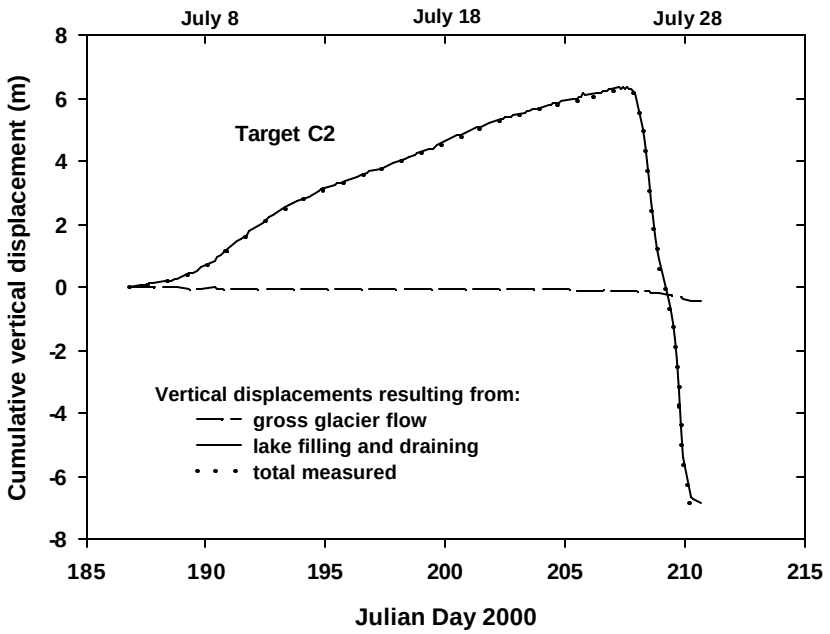


Figure 4.9 Example of the cumulative vertical displacements measured at target C2 and its components associated with changes in lake level and gross glacier flow along a reference plane.

*Crevasse orientations*

Two major crevasse types are seen at the glacier surface prior to the flood (Figure 4.10): (1) Large, straight crevasses, within a domain that extends from the front of the ice dam to approximately 200 m from the lake with a N-S orientation. (2) Arcuate crevasses, with a domain that extends approximately 200 - 300 m from the lake back to the main body of the glacier, with a N-S orientation. A very large crevasse separates the two sets of major crevasses and appeared to be filled with water both years. Secondary crevasses include longitudinal crevasses that run roughly parallel to the flow of the ice dam into the lake and nearly perpendicular to the ice/lake interface with a primary orientation of N55ºE - N65ºE (Figure 4.11). The longitudinal

crevasses appeared to increase in number and size during the lake filling period indicating that their growth is associated with rising lake stage. The longitudinal crevasses may also be indicative of a “bowing” or arching of the ice dam. Bowing of the ice dam could occur if it remained coupled to the valley walls while simultaneously being lifted by the rising lake level. No conclusive evidence in the survey data suggests that the central portion of the ice dam was rising faster with little vertical displacement at the sides. While there is no obvious gradient in the measured displacements, the lack of survey points close to the margins makes it difficult to make a conclusive statement regarding bowing of the dam.

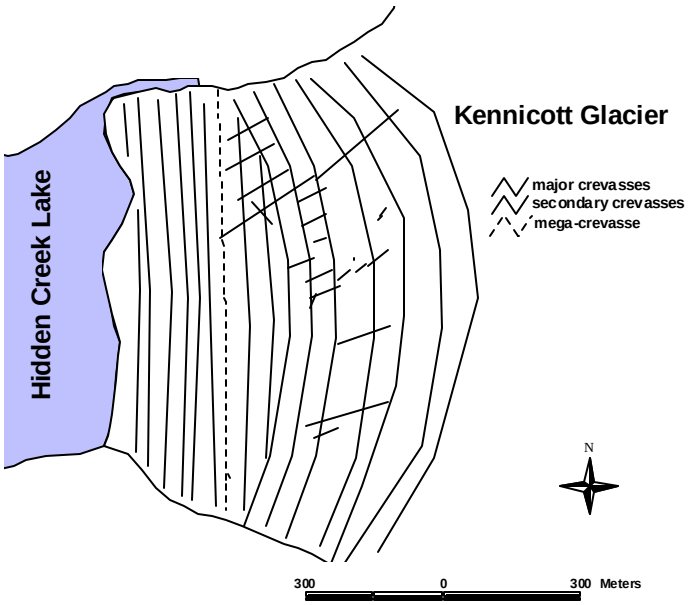


Figure 4.10 Map of the ice dam showing the major and secondary crevasse features.

Figure 4.11 Photographs of two of the same longitudinal crevasses on the ice dam that were forming and enlarging during the lake rise period. The photo on the left was taken on July 8, 2000 when the average crevasse width was 10 cm. The photo on the right was taken on July 15, 2000 when the average crevasse width was 46 cm.

*Horizontal displacements*

Horizontal displacements are plotted incrementally with time for each field season. In addition, total horizontal vector plots exhibiting displacement prior to the flood and during/after the flood are included.

Figure 4.12 shows the horizontal ice dam displacements for a subset of the 1999 survey targets for the period after the lake began to drain. Figure 4.13 shows the horizontal vector motion of the targets during the flood period. The pre-flood data is missing due to the unfortunate timing of the flood. The magnitudes have been exaggerated 10x for clarity. The trajectories for targets F4, F5, and F6 were to the SW. The trajectory of target F3 was initially to the NW but shifted to the SW after just over a day. Target F3 is located near the center of the dam.

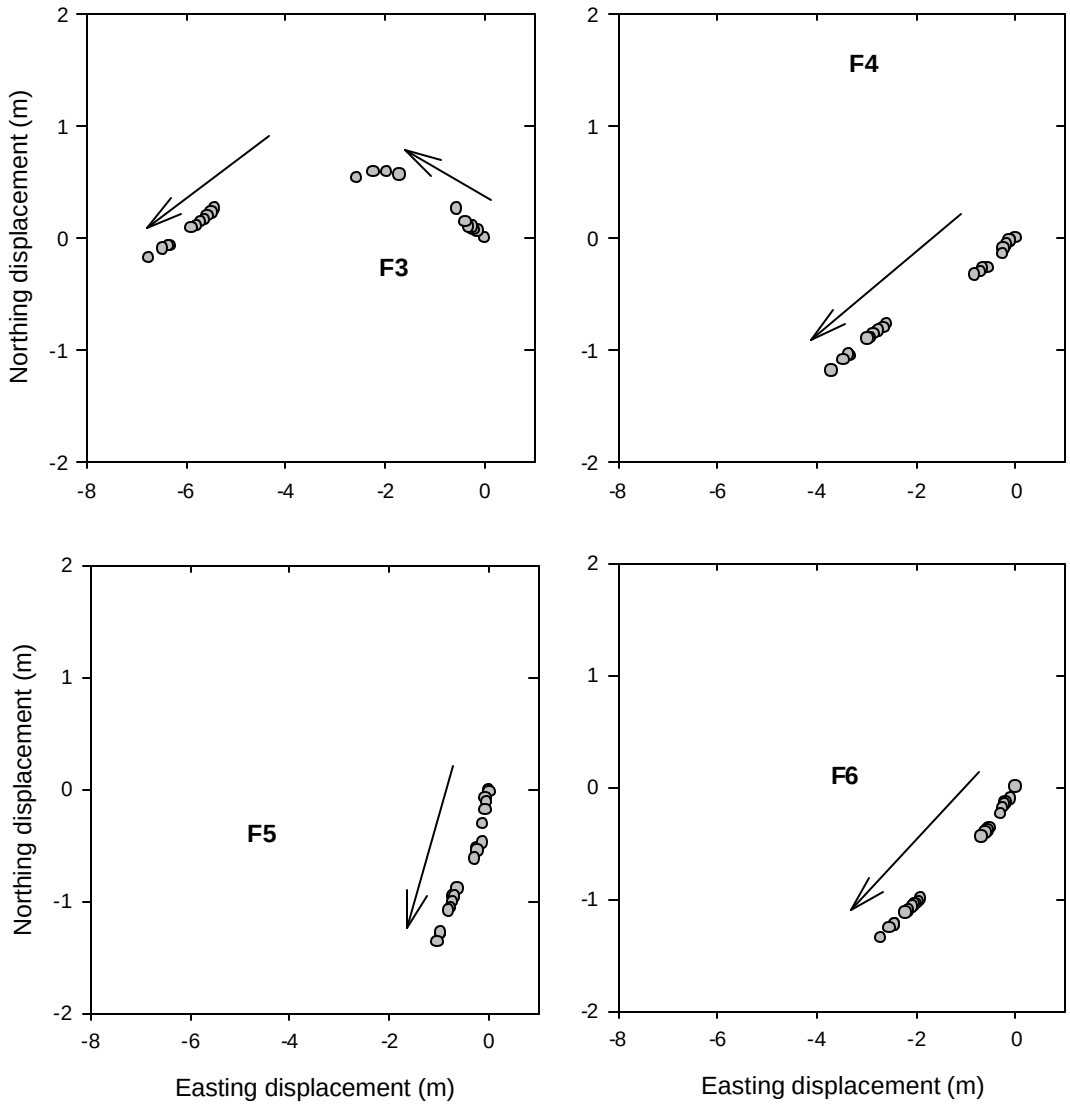


Figure. 4.12 Horizontal displacements for a subset of the 1999 survey targets during the flood period. The arrows indicate the direction of motion through time.

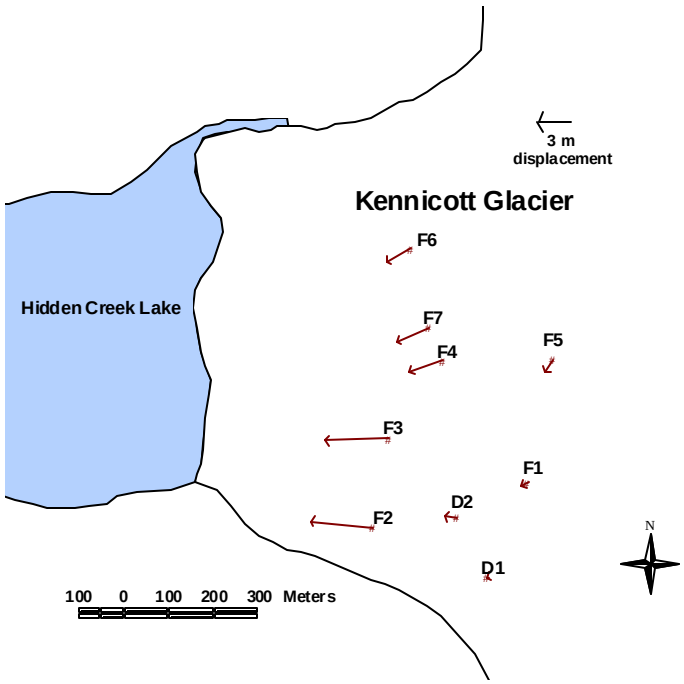


Figure 4.13 Horizontal vector displacements for all of the 1999 survey targets during the flood period. The magnitude has been increased 10 x.

A representative subset of the horizontal displacements measured during the 2000 field season are plotted in Figure 4.14. The horizontal vector plots are separated into pre-flood and during/post-flood periods (Figure 4.15). Prior to the flood, most of the trajectories were to the SW, exceptions were target F6, which had a trajectory to the NW and the two far targets, BL1 and MLN, which had trajectories to the south (Figures 4.12, 4.13). All of the targets (except BL1 and MLN) show a significant change in orientation towards the lake (west) after the lake has started to drain.

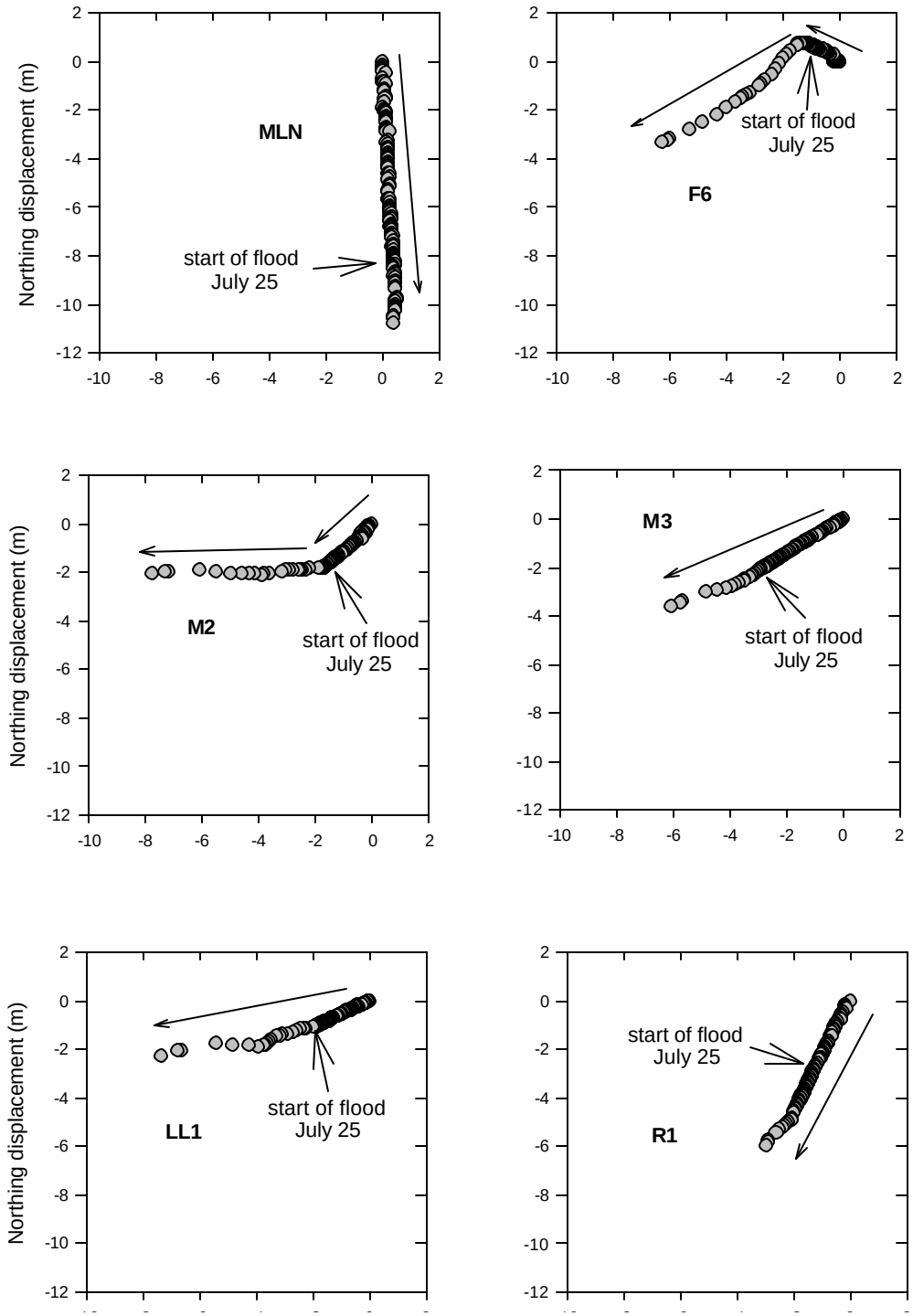


Figure 4.14 Horizontal displacements for a subset of representative targets from the 2000 field season. The arrows indicate the direction of motion through time and the time at the beginning of the flood period is indicated.

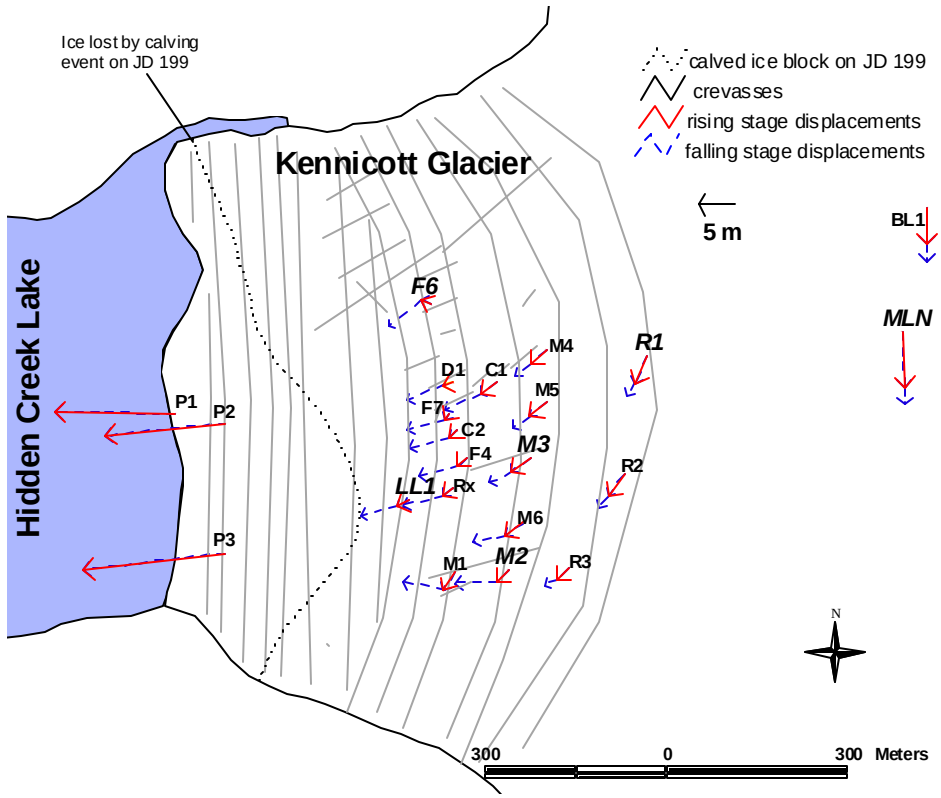


Figure 4.15 Horizontal vector displacements for all of the targets from the 2000 field season prior to the flood (solid arrows) and during/after the flood (dashed arrows). The magnitude has been exaggerated 10 times.

*Ice-dam velocities*

Figure 4.16 shows the horizontal velocity vectors during the lake filling period (solid) and during the lake drainage period (dashed) for the year 2000. The data are reported in Table 4.2, according to lake stage. The transition from lake filling to draining was accompanied by a significant increase in horizontal velocity as well as a dramatic shift in direction. In general, the velocity increase was greatest nearest the lake (~ factor of 21) and decreased with distance from the lake, with a factor of less

than 2 increase in velocity for the two targets located over 1 km from the lake. The change in target displacement direction associated with lake drainage appears to be oriented towards the area of greatest ice loss from the large calving event that occurred on JD 199. The direction of horizontal motion during the drainage period could be a possible explanation for the origination and continuance of the longitudinal crevasses.

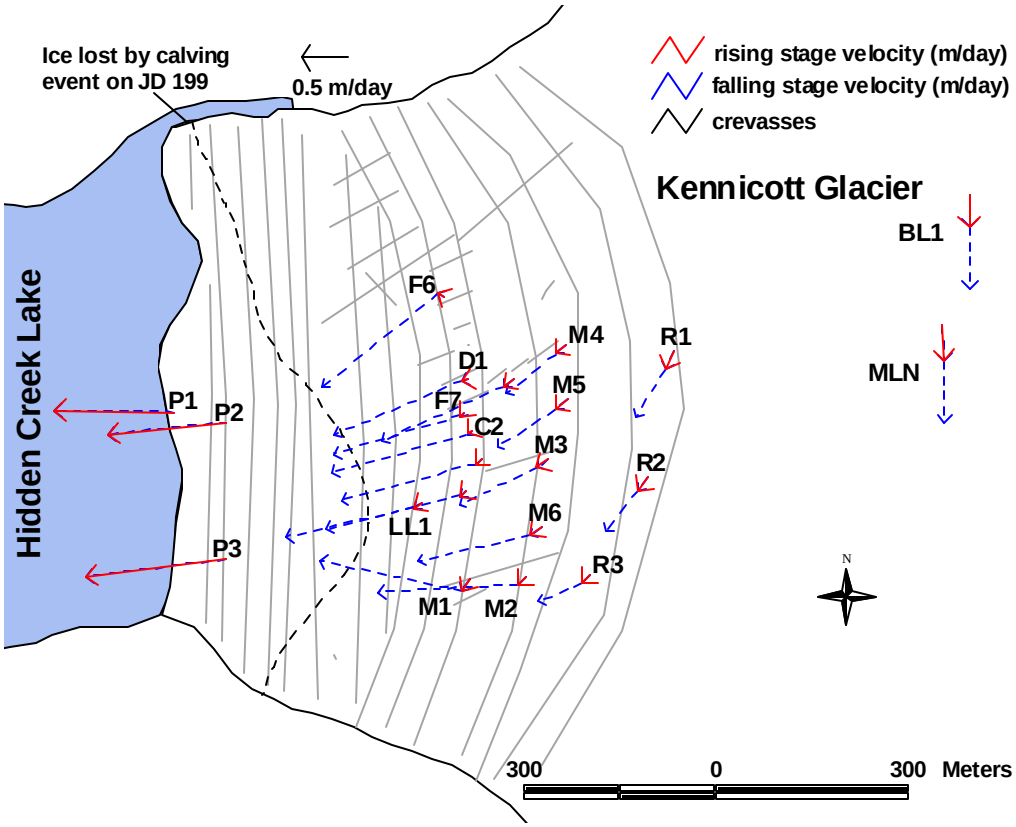


Figure 4.16 Horizontal vector velocities for the 2000 season during the rising stage (solid vectors) and during the falling stage (dashed vectors).

Table 4.2 Changes in target orientation and velocity during the lake rising and lake falling stages. The targets are listed in order of increasing distance from the lake.

| | rising stage | | falling stage | |
|---|---|---|---|---|
| target | bearing | velocity (m/day) | bearing | velocity (m/day) |
| P1 | 271 | 1.36 | - | - |
| P2 | 264 | 1.37 | - | - |
| P3 | 263 | 1.61 | - | - |
| LL1 | 241 | 0.11 | 257 | 1.50 |
| F6 | 299 | 0.08 | 231 | 1.71 |
| Rx | 233 | 0.09 | 256 | 1.60 |
| F7 | 221 | 0.06 | 253 | 1.51 |
| C2 | 232 | 0.07 | 254 | 1.62 |
| F4 | 226 | 0.09 | 255 | 1.60 |
| D1 | 256 | 0.07 | 247 | 1.58 |
| M1 | 211 | 0.16 | 282 | 1.67 |
| C1 | 234 | 0.15 | 246 | 1.52 |
| M2 | 224 | 0.12 | 267 | 1.61 |
| M3 | 234 | 0.17 | 244 | 0.99 |
| M6 | 235 | 0.16 | 257 | 1.32 |
| M4 | 227 | 0.16 | 231 | 0.72 |
| M5 | 229 | 0.17 | 237 | 0.80 |
| R3 | 224 | 0.13 | 247 | 0.55 |
| R2 | 218 | 0.19 | 218 | 0.60 |
| R1 | 204 | 0.21 | 211 | 0.64 |
| BL1 | 180 | 0.38 | 179 | 0.70 |
| MLN | 177 | 0.41 | 180 | 0.70 |

## 4.4 Ice dam analysis

*Net vertical displacements*

Figure 4.17 shows a comparison of vertical displacements for the 1999 and 2000 survey data. The greatest vertical downdrop during the 1999 drainage period - 11.48 m, occurred at target F3, which was the target located closest to the lake (409 m). The vertical downdrop during the drainage period for the rest of the targets, 522 –

785 m from the lake, were smaller, ranging from -0.31 to -1.73 m. The behavior of target D1 deviated from the rest of the targets in that the target oscillated up and down by as much as ± 0.05 m during the drainage period. Some of this variation is within the survey error but the atypical behavior of the target may also be due to its location, which was located further from the lake than the other targets.

The adjusted maximum downdrop in 2000, during lake drainage, -21.45 m, again occurred at the target closest to the lake (LL1), approximately 300 m from the lake. The smallest vertical downdrop, -0.13 m, occurred at target BL1, approximately 1.2 km from the lake. At the end of the measurements, the elevation of BL1 was above the elevation that it should have been at if it had been simply advected parallel to local slope. In general, the vertical displacements for 2000 were consistently greater than in 1999, possibly correlated with the larger lake volume in 2000.

During lake rise in 2000, several targets nearest the lake (5 – 300 m) rose at a faster rate than the lake. The targets nearest the ice front (group 1) were initially rising at the same rate as the lake but began to deviate after Julian Day 193 and began rising faster than the lake. In the field, we observed calving and/or rotation of the ice blocks near the lake that may account for a change in rate of ice rise. At a distance of 300 – 400 m from the lake, the ice rose at roughly the same rate as the lake (about 0.5 m/day), while the ice 400 – 600 m from the lake rose at a significantly slower rate, about 10% as fast as the lake stage. Coincidently, 600 m is roughly twice the local ice thickness. Vertical displacements of the two targets located > 1 km from the lake (BL1 and MLN), were initially downward during the lake rise period. These two targets

were far enough from the lake that their vertical displacement is probably dominated by normal glacier flow. However, after Julian Day 196, these two far targets began to lift slightly, presumably exhibiting a delayed response to the rising lake level or to an increase in water storage at the bed. The lifting would be due to normal stresses transmitted laterally through the glacier. The latter case may indicate that meltwater is locally going into storage, which could have important implications in terms of flood volume.

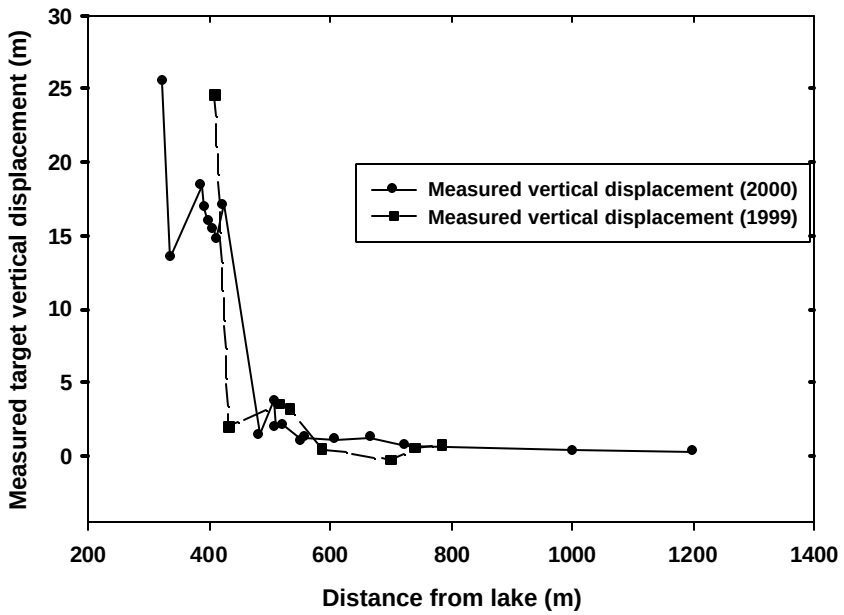


Figure 4.17 Comparison of measured vertical displacement with distance from the lake from the 1999 and 2000 survey targets.

*Horizontal displacements and velocity*

The survey data are used to determine the ice strain during the lake rise period. Changes in target easting position are used as there are very little changes in northing

position during the lake rise period. As a first approximation, apparent “strains” are plotted only in the easting direction by subtracting the easting position through time between two targets (Figure 4.18). These plots reveal that closer to the ice front between targets LL1 – M3 and D1 – M4 compression is prevalent prior to the flood, and between targets M5 – R1 and R2 – MLN tensional strain are prevalent prior to the flood.

The increase in horizontal velocity after the lake begins to drain is not instantaneous. In general, there is a delay of approximately 24 – 28 hours for group 2 targets, 46 hours for group 3 targets and 52 hours for group 4 targets before there is a noticeable change in horizontal target orientation.

*Mechanical behavior in 2000*

Once the lake level began to drop, survey targets at distances greater than 300 m from the lake continued to rise for a period of time before dropping. This “lag time”, defined as the time difference from when the lake began to drop until the ice surface was observed to drop, increased with distance from the lake. The shortest lag time was 12 hours at about 400 m from the lake (target F7) and the longest was 60 hours at about 1.2 km from the lake (target BL1) (Figure 4.19). For some targets it was not clear exactly when they began to drop; the error bars indicate this uncertainty. The lake drained completely in approximately 75 hours.

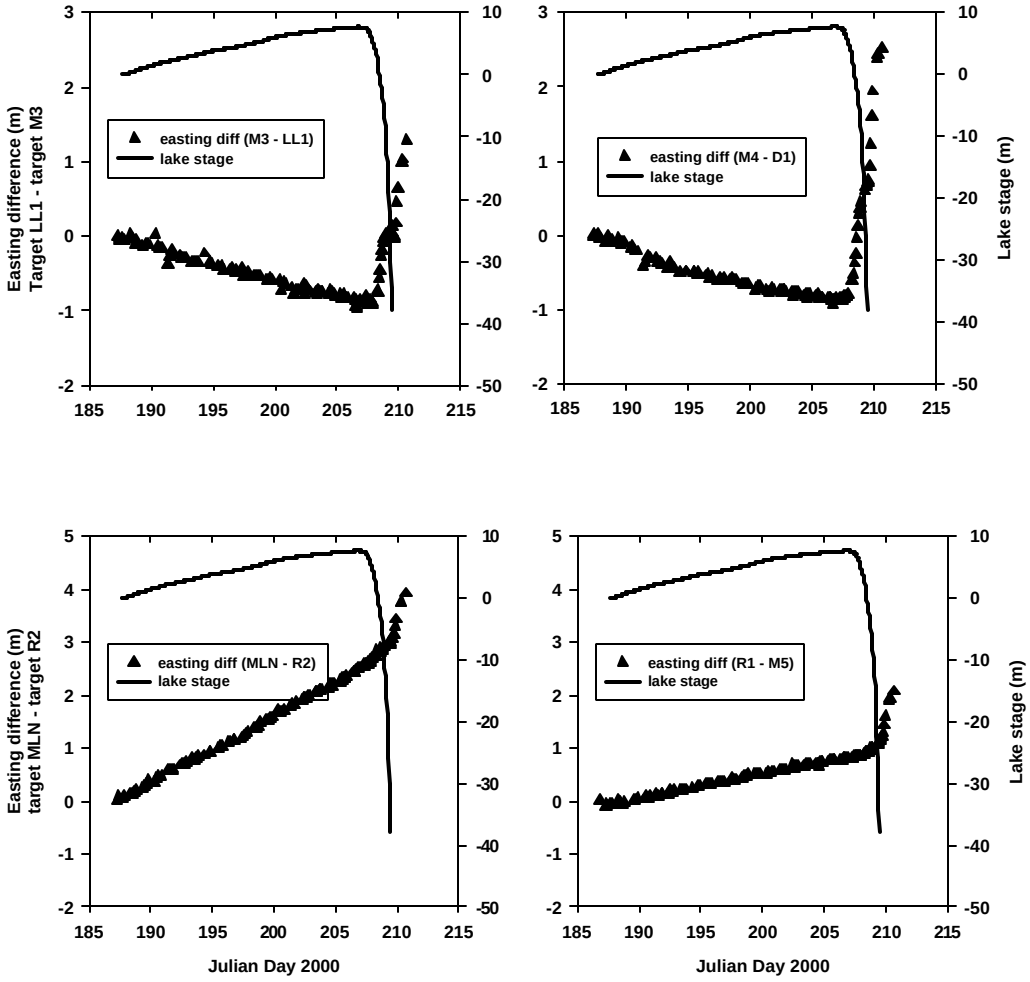


Figure 4.18 Plots demonstrating the progressive difference in easting position between two survey targets. A decreasing difference prior to the flood indicates a compressive strain and an increasing difference indicates a tensional strain in the east-west direction.

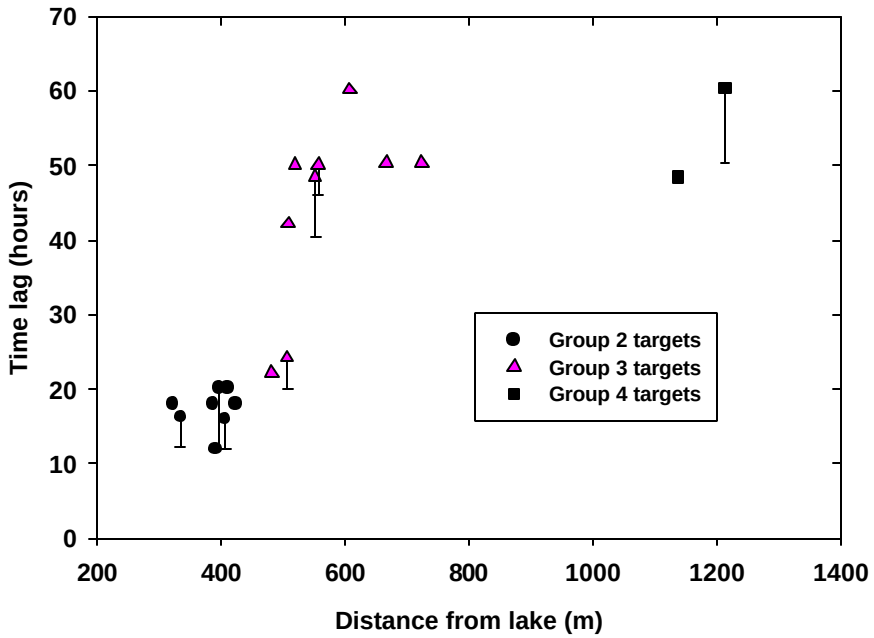


Figure 4.19 Plot showing the difference in hours from the lake began to drain to when the ice surface began to drop at the various survey targets. The lower error bars indicate the smallest time lag possible based on when the targets are interpreted to begin dropping.

To gain some insight into the mechanical behavior of the ice dam during the rising and falling lake periods, the difference in target elevations at a given lake stage before and during the flood were plotted. If the ice were behaving elastically, the target should be at approximately the same elevation as the lake passes through a given elevation or stage as it rises then falls. Figure 4.20 shows the difference in target elevation for a given lake stage during the flood and prior to the flood. For any given lake stage, the survey targets were invariably at a higher elevation as the lake drained than during the rising lake phase.

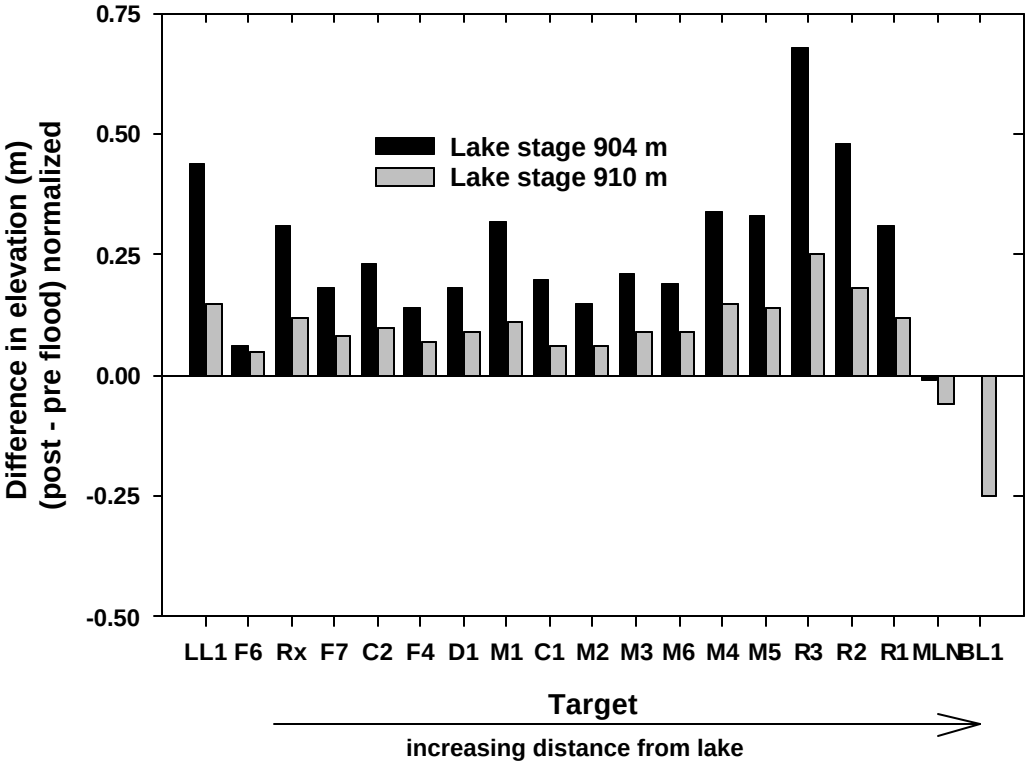


Figure 4.20 Plot showing the difference in target elevation for a given lake stage during the flood and before the flood. A positive value indicates that the target elevation was higher during the flood period even though the lake stage was the same.

Target F7 (target group 2) was selected to illustrate the mechanical ice behavior because it is located in the center of the ice dam where the displacements are less influenced by side drag. Target F7 is also located close to the lake where the displacements appear to be greatly influenced by lake stage. Figure 4.21 illustrates the trajectory of target F7 located approximately 400 m from the lake and is representative of group 1. Over the survey period in which the lake was rising, target F7 rose by 5.94 m while the lake level rose by 7.71 m. The steep falling trajectory of target F7 suggests that it was situated on a block, bounded by steep normal faults, that shifted or

began rotating after JD 193. If this notion is correct then the portion of the ice dam where target group 1 was located was not well connected, mechanically, to the rest of the ice dam. The fact that the large calving event on JD 199 had no apparent effect on the velocity or displacement of the ice dam supports this interpretation of the displacement data.

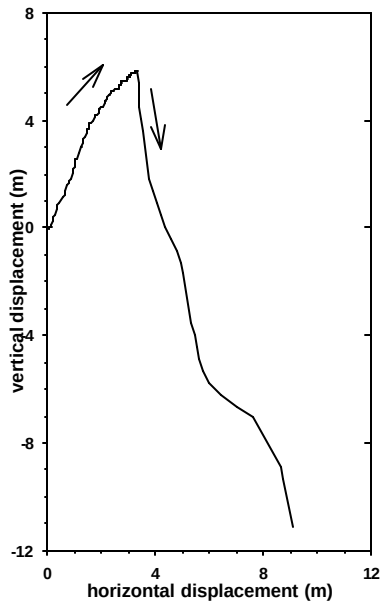


Figure 4.21 Trajectory for target F7 with no vertical exaggeration.

*Ice dam geometry*

The depth to the bedrock combined with the surface elevation provided us with information about the subglacial topography and ice thickness. However, due to the irregular distribution of our radar transects we were unable to combine the information obtained from the lake basin survey and ice radar to create a contour map of the

subsurface topography without extrapolating over large areas. Instead the data was used to create a longitudinal cross section (striking N75ºE) showing the ice geometry and the lake at maximum stage (Figure 4.22). In small areas where there are no radar data, the glacier thickness was interpolated or extrapolated (indicated by dashed lines in Figure 4.22). Survey targets at the ice dam/lake interface were lost during the calving event and the elevation at maximum lake stage is not precisely known. However, we were able to estimate the maximum thickness using the vertical displacement data. The vertical displacements for the three disposable targets show that the ice rose at the same rate or faster than the lake indicating that the ice achieved isostatic equilibrium before the targets were lost. Given that the lake elevation at maximum stage was 912 m and the deepest portion of the lake nearest the ice dam is at an elevation of approximately 795 m, then the water head must have been approximately 117 m. If we assume the closest ice to the lake had reached isostatic equilibrium at the time of maximum lake stage we can use the density difference between ice and water to calculate a minimum local ice thickness of 130 m.

The combination of lake bathymetry and radar data reveals that the lake forms in a hanging valley that is truncated by Kennicott Glacier. The ice thickness also increases from the lake to a distance of approximately 600 m then it appears to decrease slightly. The thinning of the glacier in this area is probably a localized feature on the glacier.

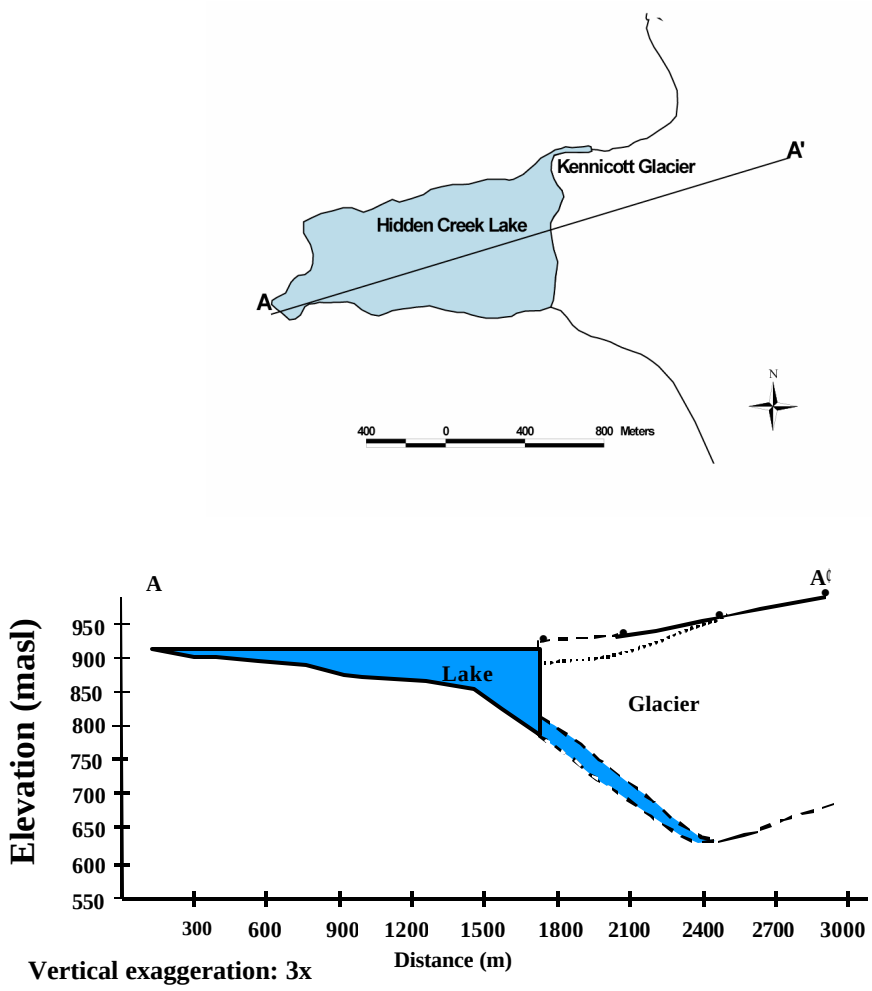


Figure 4.22 Cross section of the ice dam showing the interpolated (dashed line) and measured (solid line) geometry of the lake and ice dam at maximum lake stage. The points indicate the approximate location of survey groups 1 – 4. The dotted line shows the ice surface after the lake has drained. The blue area beneath the dam indicates the amount of stored water if we assume that the total ice displacement is due to the evacuation of water.

There is a strong correlation between ice thickness and the magnitude of vertical displacements. The thickness of the glacier was estimated for each survey target that was situated near or coincided with the radar transects and was compared

with the total vertical deflection at those same targets (Figure 4.23). In general, there is greater vertical displacement of the ice-dam nearest the front, where the ice is relatively thin (230 – 260 m) and less vertical displacement farthest from the lake where the ice is relatively thick (~355 m). There is a significant decrease, in the magnitude of vertical displacements at a distance of approximately 420 to 480 m that corresponds to a significant increase in ice thickness. The vertical displacements decrease from a total displacement of 15 m to a total displacement of 3 m over a distance of 60 m.

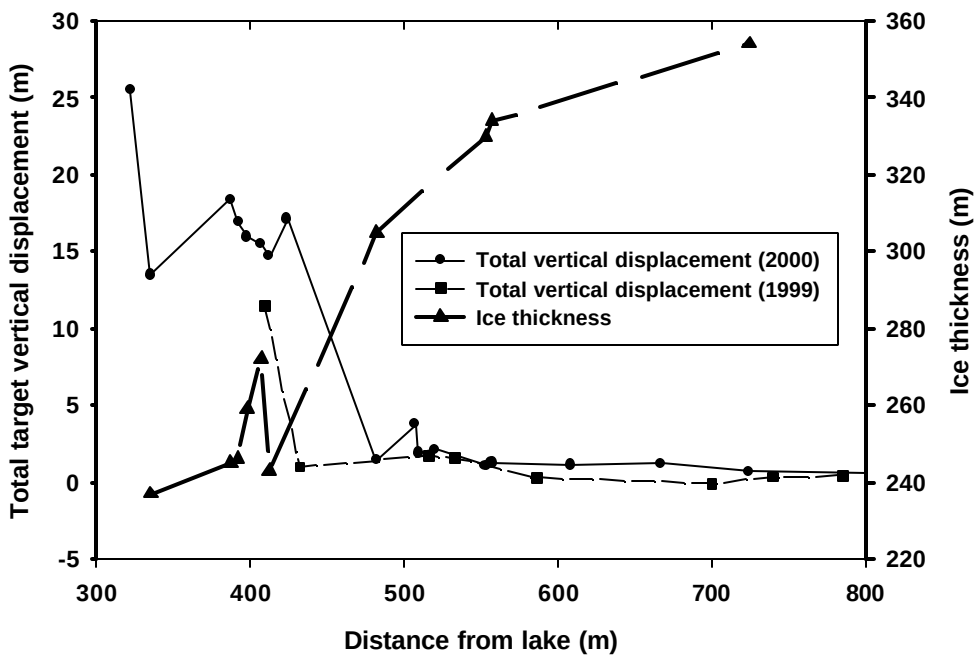


Figure 4.23 Graph comparing the total vertical deflection with distance from the lake and ice thickness with distance from the lake (secondary axis) for a subset of the survey targets.

*Water Storage*

During the uplift period, ice as far as 400 m from the lake rises at roughly the same rate or faster than the rate of lake level rise. The likeliest cause for this uplift is water going into storage at the bed, possibly in the form of a subglacial "wedge" connected directly with the subaerial lake but disconnected from the glacier's main drainage system by a drainage divide. If we make the assumption that the net vertical downdrop of the ice dam is due entirely to the evacuation of water from beneath the ice dam, we can use the measured displacements to estimate the volume of water stored beneath the ice dam. Additionally, the ice dam at a distance of 400 – 600 m from the lake is also being lifted from the bed as a result of the normal stresses imposed at the front of the dam. It is probable that lake water and/or glacier melt water is entering into this area as well.

To make a plausible estimate of the volume of stored water, the shape of the subglacial wedge must be approximated. The basis of our estimate is the adjusted vertical target displacements plotted at several times ($t$) in terms of easting position. There were no systematic variations with northing position. The vertical displacement data from JD 188 was then fit with a Sigmoidal curve (Figure 4.24 a) and the coefficients determined by regression with the following equation:

$$h(x) = \frac{a}{[1 + e^{-(x - x_0)/b}]} \quad (4.5)$$

where $h(x)$ is the height of the ice dam during the lake filling period, $x$ represents the easting position and the parameters $a$, $x_0$ and $b$ represent constants defined by the

regression. The $R^2$ for the JD 188 fit is 0.98. As the lake stage continues to rise, the goodness of the Sigmoid curve fit declines. The lowest $R^2$ value is 0.67, on JD 208 (Figure 4.24 b). The progressive decrease in the $R^2$ value is accounted for by target LL1, whose behavior deviated with time from the pattern of the other targets. The variables and $R^2$ values for each time period calculated are in Appendix B.2. The area under the curve is simply the integral of the Sigmoid equation:

$$A = \int_{m}^{m'} ab \ ln \ [e^{\frac{x}{b}} + e^{\frac{x_0}{b}}] \, dx \quad (4.6)$$

where *m and m'* represent the bounds in easting position from the target locations. The integrated area is multiplied by the width of the ice dam to determine the water volume.

Equation 4.6 is used to estimate the water volume stored beneath the ice dam based on the vertical displacement data. Although the vertical displacement is not uniform across the full width of the ice dam, a constant width of 900 m (width at the ice front) was used for all the time steps because the vertical displacement across the width of the glacier is not as variable as the longitudinal vertical displacement. The farthest integral bounds correspond to the targets in group 3 and excludes the two farthest targets in group 4 due to their negligible vertical motion. To calculate an upper bound of the volume, it was first assumed that the vertical displacements measured at the targets longitudinally across the dam were uniform across the width of the glacier.

This is most likely not accurate because we would expect some degree of coupling between the ice dam and the valley walls. To estimate a lower bound that represents complete coupling of the ice dam at the margins with no vertical deflection, all of the upper bound volumes were multiplied by ½ (Figure 4.25). The volumetric difference between the two lines in Figure 4.25 represent the upper boundary of water storage. The heavy solid line represents the ice surface if we assume completely coupling of the valley walls at full deflation. The volumetric difference between this line and the dashed line represents the lower boundary of water storage, which equates to approximately one half of the upper boundary volumes.

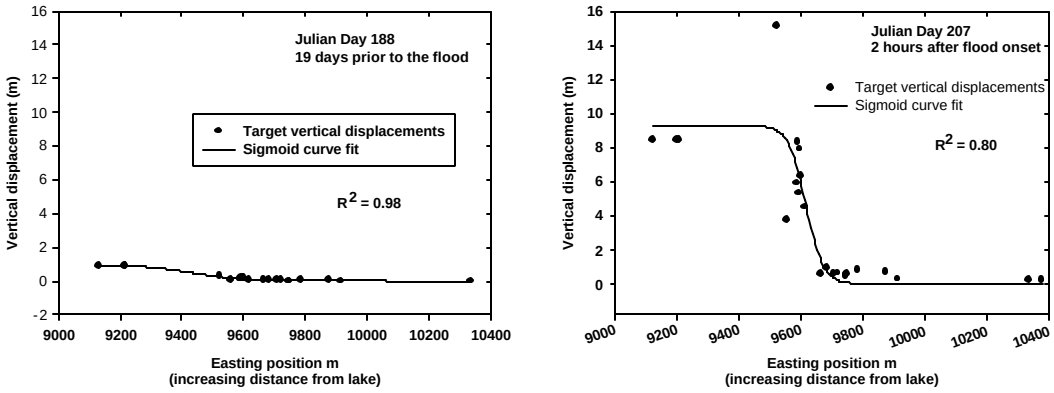


Figure 4.24 Target vertical displacements on JD 188 with easting position (a) and on JD 207 with easting position (b). The curves represent a sigmoid regression with an r – squared value of 0.98 and 0.80 respectively.

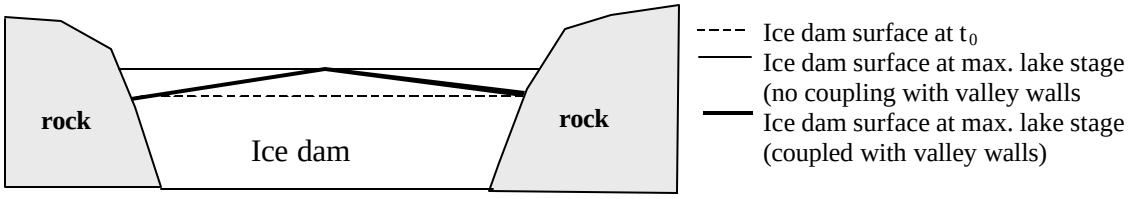


Figure 4.25 Schematic diagram showing a cross section across the width of the ice dam and the intersection with the valley walls. The dashed line shows the ice surface at time $t_0$ and the solid thin line shows the surface of the ice dam at its full deflation.

The change in storage volume since the start of measurements and the cumulative storage volume are shown in Figure 4.26. The total estimated volume was determined by taking the lowest ice dam elevation after the flood as the zero volume (datum) that indicates the volume of water stored prior to the beginning of our survey measurements. The total water storage is likely between 4 to 8 x $10^6$ $m^3$ with about 2 to 4 x $10^6$ $m^3$ entering storage during our observations (JD 186 – 210), over the 2000 field season.

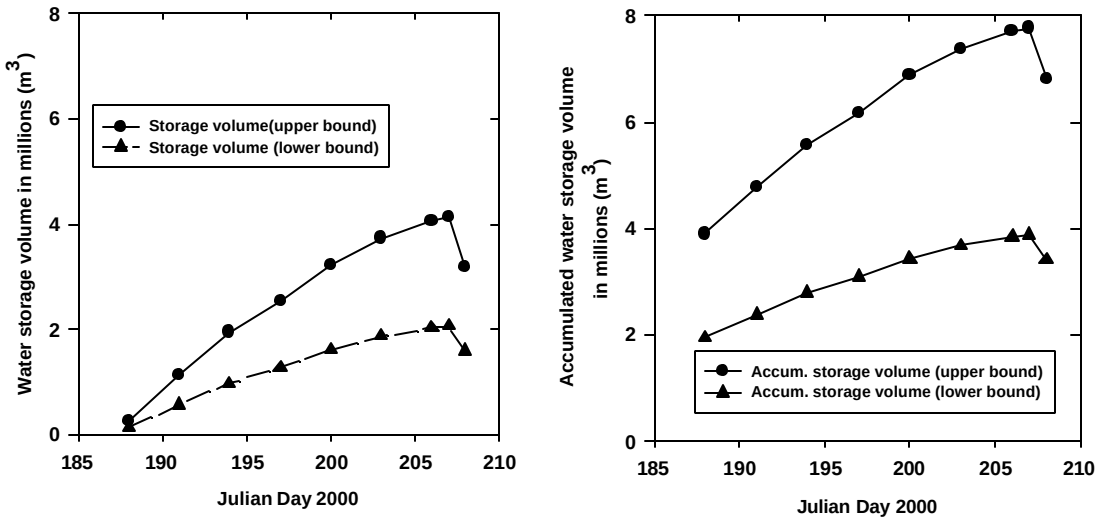


Figure 4.26 Water storage volume results based on a) ice dam inflation from the beginning of our survey measurements and b) accumulated water storage volume including water stored prior to the beginning of our survey measurements.

## 4.5 Ice dam discussion

*Vertical displacements*

The decrease in the total amount of downward displacement with distance from the lake at HCL is similar to Kasper's (1989) results from her research on outburst floods at Kaskawulsh Glacier. The Kaskawulsh survey data contains more measurement errors than for the data presented here for HCL, and was conducted at longer time intervals (3 days). Kasper also measured the largest vertical displacements nearest the lake with decreasing displacements with distance from the lake. However, due to the different geometries, direct comparison between the data is not possible.

The upward displacement of survey points far from the lake (BL1 and MLN) exhibited after JD 196, may be due to stresses in the ice imposed by the lake water, increased water storage at the bed, or other dynamic factors unmeasured. Iken et al., (1983) measured up to 0.4 m of vertical uplift of Unteraargletscher at the beginning of the melt season attributed to water storage at the bed. Based on the estimated location of the drainage divide presented in Chapter 3, we estimate that this area is not hydraulically connected to the lake, but we have no pertinent data to determine whether water storage was responsible for the uplift observed at targets BL1 and MLN.

A few of the targets nearest the ice front (P1, P2, P3, and LL1) were at times rising faster than the lake stage. Targets P1, P2, and P3 were lost after JD 199 but target LL1 continued to rise faster than the lake while other targets in group 2 were rising at the same rate or slightly slower than the lake. One possible reason for the

faster moving targets is that prior to our survey observations, the ice may have been held below hydrostatic equilibrium by the still grounded ice. As the water pressure in the lake became high enough the ice would then "rebound" in order to attain isostatic equilibrium with the current lake level. This type of "inverse Reeh" mechanism was first proposed by Lingle et al. (1993) to explain calving of icebergs from below the water surface at Vitus Lake, situated at the terminus of the Bering Glacier.

*Horizontal displacements and velocity*

The horizontal displacements of targets on the ice dam prior to the onset of lake drainage follow a southwest trajectory. The horizontal motion is probably controlled partially by flow due to deformation of the ice directed down valley to the south with a side-drag component derived from ice that is flowing into the tributary valley to the west, and basal drag. After the lake begins to drain, the target trajectories shift to the west, in the direction of the lake.

The presence of water at the base of glaciers is known to increase their sliding velocity (Iken and Truffer, 1997). The sliding velocity is greatest under transient water pressures (Iken et al., 1983). However, horizontal velocities of the Kennicott ice dam were nearly constant during the period of lake rise, despite a potentially large volume of stored water beneath the ice dam. The nearly constant horizontal velocity during lake rise indicates that there is resistance to the gravitational driving stress either due to side drag along the valley walls or basal drag. Due to the short length of the ice dam, longitudinal coupling is probably another important factor in the ice behavior.

Even with the presence of water at the bed, it is possible that basal drag is an important factor if there are significant bumps in the bed that never get completely flooded and serve to impede ice flow. The arcuate crevasses across the ice dam suggest that side drag does occur and is probably an important resistance factor.

During lake drainage the horizontal velocities increased dramatically, from 2 to 21 times the pre-flood speeds. The drop in hydrostatic pressure at the free face during lake drainage causes the longitudinal tension to dominate over the force of the side drag thereby increasing the horizontal velocity. The ice dam also slopes a lot more during drainage thus increasing the shear stress.

*Mechanical behavior*

The time lag associated with the delay between lake level drop and vertical downdrop of the ice dam in addition to the departure from reversibility between the lake filling and draining periods may be explained by a viscous response of the ice dam to the flexural stresses imposed by the buoyantly supported ice. In other words, it takes a finite time for the ice to attain isostatic equilibrium with the rising and falling lake levels because the whole ice mass is not simply floating rather is supported by both hydrostatic pressure and internal stresses within the ice. Therefore, the ice does not immediately respond to the changing water pressure conditions at the front of the ice dam.

*Water storage*

There is a significant difference between the calculated volume of outflow from HCL and the integrated flood discharge measured from the Kennicott River near the terminus of the glacier. The total flood volume for 2000 from the Kennicott River was 38 million $m^3$ (S. Anderson, S. pers comm., 2000) whereas the total volume in the visible part of HCL was 28 x10 $m^3 \pm 3.0 \times 10^6$ $m^3$. The approximate error associated with the flood volume recorded at the Kennicott River is unknown at this time, however it is expected to be significant.

The vertical ice displacement data from HCL reveal that there is a subglacial "wedge" of water that extends to approximately 400 – 500 m from the lake that is hydraulically connected to the lake. The buoyantly supported portions of the ice cause the grounded ice to be lifted off the bed allowing additional water to go into storage. The calculated volume of water in storage beneath the ice dam determined from the vertical ice displacements prior to the flood (between 4 and 8 x $10^6$ $m^3$) may account for some of the deficit in the volume of water measured in the lake compared to the much larger volume measured downstream in the Kennicott River. Kasper (1989) made a similar calculation based on vertical ice displacements and estimated a water storage that equated to 7% of the total volume of the visible lake at Kaskawulsh Glacier. In comparison the water storage calculated at HCL was 4 to 29 % of the total volume of the visible HCL. The range of 4 to 8 x $10^6$ $m^3$ is a realistic storage volume at HCL due to the magnitude of the flood volume measured at the glacier terminus,

which was significantly higher than the calculated volume of water stored in the visible part of HCL.

Although there is no conclusive evidence from the HCL data, drainage of the lake may coincide with the release of water stored within the main part of the glacier as well as with water draining from other hydraulically connected ice-dammed lakes in the basin such as Donoho Falls Lake. Several studies have revealed that later in the summer months, the discharge from glaciers often exceeds ablation, implying the release of water that was stored within the glacier (Stenborg, 1970; Tangborn et al., 1975). Bezinge (1973) suggested that stored water was released in conjunction with drainage of the Gornersee and even dominated the outflow at the terminus of the glacier.

The possibility of water being stored beneath the ice dam prior to the flood has not been fully addressed in the outburst flood literature and is important in understanding outburst flood triggering mechanisms as well as flood volumes. Water storage prior to the flood suggests that flotation of the ice dam may not be the controlling mechanism behind lake drainage, otherwise the lake would drain much sooner. Also, some studies have focused on lake volume as an indicator of peak discharge but have not included water stored beneath the ice dam that may significantly alter the volume of water discharged through the system. While we propose that the stored water is hydraulically isolated from the glacier's main drainage system via a local drainage divide, this idea needs to be more rigorously tested. Dye tracing experiments performed by Fisher (1973) revealed that water from ice-dammed

Summit Lake, British Columbia leaked into the main drainage system prior to an outburst flood from the lake. Further studies analogous to Fisher's, made in conjunction with ice displacement measurements, could provide important evidence for or against our hypothesis.

### 4.6 Summary and conclusions

The survey data from the ice dam reveal a straightforward pattern of displacements due to the lake. During lake rise, several of the targets closest to the lake rose at faster rate than the lake, suggesting that the ice in this area may have been rebounding to attain isostatic equilibrium after a period of being held below hydrostatic equilibrium by the still grounded ice. At a distance of 300 – 400 m from the lake, the ice rose at roughly the same rate as the lake. The ice at a distance of 400 – 600 m from the lake rose at a slower rate than the lake. The farthest two targets, located over 1 km from the lake, did not begin to rise until after JD 196 and may be unaffiliated with the lake rather may be due to water storage at the bed in the main portion of the glacier.

Displacements were greatest at those targets situated closest to the lake and decreased with distance from the lake in both years. In 1999, the largest measured downward displacement of the ice was –11.48 m and the smallest was 0.31 m, while in 2000 the largest was –25.47 m and the smallest was –0.13 m. The dramatic decrease in the magnitude of vertical displacements at a distance of 400 – 600 m from the lake also coincides with a significant change in ice thickness.

The delay in the response of the ice dam to the drainage of the lake can be explained by the temporary storage of water beneath the ice dam as the lake drains. In addition, during the lake rising period, it takes a finite period of time for the ice to attain isostatic equilibrium. Therefore, during the initial stages of lake drainage the ice may continue to rise in an effort to reach equilibrium.

The vertical displacement data show that there is a body of stored water beneath the ice dam that extends approximately 400 to 500 m from the lake. The stored water is presumed to be hydraulically isolated from the glacier's main drainage system but is hydraulically connected to the lake. An estimate of this potential water storage volume (between 4 and 8 million $m^3$) was calculated based on vertical downward displacement of the ice after the flood. This volume is 14 to 28% of the total volume of the lake.

# CHAPTER 5

# SUMMARY OF RESULTS

## 5.1 Water storage

The vertical displacements of the ice dam, the sub-ice storage volume accumulated over the measurement period is estimated at 2 - 4 x $10^6$ $m^3$. This range is similar to the estimated change in lake storage volume from the water balance of 1.3 million $m^3$ ± 1.2 million $m^3$. The calculated volume of water storage beneath the ice dam combined with the total volume of the visible lake (28 million $m^3$) does not entirely account for the flood volume (38 million $m^3$) measured at the Kennicott River near the terminus of the glacier. Unfortunately, the measurement errors make a precise comparison difficult. It seems reasonable that the flood volume measured at the terminus would be much higher than the combined volume from the visible lake and "wedge" beneath the ice dam because during the flood event, water could be released from storage within the main portion of the glacier. Figure 5.1 shows the cumulative water volume inputs for Hidden Creek, Hidden Creek Lake and from storage beneath the ice dam. Although this plot does not take into account the variables included in the water balance and may give a false impression that the volumes do not match well, it does provide an idea of the rates of input. In general, although the Hidden Creek inputs are close to the Hidden Creek Lake inputs, the errors are large enough in the Hidden Creek data to mask the storage volume beneath the ice dam.

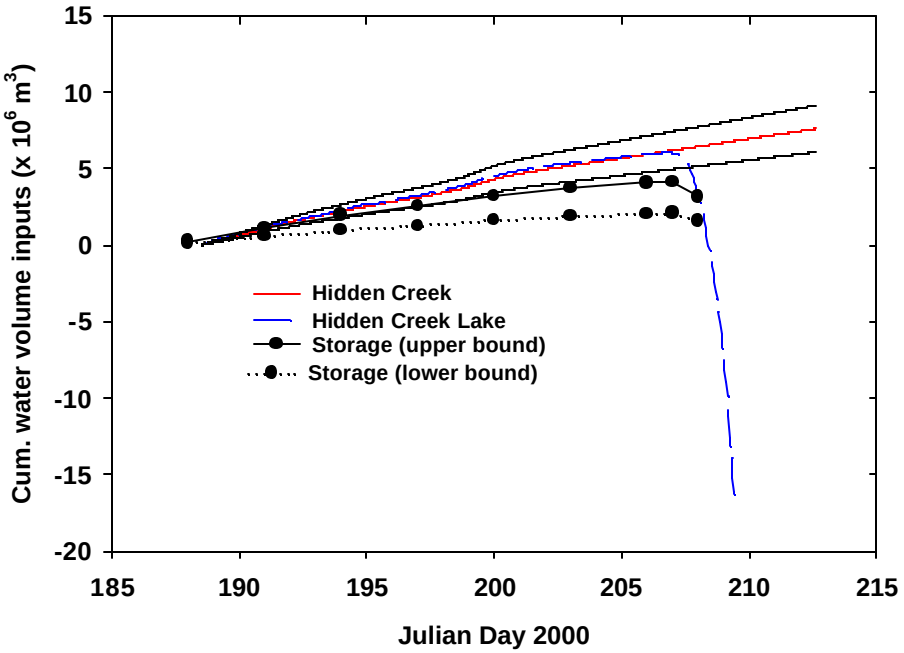


Figure 5.1 Comparison of cumulative water volume inputs for Hidden Creek, Hidden Creek Lake, and from calculated storage beneath the ice dam. The solid lines are error bounds on the Hidden Creek data.

## 5.2 Ice deformation

Our survey measurements from both years reveal that the ice dam experiences large vertical and horizontal displacements in response to changing lake levels. The magnitude of vertical and horizontal displacements generally decreases with distance from the lake and are likely associated with an increase in ice thickness with distance from the lake. A comparison between the rate of vertical displacements of the ice and the rate of lake rise shows a complicated behavior of the ice as it attempts to attain isostatic equilibrium. In addition, the vertical displacements of the three disposable

targets suggest that the front most portion of the ice was probably loosely connected to the main portion of the ice dam and probably experienced small calving events as well as fault block rotations.

The horizontal velocity of the ice increased dramatically during the drainage period from 21 at the targets located closest to the lake to a factor of less than 2 at the targets located farthest from the lake, as compared to the pre-drainage period. Prior to the flood, the horizontal velocities were temporally constant despite the presence of water stored at the bed. This suggests that prior to the flood, side drag and possibly basal drag, dominated the flow of the ice into the tributary valley. During the flood, longitudinal extension grew larger because the inward-pointing stress due to the lake water decreased. However, the increase in velocity at the farthest two targets may be more attributed to an increase in water at the bed that can decrease bed friction and increase sliding velocity or dynamic factors unmeasured.

Prior to this study, it was not well understood how an ice dam deforms in response to changing lake levels associated with an outburst flood. The findings presented here are important for understanding the mechanisms of flood initiation as well as providing information on how hydrological changes in the glacier affect glacier dynamics.

### 5.3 Triggering mechanisms

Flotation of the ice dam has been the central focus in most theories regarding the processes that control outburst floods. The data from the outburst floods at HCL

reveal that drainage does not occur when the frontal part of the ice dam is initially lifted off the bed, rather water becomes stored beneath the ice dam, apparently hydraulically disconnected from the glacier's main drainage system.

Based on the results from Hidden Creek Lake, I propose that the flood is initiated when the subglacially stored water that is hydraulically connected to the lake breaches the localized drainage divide. After the drainage divide is breached, it is not evident whether a stable leak ensues until a connection is made with the main drainage network or if a connection is made immediately upon breaching. Perhaps changing hydraulic conditions at the bed associated with increases in meltwater from the glacier may play a role.

The results presented here support Nye's (1976) theory on outburst flood triggering mechanisms. However, there is still much that can be learned about the hydrological interactions that occur once the lake water joins the main drainage system and how the water is transported through the glacier.

## 5.4 Future Research

In conclusion, further research should include a more accurate determination of the water balance in the basin to better constrain the volume of stored and released water in the lake basin. In the future this data may be useful for constructing models and/or predicting outburst floods. Suggestions for future data collection include obtaining more discharge measurements in Hidden Creek for a more accurate rating curve, determining the hypsometry of the lake in the deepest part of the basin using

sonar, and placing a rain gauge near the lake or glacier to obtain measurements of local precipitation. In addition, better control on the location of the local drainage divide would aid in constraining the inputs and outputs to the lake. Drilling more boreholes in the ice and covering a larger area of the ice dam using ice radar would provide useful information for delineating the drainage divide.

A comprehensive network of survey targets on the ice dam that includes targets near the margins of the ice dam as well as off the ice dam on the main part of the glacier would provide better baseline measurements. Also, a strain analysis of the horizontal displacements would provide useful information about the mechanical behavior of the ice dam.

## REFERENCES


Anderson, S. P., Fernald, K. M. H., Anderson, R. S., and Humphrey, N. F., 1999, Physical and chemical characterization of a spring flood event, Bench Glacier, Alaska, U.S.A.: evidence for water storage: Journal of Glaciology, v. 45, no. 150, p. 177-189.

Baker, V. R., and Fairbridge, R. W., 1981, Catastrophic flooding; The origin of the channeled scabland, Benchmark papers in geology: Stroudsburg, PA, Dowden, Hutchinson and Ross, p. 360.

Benn, D. I., and Evans, D. J. A., 1998, Glaciers and Glaciation: New York, John Wiley and Sons, Inc.

Bezinge, A., Perreten, J. P., and Schafer, F., 1973, Behavior of the glacial lake Gornersee: Symposium on the Hydrology of Glaciers; IAHS Publ. 95, p. 65-78.

Björnsson, H., 1974, Explanation of jökulhlaups from Grimsvötn, Vatnajökull, Iceland: Jökull, v. 24, p. 1-24.

Björnsson, H., 1992, Jökulhlaups in Iceland: prediction, characteristics and simulation: Annals of Glaciology, v. 16, p. 95-106.

Bretz, J. H., 1969, The Lake Missoula floods and the channeled scablands: Journal of Geology, v. 77, p. 505-543.

Clague, J. J., and Mathews, W. H., 1973, Short notes: The magnitude of jökulhlaups: Journal of Glaciology, v. 12, no. 66, p. 501-504.

Clarke, G. K. C., 1982, Glacier outburst floods from "Hazard Lake", Yukon Territory, and the problem of flood magnitude prediction: Journal of Glaciology, v. 28, no. 98, p. 3-21.

Clarke, G. K. C., Mathews, W. H., and Pack, R. T., 1984, Outburst floods from glacial Lake Missoula: Quaternary Research, v. 22, p. 289-299.

Davis, J. C., 1986, Statistics and data analysis in geology: New York, John Wiley and Sons, 646 p.

Dick, G. S., Anderson, R. S., and Sampson, D. E., 1997, Controls on flash flood magnitude and hydrograph shape, Upper Blue Hills badlands, Utah: Geology, v. 25, no. 1, p. 45-48.

Driedger, C. L., and Fountain, A. G., 1989, Glacier outburst floods at Mount Rainier, Washington State, U.S.A.: Annals of Glaciology, v. 13.

Fisher, D., 1973, Subglacial leakage of Summit Lake, British Columbia: Symposium on the Hydrology of Glaciers, v. 95, p. 111-116.

Fountain, A. G., and Jacobel, R. W., 1997, Advances in ice radar studies of a temperate alpine glacier, South Cascade Glacier, Washington, U.S.A.: Annals of Glaciology, v. 24, p. 303-308.

Fowler, A. C., 1999, Breaking the seal at Grimsvötn, Iceland: Journal of Glaciology, v. 45, no. 151, p. 506-516.

Friend, D. A., 1988, Glacial outburst floods of the Kennicott Glacier, Alaska: An empirical test [M.S. thesis]: University of Colorado.

Glen, J. W., 1954, The stability of ice-dammed lakes and other water-filled holes in glaciers: Journal of Glaciology, v. 2, no. 15, p. 316-318.

Iken, A., Rothlisberger, H., Flotron, A., and Haeberli, W., 1983, The uplift of Unteraargletscher at the beginning of the melt season - a consequence of water storage at the bed?: Journal of Glaciology, v. 29, p. 28-47.

Iken, A., and Truffer, M., 1997, The relationship between subglacial water pressure and velocity of Findelengletscher, Switzerland, during its advance and retreat: Journal of Glaciology, v. 43, no. 144, p. 328-337.

Kamb, B., 1987, Glacier surge mechanism based on linked cavity configuration of the basal water conduit system: Journal of Geophysical Research, v. 92, no. 101, p. 9083-9100.

Kasper, J., 1989, An ice-dammed lake in the St.Elias Range Southwestern Yukon Territory: Water balance, physical limnology, ice dynamics, and sedimentary processes [MS thesis]: University of Ottawa, Canada

Kite, G., 1993, Computerized streamflow measurements using slug injection: Hydrological Processes, v. 7, p. 227-233.

Kraal, E. R., 2001, The 1999 and 2000 Hidden Creek Lake outburst floods on the Kennicott River, Alaska [M.S. thesis]: University of California, 119 p.

Lingle, C. S., Hughes, T. J., and Kollmeyer, R. C., 1981, Tidal flexure of Jakobshavns Glacier, West Greenland: Journal of Geophysical Research, v. 86, no. B5, p. 3960-3968.

Lingle, C. S., Post, A., Herzfeld, U. C., Molnia, B. F., Krimmel, R. M., and Roush, J. J., 1993, Bering Glacier surge and iceberg-calving mechanism at Vitus Lake, Alaska, U.S.A: Journal of Glaciology, v. 39, no. 133, p. 722-727.

MacKevett, E. M. J., 1972, Geologic map of the McCarthy C-6 quadrangle, Alaska: U.S. Geological Survey, scale 1:63,360.

McVay, K. R., 1998, Flowvector, ESRI ArcScripts, www.esri.com/arcscripts.

Nye, J. F., 1973, Water at the bed of a glacier, Symposium on the Hydrology of Glaciers, IASH publication, no. 95, p. 189-194

Nye, J. N., 1976, Water flow in glaciers: Jökulhlaups, tunnels and veins: Journal of Glaciology, v. 17, no. 76, p. 181-207.

Raymond, C. F., Benedict, R. J., Harrison, W. D., Echelmeyer, K. A., and Sturm, M., 1995, Hydrological discharges and motion of Fels and Black Rapids Glaciers, Alaska, USA: implications for the structure of their drainage systems: Journal of Glaciology, v. 41, no. 137, p. 290-304.

Richter, D. H., Rosenkrans, D. S., and Steigerwald, M. J., 1995, Guide to the volcanoes of the western Wrangell Mountains, Alaska; Wrangell-St. Elias National Park and Preserve: U.S. Geological Survey, B 2072.

Rickman, R. L., and Rosenkrans, D. S., 1997, Hydrologic conditions and hazards in the Kennicott River basin, Wrangell-St. Elias National Park and Preserve, Alaska: United States Geological Survey Water Resources Investigations Report, v. 96-4296, p. 1-53 plus appendix.

Roberts, P. V., and Stall, J. B., 1967, Lake Evaporation in Illinois: Illinois State Water Survey Report of Investigation no. 57, p. 44

Röthlisberger, H., 1972, Water pressure in intra- and sub- glacial channels: Journal of Glaciology, v. 11, no. 61, p. 177-203.

Seaberg, S. Z., Seaberg, J. Z., Hooke, R. L., and Wilberg, D. W., 1988, Character of the englacial and subglacial drainage system in the lower part of the ablation area of Storglaciärien, Sweden, as revealed by dye-trace studies: Journal of Glaciology, v. 34, no. 116, p. 217-227.

Shreve, R. L., 1972, Movement of water in glaciers: Journal of Glaciology, v. 11, no. 62, p. 205-214.

Stenborg, T., 1970, Delay of run-off from a glacier basin: Geografiska Annaler, v. 52A, p. 1-30.

Tangborn, W. V., Krimmel, R. M., and Meier, M. F., 1975, A comparison of glacier mass balance by glaciological, hydrological, and mapping methods, South Cascade Glacier, Washington: Snow and ice symposium, IAHS - AISH, no. 104, p. 185-196.

Telford, W. M., Geldart, L. P., and Sheriff, R. E., 1990, Applied Geophysics: New York, Cambridge University Press, 770 p.

Thorarinsson, S., 1939, The ice dammed lakes of Iceland with particular reference to their values as indicators of glacier oscillations: Geografiska Annaler, v. 21, no. 3-4, p. 216-242.

Tweed, F. S., and Russell, A. J., 1999, Controls on the formation and sudden drainage of glacier-impounded lakes: implications for jokulhlaup characteristics: Progress in Physical Geography, v. 23, no. 1, p. 79-110.

van der Veen, C. J., 1986, Numerical modelling of ice shelves and ice tongues: Annales Geophysicae, v. 4B, no. 1, p. 45-54.

Vaughan, D., G., 1995, Tidal flexure at ice shelf margins: Journal of Geophysical Research, v. 100, no. B4, p. 6213-6224.

Wahl, K. L., Thomas, W. O. J., and Hirsch, R. M., 1995, Stream-gaging program of the U.S. Geological Survey: U.S. Geological Survey Circular no. 1123.

Walder, J. S., 1986, Hydraulics of subglacial cavities: Journal of Glaciology, v. 32, no. 112, p. 439-444.

Walder, J. S., and Costa, J. E., 1996, Outburst floods from glacier-dammed lakes: the effect of mode of lake drainage on flood magnitude: Earth Surface Processes and Landforms, v. 21, p. 701-723.

Walder, J. S., and Driedger, C. L., 1994, Geomorphic change caused by outburst floods and debris flows at Mount Rainier, Washington, with emphasis on Tahoma Creek Valley: U.S. Geological Survey, 93-4093.

Walder, J. S., and Driedger, C. L., 1995, Frequent outburst floods from South Tahoma Glacier, Mount Rainier, U.S.A.: relation to debris flows, meteorological origin and implications for subglacial hydrology: Journal of Glaciology, v. 41, no. 137, p. 1-10.

Walder, J. S., and Hallet, B., 1979, Geometry of former subglacial water channels and cavities: Journal of Glaciology, v. 23, no. 89, p. 335-346.

Watts, R. D., and England, A. W., 1976, Radio-echo sounding of temperate glaciers: ice properties and sounder design criteria: Journal of Glaciology, v. 17, no. 75, p. 39-48.

Willis, I. C., Sharp, M. J., and Richards, K. S., 1990, Configuration of the drainage system of Mitdalsbreen, Norway, as indicated by dye-tracing experiments: Journal of Glaciology, v. 36, no. 89-101.

# APPENDIX A

# HYDROLOGICAL MEASUREMENTS

## 1. Pressure transducer calibrations

The pressure transducers placed in Hidden Creek Lake during the 2000 field season were calibrated in the lab prior to deployment in the lake. The transducers were calibrated over a range in head from 0 to 2.5 m.

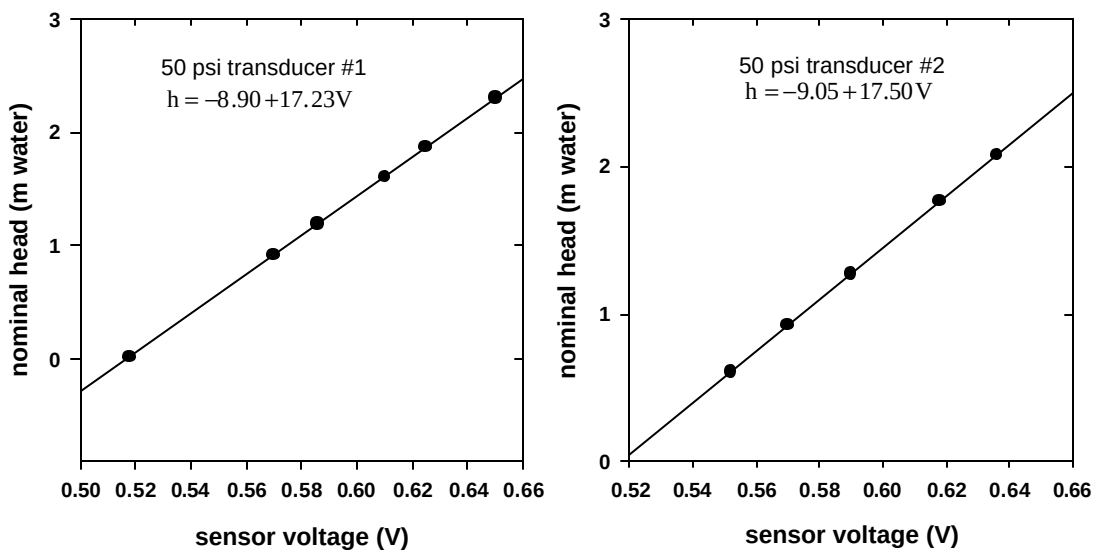


Figure A.1 Calibration records for the two 50 psi pressure transducers (2000).

## 2. Hidden Creek rating curve

The rating curve used to convert stream stage measurements to discharge is presented here for the 2000 field season.

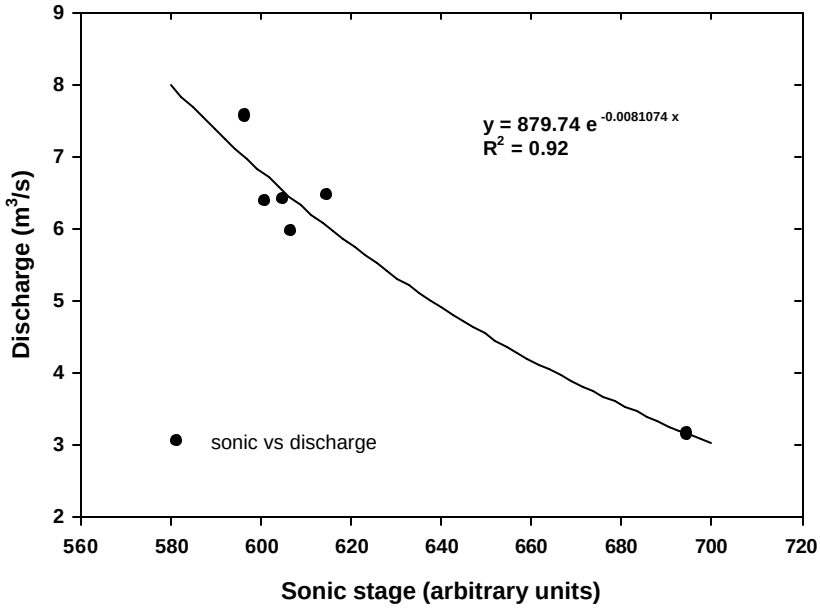


Figure A.2 Hidden Creek rating curve for the 2000 field season.

## 3. 1999 Pressure transducer records

The two 300 psi pressure transducer records are presented below for 1999.

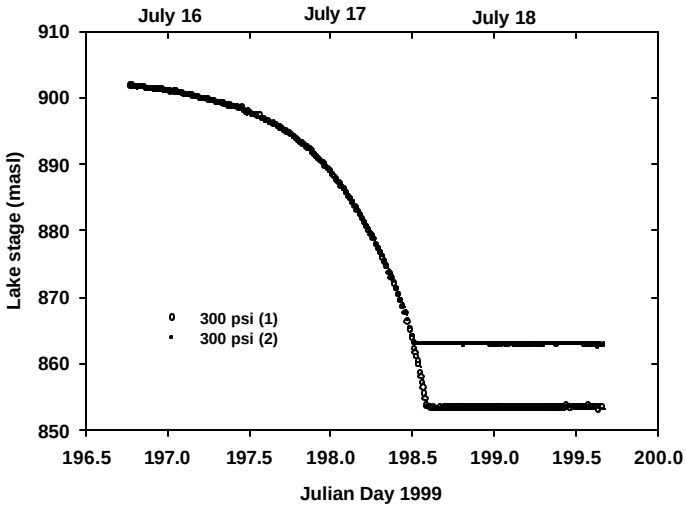


Figure A.3 Drawdown records from the two 300 psi pressure transducers placed in the lake during the 1999 field season.

## 4. Compilation of 2000 water stage records

A single record of complete drawdown was not obtained during the 2000 field season instead four different records of drawdown were compiled into a single record. These records include two shallowly placed 50 psi pressure transducers, one survey to a reflector floating in the lake (floating target), and another survey to a fixed point and the lake surface (spire angle). The first step in this process was to match and combine the data from the two 50 psi pressure transducers and to combine the two records collected from survey methods. These two records were then added to each other and the final record was smoothed.

The two 50 psi pressure transducer records were first compared to each other and the differences calculated. A plot showing the square of the residuals with time (Figure A.4) is noisy but reveals a near linear trend and a RMS (root mean square) value of 0.10 m. One transducer reading was consistently larger than the other (on average 0.07 m), so this value was subtracted from each data point in the larger transducer record resulting in a new RMS value of 0.04 m. The consistent difference is likely due to an error in the instrument calibrations. The two records were at different time intervals so they were added together and sorted in order of increasing Julian Day.

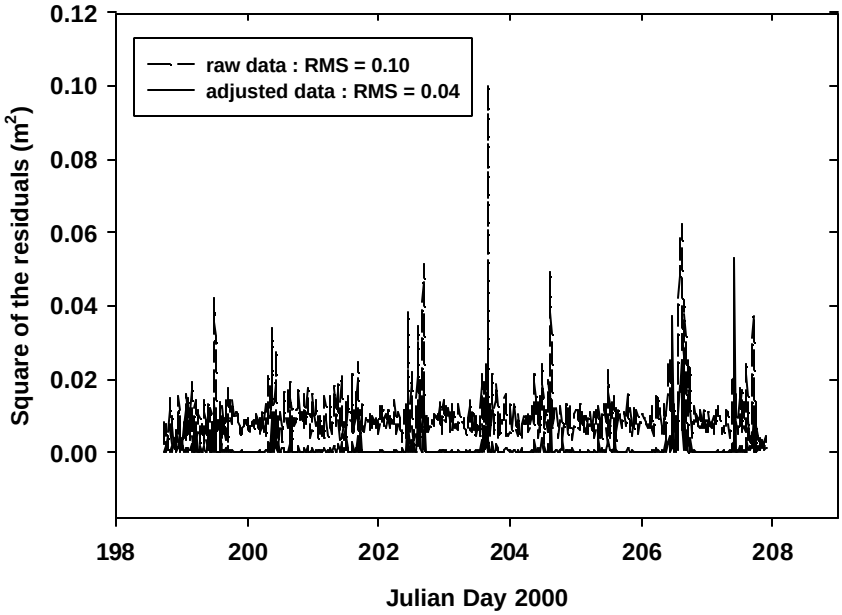


Figure A.4. Plot showing the square of the residuals with time between the two 50 psi pressure transducers before and after the data was adjusted. The average difference between the two transducer records was subtracted from the higher valued transducer and the RMS was recalculated.

In comparing the two survey records, random fluctuations occurred in the data sets that are larger than the instrument errors. The resolution of the survey measurements should be within ± 5 cm, with the floating target measurements likely more precise then the spire angle measurements since a survey reflector was not used for sighting with the latter. Without a reflector in place, it was often difficult to focus on the spire point or the lake surface in rainy or cloudy weather. The lake levels based on the spire angle measurements were consistently lower than that from the floating target record by an average of 0.088 m. This amount was added to each measurement in the spire angle record to match it to the floating target data.

The combined 50 psi transducer records were then compared to the two lake survey records by taking the difference between the two at the same time intervals. Equal time intervals were obtained by piece-wise linear interpolation at 0.25 Julian Days. The difference between the two records revealed a linear trend with time. This trend does not exist between the two transducers or between the floating target/lake spire data alone. The drift exhibits an underestimate of about 10 cm at the beginning of the comparison and 10 days later about a 10 cm overestimate (Figure A.5). There is no reason for a drift in the survey data because it was reset at the end of every measurement cycle. The drift must be due to the transducers or the data loggers.

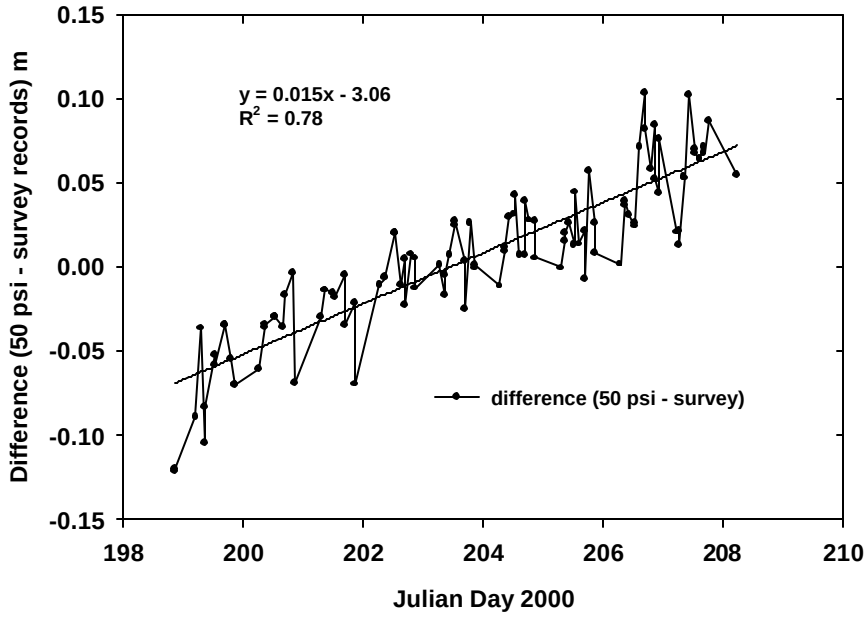


Figure A.5. Difference between the combined 50 psi records and the combined survey records with time. The plot shows the drift that occurs through time.

The drift was subtracted from the combined transducer record, and was added to the two combined survey records. A piece-wise linear interpolation of 0.05 Julian Day intervals was applied to interpolate the four data sets a regular time interval. The data were smoothed using a 5-point running average, a low pass filter. The final transducer record composed of the four separate stage measurements is shown in Chapter 3. The overall probable error in the combined data must be reported as the largest error in the survey data (± 5 cm).

### 5. Bathymetric survey locations

A bathymetric map of Hidden Creek Lake was determined by compiling survey records of the lake basin collected by Rickman and Rosenkrans (1997), survey records collected by our team during the 1999 and 2000 field season, and surrounding elevation data from a USGS topographic map (1959). To aid in contouring five points were manually interpolated in the deepest portion of the lake where survey data is lacking. In addition, one point was added near the ice front based on sonar records. The distribution of the data used to contour the lake bathymetry is shown in Figure A.6.

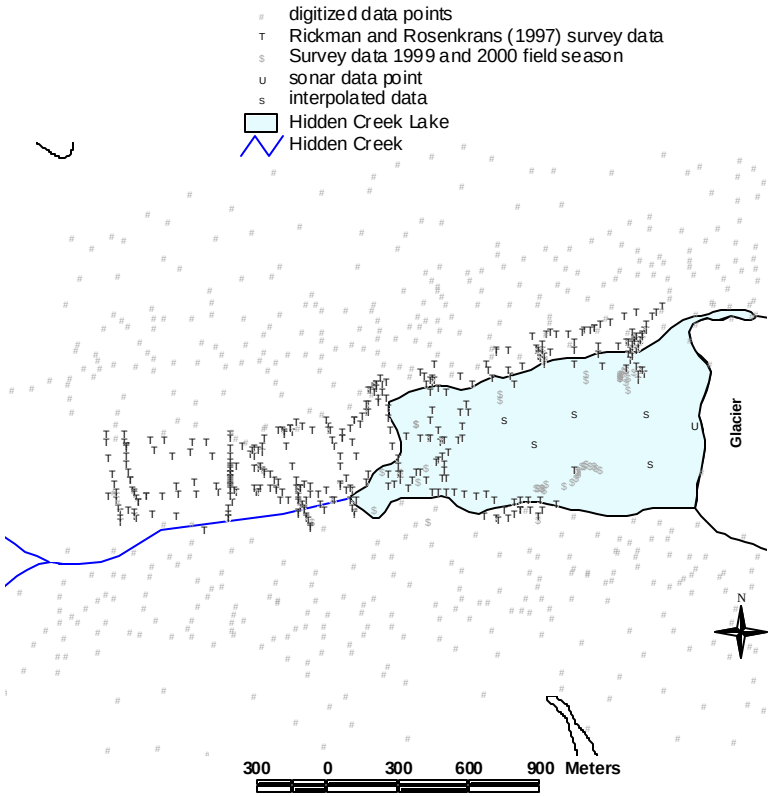


Figure A.6. Distribution of various data points used to construct the bathymetry of the lake basin.

## 6. Spatial Interpolation

*Spatial Interpolation*

The bathymetric surface was spatially interpolated by ordinary kriging. Kriging is a weighted moving average method of interpolation that is dependent on the computation and interpretation of a semivariogram. The semivariogram is used to calculate the degree of spatial correlation among data points and is used to control the way that kriging weights are assigned to data during interpolation (Davis, 1986). This method was used due to the sparse data distribution and allowed for more control over

how the data is interpolated. For this particular data set, the semivariogram model that fit the observational points best and had the lowest RMS (root mean square) value was the spherical mathematical function. The kriging and semivariograms were all completed using an Arcview GIS (Geographical Information System) Avenue script (McVay, 1998) that was run in conjunction with the ArcView Spatial Analyst extension.

# APPENDIX B

# ICE DEFORMATION MEASUREMENTS

## 1. Survey methods and accuracy

During both field seasons, the stability of the theodolite was checked before and during each set of readings to assure that the leveling bubble was centered. Because changes in the sun angle on the instrument can cause unequal expansion of the various parts in the instrument thus creating significant errors, an umbrella was positioned over the instrument to maintain instrument stability and to keep it dry. We used an external EDM and were unable to practice double survey readings (F1/F2 readings). For orientation control we taped a white (X) on a pole that was fixed to bedrock at the opposite shore of the lake from the theodolite position. At the beginning and end of each survey, two readings (one forward and one backward) were taken to this point.

Due to the long time period of our survey in the 2000 field season (24 days) we were able to measure ablation of the surrounding ice to be used in the water balance equation. However, because we were interested in relative displacements of the targets we did not correct the survey data for ablation. Also, the wood plugs that were inserted into the pole helped keep the poles from melting into the ice and eliminated the need for an ablation correction. However, due to the long time period of the survey we measured daily ablation of the surrounding ice. Ablation measurements were made for every survey stake during the last survey of the day. The amount of ablation was

measured by recording the angle difference between the reflector and the ice/stake interface. Any increase in this angle measurement was attributed to ablation.

There are several sources of error in surveying measurements that will be discussed here. Sources of error can derive from operator errors, instrument stability, instrument collimation, curvature and refraction, sight-path density variations, and distance determination errors.

Operator errors can derive from mis-reading the numbers on the total station or recording them incorrectly in the notes or computer. We did not use an electronic notebook so care was taken when surveying to ensure that these errors were limited. Plotting the data also alerted our attention to any abnormal data points that was most often traced to an error in manual data entry. Matching the data to the original field notes aided us in finding and correcting the errors. Another potential error is in the ability of the surveyor to precisely re-align the cross hairs on the same target, we estimate is ± 0.0003 to 0.0004 grad for both the horizontal and vertical readings.

Horizontal instrument stability derives from the fact the instrument is assumed to be rotating uniformly in time so that the error between opening and closing angle can be partitioned proportionally between each reading. The angular difference between each opening and closing shot is averaged and applied to each target. There should be no errors attributed to vertical stability due to a self indexing vertical reference contained in the instrument.

Collimation is an instrument error arising from the misalignment between the cross hairs in the theodolite and the bubble levels. The collimation error is reduced by

double centering on the opening and closing shots. Assuming there is no error in the sighting itself, the horizontal angles between the normal and inverted position would amount to 200 grads and the vertical angles between the normal and inverted position would amount to 400 grads. Any deviation from these sums is attributed to collimation error and is applied to the target survey data.

Curvature corrections are necessary since the measurements are taken in a plane coordinate system where in reality the earth has some curvature. Refraction occurs when rays of light are bent as a result of passing through the earth's atmosphere (Moffitt and Bouchard, 1987). Under normal conditions of pressure and temperature, refraction tends to lessen the effect of curvature by a small amount (Moffitt and Bouchard, 1987). Thus, it is difficult to separate temperature and pressure and they are often treated collectively. This correction was considered to be insignificant for the survey and was not applied.

Distance determination is dependent on the speed of light in air, dependent on the density of the air along the sight path. Based on the EDM we used and the altitudes of the instrument and targets, this error is approximately 5 ppm.

*Summary*

Taking into account all of these factors a rough estimate of the total error in the survey was determined. If we assume the average angular error to be ± 0.0005 grad we can take the tangent of the angular error and multiply this by the distance to the targets. Given the shortest target distances to the instrument station as 480 m and the

longest distance as 1,200 m, we can provide an error bound of ± 4 mm for the close targets and ± 9 mm for the farthest targets. If we double this number to account for operator errors such as being able to accurately align the cross hairs on the target the error bound would then be ± 8 to ± 18 mm. If we assume a distance error of ± 5 ppm then we can apply an error of ± 2 mm for short distances and ±6 mm for the long distances.

## 2. Water storage calculations

The variables used for each sigmoid regression at each time step are provided here as well as the integral bounds (Table B1). Since the closest targets (P1, P2 and P3) were lost after JD 199 and this portion of the ice dam was assumed to be floating, we continued to use a constant height difference between the lake and the ice surface following the last record. In other words, the ice dam at these target locations was assumed to continue to move upward at the same rate as the lake stage.

Table B.1 Table of sigmoid regression variables, integral bounds and $R^2$ values for each time step.

| | | | | | integral bounds (easting) | |
|---|---|---|---|---|---|---|
| **Julian Day** | **a** | **b** | **$x_0$** | **$R_2$** | **upper bound** | **lower bound** |
| 188.00 | 0.97413 | -84.4959 | 9432.45 | 0.98 | 10335.12 | 9133.01 |
| 191.00 | 2.82846 | -47.8788 | 9577.85 | 0.91 | 10335.09 | 9131.78 |
| 194.00 | 4.47398 | -29.4957 | 9611.10 | 0.84 | 10375.92 | 9127.50 |
| 197.00 | 5.76635 | -27.7306 | 9613.06 | 0.83 | 10375.94 | 9122.57 |
| 200.00 | 7.34919 | -29.3273 | 9611.69 | 0.83 | 10375.91 | 9122.57 |
| 203.00 | 8.46056 | -28.5608 | 9613.17 | 0.81 | 10376.00 | 9122.57 |
| 206.00 | 9.17146 | -28.0625 | 9614.67 | 0.81 | 10376.10 | 9122.57 |
| 207.00 | 9.30217 | -27.7836 | 9615.53 | 0.80 | 10376.13 | 9122.57 |
| 208.00 | 6.96727 | -18.4943 | 9628.09 | 0.67 | 10376.16 | 9122.57 |